

# Preface

This thesis constitutes the final work of the last semester, of the Master of Energy and Environmental Engineering programme, at the Department of Electric Power Engineering, at the Norwegian University of Science and Technology.

Many thanks are due to my supervisor, Professor Kjetil Uhlen, for valuable guidance and helpful insights during the process of producing this thesis. I am also grateful for working on such an interesting, and relevant, subject.

My co-supervisor, PhD Candidate Dinh Thuc Duong, is also due my gratitude. The progress and quality of the developed measurement interface, would have been diminished without basing it on the template you gave me during my specialization project last semester. Thank you.

I would also like to thank research scientist Kjell Ljøkelsøy, at SINTEF Energy Research, for sharing his invaluable knowledge regarding the laboratory components. The rewarding discussions, and good times had, during lunch breaks with fellow Master-students, are worth to mention. They will never be forgotten.

I would also like to thank my wife for her love, understanding and support throughout this process, especially during periods with high workload. Finally, a special gratitude goes to my parents, and siblings, for their encouragement and backup through all these years. Thank you for believing in me.

June 19, 2014, Trondheim

---

Kristian L. Brunsgård Ek



## Abstract

Utilization of phasor measurements units (PMUs) in wide area monitoring and control systems (WAMS), has a large potential for increased situational awareness in power system operation, especially regarding system stability surveillance. Applications utilizing PMU measurements, however, are still in their early stage.

A measurement interface (MI) based on PMU measurements was developed as part of this thesis, as an example of a possible network information system (NIS) for control room purposes. Its main objective was to display the measured voltage and current phasors, as well as other significant power system parameters that could be derived, so that the current state of the system was accurately visualized, and its voltage stability could be assessed. The laboratory power system set-up consisted of a single generator, supplying a single load, and was subjected to increasing load power demand, and varying system impedance.

A simulation model of the laboratory power system, was developed to validate the MI calculations. The theoretical basis of the voltage-power characteristic estimation, and  $VSI_{SCC}$  voltage stability indicator, were proved incorrect for the power system set-up utilized in the experiments. The indicators might perform better in a high-voltage grid, with low resistance, and less dynamic load power factors, but this should be investigated further.

During the laboratory experiments, it was discovered that only measuring a single phase in each measurement location, introduces deviations in the calculations, when applied to power systems that are not perfectly symmetrical. When implemented in an actual power grid, the PMUs should measure all three phases at each node, to increase the accuracy of the MI.

The phasor diagram behaved correctly when based on both simulated and measured phasors, and provided a highly intuitive and accurate visualization of the current state of the system. This may significantly increase the situational awareness for the grid operator, and it might even prove useful for educational purposes, because of its natural ability to visualize the current state of the system. The trend curves visualizing phasor magnitudes, phasor angles, system frequencies, calculated powers, and impedances, will be great assets in every network information system, and provide valuable information to the grid operator. They are important parameters, since pattern recognition of these can 1) predict impending faults, 2) govern the supply-demand scheduling, 3) analyse primary frequency, or 4) validate power system models off-line.

All of the parameters and displays developed in this thesis, except the voltage stability indicators and the voltage-power characteristic estimation, have been validated for power system operation, both during increasing load power demand, and varying system impedance. Even though the  $ISI$  voltage stability indicator was not tested close to its limit during real-time operation, it performed well on the simulated voltage and current phasors, and should therefore be included among the successful parameters. The

developed network information system based on PMU measurements are sufficiently accurate, greatly improves the situational awareness delivered by the SCADA systems today, and provides invaluable information for the grid operators, regarding the real-time power system operation. The MI can be considered as proof of the WAMS concept, and should be investigated and developed even further in the future.

## Sammendrag

Utnyttelse av visermåleenheter (Phasor Measurement Units, PMUs) ved overvåking og kontroll av store områder (Wide Area Monitoring and control Systems, WAMS) har et stort potensiale for økt situasjonsforståelse for kraftsystemer i drift. Dette gjelder spesielt overvåking av systemets stabilitet, men applikasjoner som utnytter PMU målinger er fortsatt i et tidlig stadium.

Et brukergrensesnitt basert på PMU målinger (Measurement Interface, MI) ble utviklet som en del av denne avhandlingen, og illustrerer et eksempel på et nettinformasjonssystem (NIS) til bruk i nettselskapers kontrollrom. Hovedmålet var å vise fram de målte spenning- og strømviserne, i tillegg til andre betydningsfulle kraftsystemparametre, som kunne utledes fra disse. Deretter skulle den gjeldende tilstanden til systemet bli illustrert, og dens stabilitet skulle kunne bli vurdert ved hjelp av indikatorer dedikert, til formålet. Laboratoriets kraftsystemoppsett besto av en enkelt generator som forsynte en enkelt last. Dette oppsettet ble deretter utsatt for en gradvis økende belastning, og en varierende systemimpedans, for å undersøke dens respons.

En simuleringsmodell av kraftsystemoppsettet ble utviklet for å validere MI-beregningene. Det teoretiske grunnlaget for estimeringen av spennings-effekt karakteristikkene, og  $VSI_{SCC}$ -indikatoren for spenningsstabilitet, ble implementert og testet. Det ble bevist at denne ga feil svar for kraftsystemoppsettet benyttet i denne avhandlingen. Indikatorene kan antageligvis prestere bedre i et høyspentnett med lav motstand, og mindre dynamisk lasteffekt faktor, men dette bør undersøkes nærmere.

Under laboratorieforsøkene viste det seg at å bare måle en enkelt fase på hvert målested introduserer avvik i beregningene, spesielt når PMU'ene måler i kraftsystemer som ikke er helt symmetriske. Om PMU'ene blir installert i et faktisk strømmnett, bør de måle alle tre faser i hver node av systemet for å øke nøyaktigheten av målegrensesnittet.

Viserdiagrammet opptrådte korrekt både med simulerte og målte viserverdier, og ga en svært intuitiv og nøyaktig oversikt over den nåværende tilstanden til systemet. Diagrammet kan i betydelig grad øke situasjonsforståelsen til driftsoperatørene, men det kan også være nyttig i pedagogiske sammenhenger på grunn av sin naturlige evne til å illustrere den nåværende tilstanden i systemet. Trendkurver som illustrerer viserlengder, viservinkler, systemfrekvenser, beregnede effekter og impedanser, vil kunne være verdifulle ressurser i nettinformasjonssystemer, og gi viktig informasjon til driftsoperatørene. Siden mønstergjenkjenning av disse kan 1) forutsi nært forestående feil, 2) hjelpe med å styre tilbud-etterspørselplanleggingen, 3) analysere primærfrekvensen, eller 4) validere kraftsystemmodeller i ettertid, er det verdifullt å inneha informasjon om alle disse parametrene.

Systemparametrene og fremvisningsverktøyene som ble utviklet i denne avhandlingen, unntatt spenningsstabilitetsindikatorerne og spenning-effekt karakteristikkestimeringen, har blitt validert for denne avhandlingens kraft-

system under drift, med både økende belastning og varierende systemimpedans. Selv om spenningsstabilitetsindikatoren ISI ikke ble testet nær grensen i laboratorieforsøkene, så gjorde den det gjorde bra på de simulerte viserverdiene, og bør derfor inngå blant de vellykkede parametrene. Det utviklete nettinformasjonssystemet, som er basert på PMU målinger, er bekræftet tilstrekkelig nøyaktig. Den forbedrer situasjonsforståelsen i kontrollrom i forhold til det SCADA-systemer kan levere idag, og den gir uvurderlig informasjon for driftsoperatørene om kraftsystemets sanntidsdrift. Bruker-grensesnittet for målinger kan betraktes som et bevis på WAMS-konseptet, og bør undersøkes og utvikles ytterligere i fremtiden.

# Table of Contents

<b>Preface</b>	<b>i</b>
<b>Abstract</b>	<b>iii</b>
<b>Sammendrag</b>	<b>v</b>
<b>Table of Contents</b>	<b>vii</b>
<b>Lists of Figures</b>	<b>ix</b>
<b>Lists of Tables</b>	<b>xiii</b>
<b>Abbreviations and Acronyms</b>	<b>xv</b>
<b>1 Introduction</b>	<b>1</b>
1.1 Background and Objective . . . . .	1
1.2 Scope of Work . . . . .	2
1.3 Outline of Thesis . . . . .	2
1.4 Connection with the Specialization Project . . . . .	3
References . . . . .	4
<b>2 Theoretical Basis</b>	<b>5</b>
2.1 Signal Representation . . . . .	6
2.2 Voltage and Current Conversions . . . . .	10
2.3 Phasor Measurement Technology . . . . .	13
2.4 LabVIEW: A System Design Software . . . . .	19
References . . . . .	25

---

<b>3</b>	<b>Network Information Systems</b>	<b>27</b>
3.1	Power System State Estimation . . . . .	28
3.2	Synchrophasor Applications . . . . .	31
3.3	System State Visualization Displays . . . . .	39
	References . . . . .	48
<b>4</b>	<b>Power System Set-Up Description</b>	<b>49</b>
4.1	Stationary Laboratory Components . . . . .	50
4.2	Laboratory Measurement Device . . . . .	56
4.3	Measurement Interface . . . . .	59
4.4	Simulation Model in PowerFactory . . . . .	76
	References . . . . .	78
<b>5</b>	<b>Case Studies and Results</b>	<b>79</b>
5.1	Model Simulations . . . . .	80
5.2	Measurement Interface Validation . . . . .	98
5.3	Laboratory Experiments . . . . .	108
<b>6</b>	<b>Discussion</b>	<b>119</b>
6.1	Network Information System . . . . .	119
6.2	Network Information System Abilities . . . . .	120
6.3	Measurement Interface Validation . . . . .	122
<b>7</b>	<b>Conclusion</b>	<b>127</b>
<b>8</b>	<b>Suggestions for Further Work</b>	<b>129</b>
	<b>Appendices</b>	<b>131</b>



# List of Figures

2.1	Correlation between sinusoidal signal and corresponding phasor . . . . .	7
2.2	Time and frequency representation of a $0^\circ$ and a $90^\circ$ signal . . . . .	9
2.3	Angular relationships between the phase and line voltages . . . . .	10
2.4	Illustration of the Y- $\Delta$ -connection of a transformer . . . . .	12
2.5	The Fourier filter in the phasor measurement unit . . . . .	13
2.6	Flowchart of a PMU's behaviour . . . . .	14
2.7	PMU and PDC placement in the North-American Power Grid . . . . .	15
2.8	Power oscillations measured with SCADA and synchrophasor . . . . .	16
2.9	The front panel and block diagram connections in a LabIEW application . . . . .	20
2.10	A flow chart illustration of the measurement data's path to the user . . . . .	21
2.11	A screen shot of the PMU Recorder Light . . . . .	22
2.12	PRL access components for a custom NI LabVIEW application . . . . .	23
3.1	Difference in SCADA and PMU measurements during a fault-induced delayed voltage recovery event . . . . .	32
3.2	Difference in SCADA and PMU measurements during voltage oscillations . . . . .	32
3.3	Diverging voltage angles indicating imminent power system separation . . . . .	34
3.4	Generator failure discovered by calculated negative sequence current . . . . .	35
3.5	The course a tripped line causing an unstable mode of operation . . . . .	35
3.6	Power oscillation representations with SCADA vs PMU measurements . . . . .	36
3.7	A Mode Meter operational tool based on synchrophasor measurements . . . . .	37
3.8	The frequency in Nedre Røssåga and Hasle in Norway . . . . .	38
3.9	The power transfer in Hasle from southern Norway to Sweden . . . . .	38
3.10	Thévenin equivalent for the system from the load terminals . . . . .	40
3.11	Phasor diagram with exemplified impedance ratios . . . . .	40

---

3.12	Voltage-power characteristic estimations based on measurement sample . . . . .	45
3.13	The relationship between the system and load impedances, including the voltage stability limit . . . . .	46
4.1	A part of the laboratory layout from Appendix C . . . . .	51
4.2	Equivalent line diagram of the power system that is to be studied.	53
4.3	CompactRIO Programming Model . . . . .	57
4.4	The compactRIO programmed as a PMU utilized for the measurements . . . . .	58
4.5	Illustration of the simplified laboratory set-up . . . . .	61
4.6	The control display for the <i>Signal Converting Choices</i> of the subVI named <i>LabMeasurementConverter</i> . . . . .	62
4.7	Inputs and outputs of the subVI named <i>LabMeasurementConverter</i>	62
4.8	Inputs and outputs of the subVI named <i>SaveLoadMeasurementData</i>	63
4.9	Inputs and outputs of the subVI named <i>FindingMostRecentIndex</i>	63
4.10	Inputs and outputs of the normalizer subVIs . . . . .	64
4.11	Inputs and outputs of the subVI named <i>GraphPlotter</i> . . . . .	65
4.12	Waveform chart of the calculated impedances during an increased load power event performed on the system model in PowerFactory.	66
4.13	Inputs and outputs of the subVI named <i>CalculateImpedanceSystem</i>	66
4.14	Inputs and outputs of the subVI named <i>CalculateImpedanceLoad</i>	67
4.15	Inputs and outputs of the subVI named <i>CalculateImpedanceSystemWfrequency</i> . . . . .	67
4.16	Inputs and outputs of the subVI named <i>CalculatePhasorRepresentations</i> . . . . .	68
4.17	An array displaying the voltage and current phasors . . . . .	69
4.18	The built-in vector diagram provided by LabView . . . . .	70
4.19	The phasor diagram developed for this thesis. . . . .	71
4.20	Inputs and outputs of the subVI named <i>CalculatePowerFlow</i> . .	72
4.21	Inputs and outputs of the subVI named <i>Indicator_PVcurve</i> . . .	73
4.22	Inputs and outputs of the subVI named <i>Indicator_ISI</i> . . . . .	73
4.23	Inputs and outputs of the subVI named <i>Indicator_VSI</i> . . . . .	74
4.24	Example of a measurement interface utilizing the developed library	75
4.25	Simulation model developed in PowerFactory . . . . .	76
5.1	The simulated phasor magnitudes during scenario Load: Theoretical	84
5.2	The simulated phasor angles during scenario Load: Theoretical .	84
5.3	The simulated power flows during scenario Load: Theoretical . .	85
5.4	The simulated PV-curve during scenario Load: Theoretical . . .	85
5.5	The simulated phasor magnitudes during scenario Load: Lab-start	86

---

5.6	The simulated phasor angles during scenario Load: Lab-start . .	87
5.7	The simulated power flows during scenario Load: Lab-start . . .	87
5.8	The simulated PV-curve during scenario Load: Lab-start . . . .	88
5.9	The simulated phasor magnitudes during scenario Load: Lab-average . . . . .	89
5.10	The simulated phasor angles during scenario Load: Lab-average .	89
5.11	The simulated power flows during scenario Load: Lab-average . .	90
5.12	The simulated PV-curve during scenario Load: Lab-average . . .	90
5.13	The simulated phasor magnitudes during scenario System: Lab-start	92
5.14	The simulated phasor angles during scenario System: Lab-start .	92
5.15	The simulated power flows during scenario System: Lab-start . .	93
5.16	The changed relationship between the phase-voltage and three-phase power during during scenario System: Lab-start . . . . .	93
5.17	The simulated phasor magnitudes during scenario System: Arbitrary . . . . .	95
5.18	The simulated phasor angles during scenario System: Arbitrary .	95
5.19	The simulated power flows during scenario System: Arbitrary . .	96
5.20	The changed relationship between the phase-voltage and three-phase power during during scenario System: Arbitrary . . . . .	96
5.21	Illustration of the reduced voltage-power characteristic as a result of increased system impedance . . . . .	97
5.22	LabView interface power flow estimations during scenario Load: Lab-average. . . . .	100
5.23	LabView interface complex impedance estimations during scenario Load: Lab-average. . . . .	101
5.24	LabView interface absolute impedance estimations during scenario Load: Lab-average. . . . .	102
5.25	Measurement interface indicator values during scenario Load: Lab-average. . . . .	102
5.26	Measurement interface phasor representation at the end of scenario Load: Lab-average. . . . .	104
5.27	The measured phasor magnitudes during increasing load power demand . . . . .	110
5.28	The measured phasor angles during increasing load power demand	110
5.29	The calculated power flow during increasing load power demand	111
5.30	The measured frequency during increasing load power demand .	112
5.31	The estimated complex impedances during increasing load power demand . . . . .	113
5.32	The estimated absolute impedances during increasing load power demand . . . . .	113
5.33	The visualized phasor diagram at the maximum load power demand	114

---

5.34	The indicator values calculated during increasing load power demand	115
5.35	The measured phasor magnitudes during varying system impedance	116
5.36	The measured phasor angles during varying system impedance . . .	116
5.37	The calculated power flow during varying system impedance . . .	117
5.38	The estimated complex impedances during varied system impedance	118
5.39	The estimated absolute impedances during varied system impedance	118
A.1	The block diagram actions corresponding to step 1 and 2 . . . . .	3
A.2	The block diagram actions corresponding to step 3 and 4 . . . . .	4
A.3	The block diagram actions corresponding to step 5, 6 and 7 . . . . .	5
A.4	The block diagram illustrating the saving of measurements . . . . .	6
C.1	Distribution Network Model of the Renewable Energy Laboratory	9
F.1	Measurement interface deviations in the power calculations . . . . .	19
F.2	Impedance calculations performed in Matlab based on simulation model . . . . .	20
F.3	Measurement interface deviations in the impedance calculations . . . . .	20
G.1	First phasor state during scenario Load: Lab-average . . . . .	21
G.2	Second and third phasor state during scenario Load: Lab-average . . . . .	22
G.3	Fourth and fifth phasor state during scenario Load: Lab-average . . . . .	23
H.1	All current phases measured at the generator by a PMU . . . . .	26
H.2	All line-voltage phases measured at the load by a PMU . . . . .	26

# List of Tables

3.1	Real-time synchrophasor applications, courtesy of [?, p. 3] and [?, p. 3] . . . . .	33
4.1	Initial switch states in the laboratory set-up illustrated in Figure 4.1	50
4.2	Base values for calculating pu representations of parameters . . .	52
4.3	Synchronous generator data, courtesy of [?, p. 27] . . . . .	53
4.4	The properties of the different measurement points in the laboratory, referred to the labels given in Figure 4.1. The input columns indicate the measured values when the parameter is equal to 1 pu	60
4.5	Impedance in [ $\Omega$ ] and [pu] of the flexible line equivalent sections that result in the largest line impedance . . . . .	77
5.1	Parameters for the increased load power demand event . . . . .	80
5.2	Parameters for the line impedance increase event . . . . .	82
5.3	Overview of the changed settings in the different scenarios . . . .	82
5.4	Model simulation results used as input for the measurement interface	98
5.5	Maximum deviations in parameter calculation . . . . .	99
5.6	Parameters calculated by the MI and deviations when compared to laboratory panels . . . . .	107
D.1	Overview of the different subVIs contained in the measurement interface library. . . . .	11
H.1	PMU input socket measurement's connection with laboratory phases	25



# Abbreviations and Acronyms

AVR	Automatic Voltage Regulator
cRIO	CompactRIO, a programmable hardware made by National Instruments
FPGA	Field-Programmable Gate Array
ISI	Impedance Stability Index, a voltage stability indicator
MI	Measurement Interface
NTNU	Norwegian University of Science and Technology
PDC	Phasor Data Concentrator
PMU	Phasor Measurement Unit
PRL	PMU Recorder Light, software developed by [?]
PV-curve	Voltage-power-characteristic for the load
SEL	Schweitzer Engineering Laboratories, Inc
subVI	Secondary virtual instrument (VI)
Synchrophasor	Synchronized phasor measurement
VI	Virtual Instrument
VSI <sub>SCC</sub>	Short-Circuit Capacity Index, a voltage stability indicator
WAMS	Wide area measurement system





# Introduction

## 1.1 Background and Objective

The utilization of phasor measurements units (PMUs) in wide area monitoring and control systems (WAMS), has a large potential for increasing system stability surveillance. Voltage and current phasors, calculated from analog sinusoidal signals with high time resolution, might improve the real-time state estimations, when compared to the SCADA systems used by the grid operators today.

Applications utilizing PMU measurements are still in their early stages, albeit several research communities are working on implementations for WAMS purposes. The Smart Transmission Grid Operation and Control [STRONGrid, 2013] project and the North American SynchroPhasor Initiative [NASPI, 2013] represent two such organizations that develop tools and study the results obtained through their usage.

One such tool, named *PMU Recorder Light*, collects the PMU measurements and makes them available for calculations and visualization in NI LabVIEW, a system design software provided by National Instruments [Aarstrand, 2013]. Various voltage stability indices have been thoroughly examined in a previous thesis [Storvann, 2012], and they may provide valuable information to the grid operator.

In this thesis, a new PMU will be installed in the Renewable Energy Laboratory, also known as the smart-grid laboratory, at the Norwegian University of Science and Technology (NTNU). The main objective is to develop an application containing the visualization of the voltage and current phasors measured by the PMU, together with some important power system parameters calculated from the measurements. Different system configurations and disturbances imposed

upon the system will be explored through this application, in addition to some algorithms for monitoring the voltage stability.

## 1.2 Scope of Work

A single generator supplying a single load will constitute the power system studied in the laboratory. At both the generator and the load, measurements of the voltage and the current phasor will be performed by a PMU. A measurement interface will be developed in LabVIEW, and utilize the *PMU Recorder Light* to acquire the measurements from the PMU.

The application will be specifically designed for this power system set-up. Some control parameters, though, will be supplied in order to define from which measurement points the PMU is connected. Interface components, for calculating and visualizing power flows, voltage stability indices and phasor diagrams, will be developed as part of creating the measurement interface. This will serve as a state estimator, based on voltage and current measurements obtained from the system.

The system will be subjected to events where either the power demand at the load is increased, or the system impedance is increased, which may be a result of disconnecting load-supplying power lines.

Before performing the various tests in the laboratory, the theoretical behaviour of the power system should be studied. A simulation model will be developed in DigSILENT PowerFactory 14.1, and subjected to events that simulate the performed in the laboratory. The accuracy of the interface should be validated by utilizing the simulation model.

## 1.3 Outline of Thesis

First, the theoretical basis of voltages and currents in a power system, as well as the relevant PMU measurement technology and system design software, are reviewed in Chapter 2. Second, Chapter 3 outlines the approach for estimating the current state of a power system, the possible PMU measurement applications known to date, and how the different derived parameters may be displayed in a network information system.

Then Chapter 4 presents the chosen power system with its stationary components and limitations. Also the PMU and the measurement interface, that has been utilized and developed through the course of this thesis, are studied in greater detail, before moving on to describe the simulation model and its parameters. The experiment and simulation descriptions are given in Chapter 5, which also presents and discusses the obtained results.

The results are then viewed in a broader perspective during the discussion in Chapter 6, before reaching a conclusion in Chapter 7. Last, Ideas for future work, to expand on the knowledge and tools acquired from this thesis, are presented in Chapter 8.

## 1.4 Connection with the Specialization Project

This thesis extends some of the work contributed to the "specialization project", performed at NTNU during the autumn of 2013. Although the project concerned mainly PMU measurements performed in power systems spanning across a large geographical area, and developing a real-time network information system for the Nordic grid operators, parts of the project report are still somewhat relevant for this thesis as well. The material reused from [Ek, 2013] are:

- Chapter 2: Technology
- Chapter 3: Synchrophasor Applications (Section 3.1-3.2)
- Chapter 4: PMU System Installation at NTNU (Section 4.2-4.5)
- Chapter 5: Measurement Visualization

## References

- Aarstrand, V. H. (2013). *PMU Recorder Light (PRL) - Documentation*. Enfo Technology AS, Lysaker Torg 15 Postbox 374, 3 edition.
- Ek, E. B. (2013). Wide-area monitoring and control. Specialization project, Norwegian University of Science and Technology.
- NASPI (2013). North american synchrophasor initiative. Website.
- Storvann, V. (2012). Maintaining voltage stability - an analysis of voltage stability indicators and mitigating actions. Master's thesis, Norwegian University of Science and Technology.
- STRONGrid (2013). Smart transmission grid operation and control. Website.

# Chapter 2

## Theoretical Basis

This chapter describes in detail the theoretical foundation of which the rest of this thesis is based upon. The signal conversion equations, outlined in Section 2.1, are fundamental for understanding how the voltages and currents may be measured as phasors. The parameter conversions, which are dependent of the power system set-up in question, are examined in Section 2.2. How the acquired phasors are transmitted from the phasor measurement unit to the phasor data concentrator and further, is elaborated on in Section 2.3. The software utilized for presenting the measurements, are introduced in Section 2.4, providing some insight into the application development. This might facilitate further development on the application, performed by the reader, if desired.

### Chapter Contents

---

2.1	Signal Representation . . . . .	<b>6</b>
2.1.1	Sinusoids . . . . .	6
2.1.2	Phasors . . . . .	6
2.2	Voltage and Current Conversions . . . . .	<b>10</b>
2.2.1	Line Voltage versus Phase Voltage . . . . .	10
2.2.2	Transformer Y- $\Delta$ Phase Shift . . . . .	11
2.3	Phasor Measurement Technology . . . . .	<b>13</b>
2.3.1	Motivation For Performing Phasor Measurements . . . . .	13
2.3.2	The Phasor Measurement Unit . . . . .	14
2.3.3	Encoding Standard: IEEE C37.118-2005 . . . . .	15
2.3.4	Phasor Data Concentrator . . . . .	17
2.4	LabVIEW: A System Design Software . . . . .	<b>19</b>
2.4.1	Software Structure . . . . .	19

	2.4.2 PMU Recorder Light . . . . .	19
	2.4.3 Custom Application . . . . .	22
	References . . . . .	25

---

## 2.1 Signal Representation

The currents in an AC grid are precisely that, alternating currents. The voltages are also alternating, usually modelled as a function including either the cosine or the sine trigonometric identity with respect to time. However, it is often more appropriate to transform it into the frequency plane, both for comprehension, and for simplifying the equations.

### 2.1.1 Sinusoids

In the time domain, the voltages and currents are usually described as sinusoidal signals  $s$ , and can be modelled mathematically as the following:

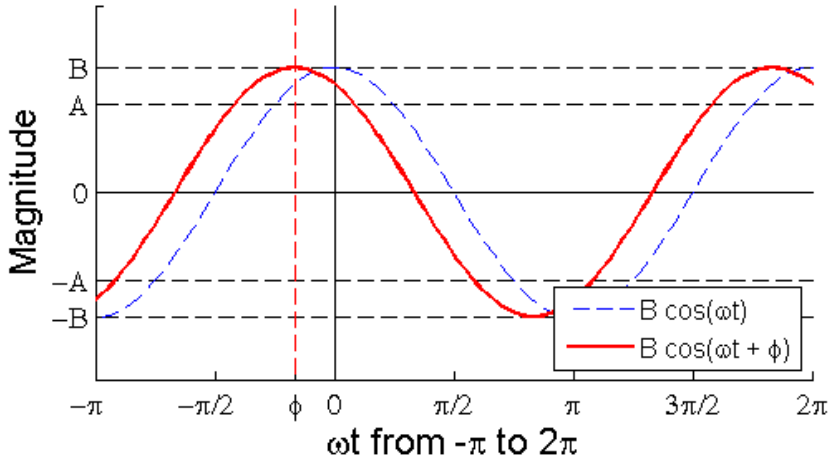
$$s(t) = B \cos(\omega t + \phi) \tag{2-1}$$

Here  $B$  describes the amplitude of the signal, and  $2B$  is therefore the peak-to-peak magnitude.  $\omega$  is the frequency of the signal [ $\frac{\text{rad}}{\text{s}}$ ], which in power systems is defined as  $2\pi f$  with  $f$  being the frequency of the system.  $t$  is the time [s], and  $\phi$  is known as the phase angle [rad], which in general can be referred to any chosen reference. The sinusoidal signal, and how the different variables relate to it, is illustrated in Figure 2.1.(a).

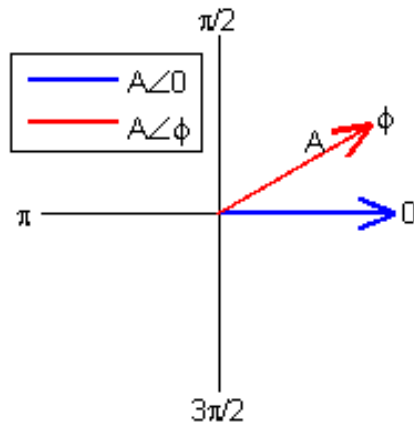
### 2.1.2 Phasors

A phasor is a time-independent method of describing the magnitude of the sinusoidal signal, and its angle, based on the angular separation between a chosen reference time and the peak of the sinusoid. Equation 2-1 shows the time domain representation of the signal, and the frequency domain representation will be derived in this section. The phasor representation of the sinusoidal signals presented in Figure 2.1.(a), is illustrated in Figure 2.1.(b).

Let  $t_{\text{peak}}$  be the time when the phase-shifted sinusoidal signal reaches its peak value, and  $t_0$  be the chosen reference time. Figure 2.1 illustrates how  $\phi$  is defined as positive when  $t_{\text{peak}} < t_0$ . If assuming  $t_0 = 0$ , Equation 2-1 results in  $s(t_0 = 0) = B \cos(\phi)$ . The property of the chosen time, as the peak of the sinusoid, yields  $s(t_{\text{peak}}) = B$ . By inserting  $t_{\text{peak}}$  into the same equation as above, the value for  $\phi$  can be found, as displayed in Equation 2-2.



(a) Sinusoidal representation



(b) Phasor representation

Figure 2.1: Correlation between sinusoidal signal and corresponding phasor.

$$\begin{aligned}
 B \cos(\omega t_{\text{peak}} + \phi) &= B \\
 \cos(\omega t_{\text{peak}} + \phi) &= 1 \\
 \omega t_{\text{peak}} + \phi &= \arccos(1) \\
 \phi &= -\omega t_{\text{peak}}
 \end{aligned} \tag{2-2}$$

By applying the root mean square method on the signal, which will not be elaborated on in this thesis (see [Nilsson and Riedel, 2008, p. 333, 399] for a review on the topic), we obtain the needed rms-quantity  $A$  :

$$A = \frac{\text{amplitude}}{\sqrt{2}} = \frac{B}{\sqrt{2}} \tag{2-3}$$

This result in the equivalent phasor representations of the sinusoidal time signal, which was stated in Equation 2-1, formatted either as absolute magnitude and angle (Equation 2-4), as polar coordinates (Equation 2-5), or as a complex number (Equation 2-6):

$$\vec{S} = A \angle \phi \tag{2-4}$$

$$= A e^{j\phi} \tag{2-5}$$

$$= A(\cos \phi + j \sin \phi) \tag{2-6}$$

If the peak of the sinusoid and the time reference coincide, Figure 2.2(a) yields that the phase angle is zero degrees, and through Equation 2-4 we have  $\vec{S} = A \angle 0$ . If the sinusoid peak leads the time tag,  $t_{\text{peak}} > t_0$ , meaning the signal is increasing and crosses zero at  $t_0$  (see Figure 2.2(b)),  $\frac{1}{4}$  of the period of the signal has crossed the reference time tag, permitting the  $t_{\text{peak}}$  to be described as  $\frac{\pi}{2\omega}$ . This results in a phase angle of  $-90^\circ$ , which is in accordance with the IEEE standard described in [Martin et al., 2008, p. 1].



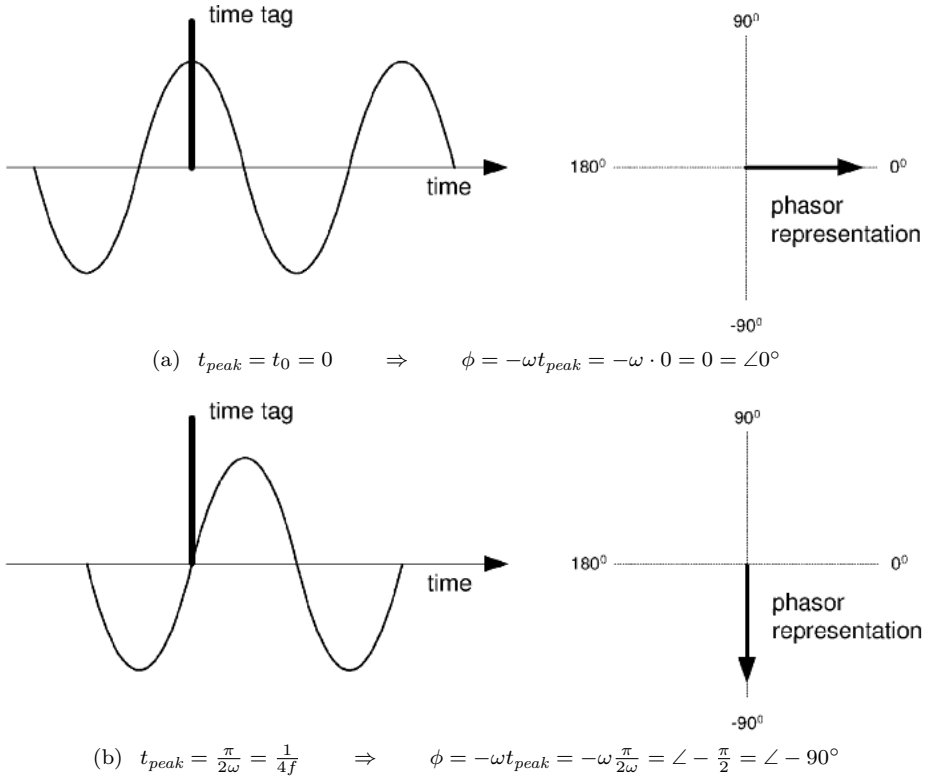


Figure 2.2: With the time tag as the chosen reference time,  $\Delta t$  is calculated as  $t_{peak} - t_0$ , where  $t_{peak}$  is the time when the peak of the sinusoidal voltage signal is occurring. In these captions,  $t_0$  is assumed equal to zero for simplicity. Courtesy of [Martin et al., 2008].

## 2.2 Voltage and Current Conversions

A three-phase power system may provide different types of voltage measurement points, and contain transformers that introduce phase-shifts between the measurement signals. When simultaneously comparing measurements from various locations and performing calculations based upon them, these aspects must be taken into consideration. The conversions necessary to transform the measurements from the power system components relevant to this thesis into having the same basis, are presented below.

### 2.2.1 Line Voltage versus Phase Voltage

The voltages in a three-phase power system can be measured as the electrical potential difference between two of the phases, or between one phase and the neutral. These measurements are called line voltages and phase voltages respectively. In order to represent the system as a single phase diagram, the line voltages must be converted into phase voltages. The relationships between these voltages in a balanced three-phase power system (i.e.  $u_a(t) + u_b(t) + u_c(t) = 0$ ) are illustrated in Figure 2.3, and Equation 2-7, 2-8 and 2-9 define the phase voltages represented as phasors, where  $U_m$  is the single-phase rms-value calculated in Equation 2-3 [Nilsson and Riedel, 2008, p. 434, 439].

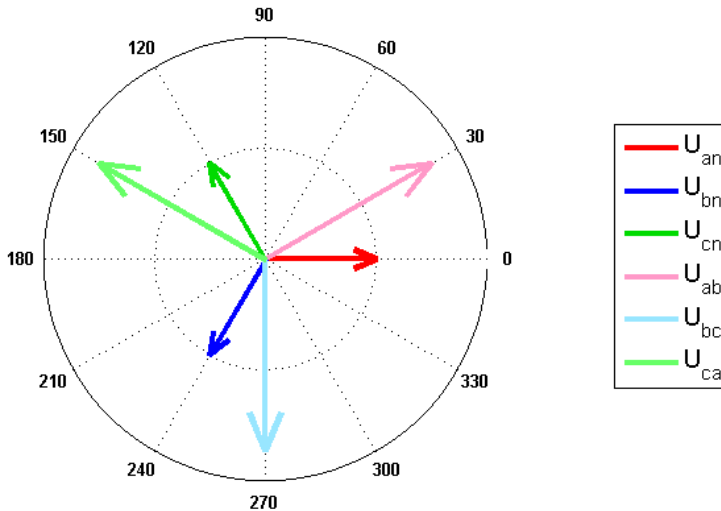


Figure 2.3: *Angular relationships between the phase voltages and the line voltages in a balanced three-phase power system.*

$$\vec{U}_{an} = U_m \angle 0^\circ \quad (2-7)$$

$$\vec{U}_{bn} = U_m \angle -120^\circ \quad (2-8)$$

$$\vec{U}_{cn} = U_m \angle +120^\circ \quad (2-9)$$

The different line voltages can be found by applying vector principles, so that:

$$\begin{aligned} \vec{U}_{ab} &= \vec{U}_{an} - \vec{U}_{bn} \\ &= U_m \angle 0^\circ - U_m \angle -120^\circ \\ &= \sqrt{3} U_m \angle 30^\circ \end{aligned} \quad (2-10)$$

The same is true for  $\vec{U}_{bc}$  and  $\vec{U}_{ca}$ , which respectively are phase-shifted to  $\angle -90^\circ$  and  $\angle +150^\circ$ . Reversed, this result in the conversion from line voltage to phase voltage, with the line voltage from phase a to phase b defined as  $\vec{U}_{ab} = U_M \angle 0^\circ$ :

$$\vec{U}_{an} = \frac{U_M}{\sqrt{3}} \angle (0^\circ - 30^\circ) \quad (2-11)$$

The introduced magnitude difference and phase shift between a phase voltage and a line voltage are important to be aware of, especially when comparing voltage measurements from different locations.

### 2.2.2 Transformer Y- $\Delta$ Phase Shift

The three-phase Y- $\Delta$  transformer connections are illustrated in Figure 2.4, where the phases at the Y-side are denoted with capital letters, and the phases at the  $\Delta$ -side are non-capital letters. Heavy lines indicate the transformer windings, where the parallel windings are located on the same core, and consequently the voltages are in phase [Saadat, 2010, p. 114].

In a Y- $\Delta$  transformer, the phase-voltage between phase  $A$  and the neutral  $n$  on the Y-side is wound on the same core as the voltage between phase  $a$  and phase  $b$  on the  $\Delta$ -side. Thus  $\vec{U}_{ab} = \vec{U}_{An}$  when the core winding ratio is equal, according to [Saadat, 2010, p. 73-74]. The voltage magnitude, resulting from unequal winding ratio, can be calculated by multiplying the  $\Delta$ -side with the coefficient  $a$ :

$$a = \frac{N_Y}{N_\Delta} = \frac{|\vec{U}_{An}|}{|\vec{U}_{ab}|} \quad (2-12)$$

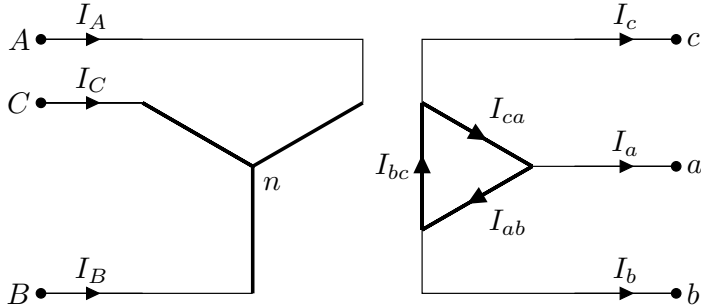


Figure 2.4: *Illustration of the Y- $\Delta$ -connection of a transformer. Parallel, heavy lines indicate voltages that are in phase with each other.*

Here  $N_Y$  is the number of windings on a single phase on the Y side, and  $N_\Delta$  is the number of windings on the corresponding phase on the  $\Delta$ -side [Saadat, 2010, p. 115].

With the previous statement in mind, the relationship between the line-voltages from each side of the transformer can be calculated relative to the Y-side from Equation 2-11:

$$\begin{aligned}\vec{U}_{ab} &= a \cdot \vec{U}_{An} \\ &= a \frac{|\vec{U}_{AB}|}{\sqrt{3}} \quad (\angle \vec{U}_{AB} - \angle 30^\circ)\end{aligned}\tag{2-13}$$

Equation 2-13 clearly states that the phase voltage  $\vec{U}_{An}$  of the Y-side of the transformer is in phase with the line voltage  $\vec{U}_{ab}$  of the  $\Delta$ -side of the transformer, which introduces a phase shift of  $\angle -30^\circ$  between the line voltage sets on the Y- and  $\Delta$ -side.

## 2.3 Phasor Measurement Technology

In the 1980s, the first modern applications utilizing direct measurement of phase angle differences were published in papers. The first prototype of a phasor measurement unit using GPS, was developed at Virginia Tech [Phadke and Thorp, 2008, p. 3-4]. The research has come a long way since then, and the measurement devices and connections have become even more advanced.

### 2.3.1 Motivation For Performing Phasor Measurements

The advantage of representing the sinusoidal signals of the voltages and currents in this format, becomes clear when using the same time tag for all measurement locations in the power system, because then both their magnitudes and angles can be compared. These synchronized phasor measurements are often referred to as synchrophasors, and they can yield instantaneous information about frequency, power flow, losses and other parameters in the system.

This type of measurement is dependent on the accuracy of the time tag, the quality of the communication media for all measurement locations, and a high sample rate performance. New technology for data handling and communications has enabled the development of such a measurement device, formally known as a phasor measurement unit. Its Fourier algorithm, for transforming sinusoidal signals to phasor representations, is illustrated in Figure 2.5, and the unit itself will be described in further detail in the next section.

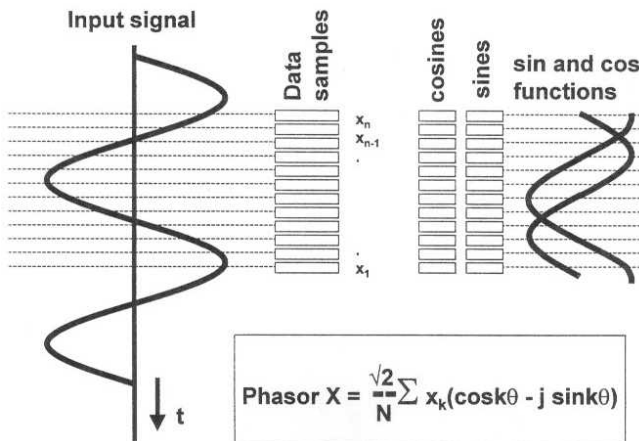


Figure 2.5: *The Fourier filter in the phasor measurement unit that represents the sinusoidal signal as a phasor, courtesy of [Phadke and Thorp, 2008].*

### 2.3.2 The Phasor Measurement Unit

A phasor measurement unit (PMU) is composed of both hardware and software. The hardware includes three-phase voltage and current transformers to transfer the analog measurement signal to the anti-aliasing filter, as depicted in Figure 2.6. The intent of this filter is to remove signals with a frequency higher than the analog-to-digital signal converter (A/D-converter) is able to sample and convert.

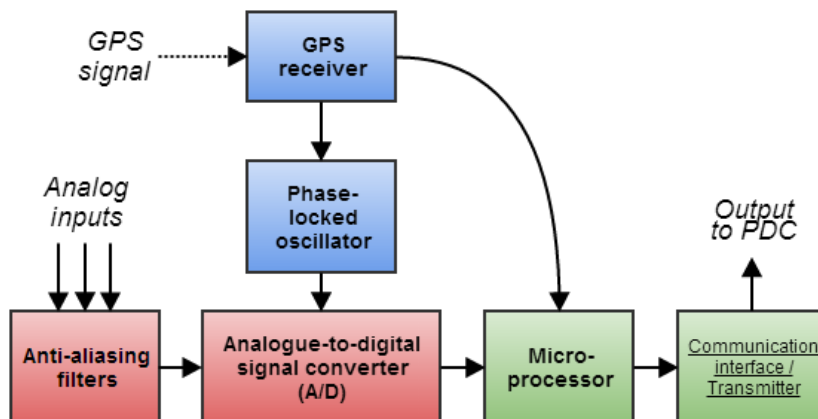


Figure 2.6: Flowchart of a PMU's behaviour, inspired by the illustration in [Machowski et al., 2012, p. 61].

The time stamp originates from a high-accuracy clock in the PMU, that is synchronized with the absolute time reference inherent in the global positioning system (GPS). The measured sample and its time stamp are sent simultaneously to the microprocessor, which stores the samples for one AC period before outputting them to the communication interface as voltage and/or current phasors (from discrete Fourier transformations of the sinusoidal signal, as described in Section 2.3.1) [Machowski et al., 2012, p. 61]. Here they are collectible through software connections for the analysts and operators.

A wide area measurement system (WAMS) usually includes several PMUs, located in different strategic connection points in a large power grid. This could be the Nordic grid including Norway, Sweden, Finland and Denmark, or on an even larger scale, such as the European or the North-American power grid, as shown in Figure 2.7. To aggregate the measurements from different PMUs, a phasor data concentrator (PDC) is used (see Section 2.3.4). A PDC can simultaneously receive signals from 20 - 30 PMUs, and through dedicated software, align the different phasor measurements according to their time stamp. This can

be utilized further in applications for monitoring, protection or control regarding the whole system.

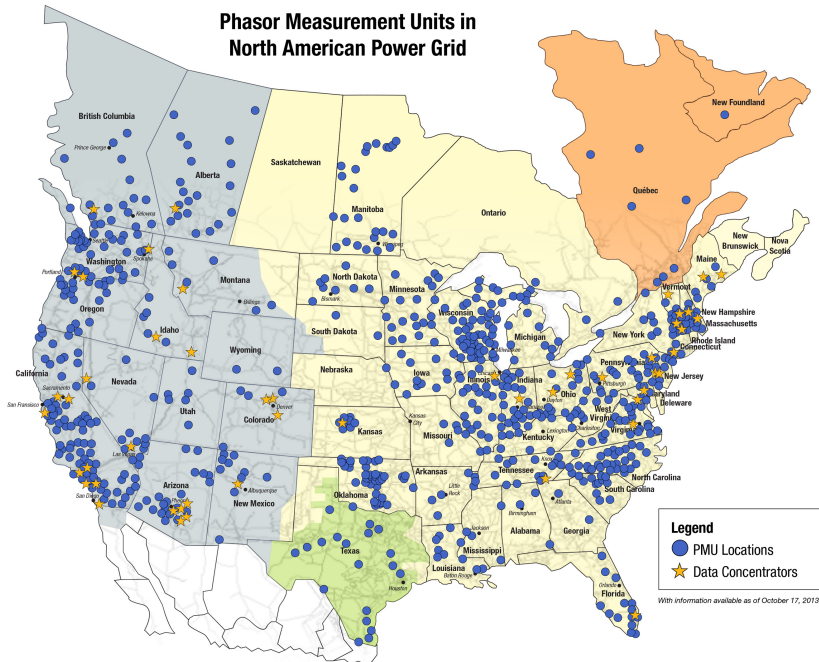


Figure 2.7: PMU and PDC placement in the North-American Power Grid, courtesy of the North American SynchroPhasor Initiative (NASPI).

A PDC can also be configured to receive signals from other PDCs to aggregate the information from even more PMUs, but for every such layer, a larger amount of time delay is introduced. This decreases the current PDC's properties to exercise protection and control, becoming more suitable for exclusively supply signals for monitoring purposes [Machowski et al., 2012, p. 62]. Either way, the obtained signal from a PMU compared to the current SCADA system provides a higher resolution, and to a greater degree assists the operator, with his visualization of the current situation in the grid, as shown with the power oscillations illustrated in Figure 2.8.

### 2.3.3 Encoding Standard: IEEE C37.118-2005

The encoding standard most used today is IEEE C37.118-2005. It defines the the data communication format for real-time data transmission of PMU measure-

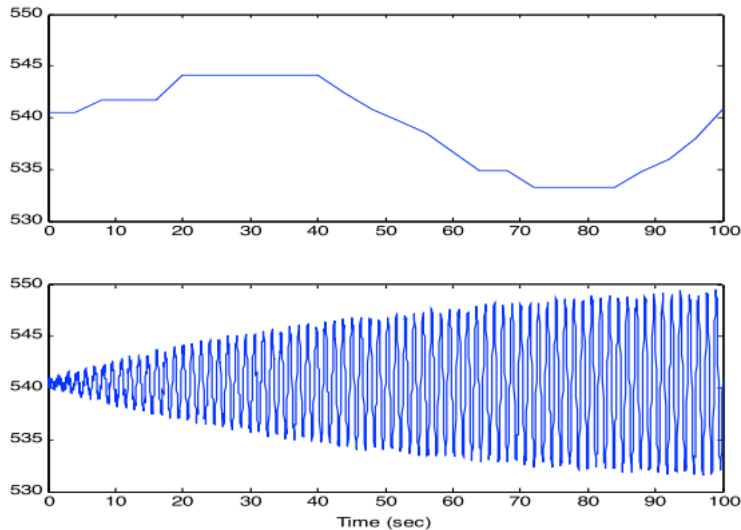


Figure 2.8: *Power oscillation representations with SCADA measurements (upper chart) and with synchrophasor measurements (lower chart), courtesy of [Kosterev and Undrill, 2011, p. 17].*

ments [Martin et al., 2008, p. 1805]. Additionally, it describes the requirements for the measurement performance of the PMU, and a method for determining the precision of the measurements. The introduction of this standard allows for different PMU distributors to develop interchangeable systems, that output the same measurements from the same input signal, and therefore make the network managers independent of the chosen PMU suppliers.

The measurement representation format that is required by the receiver, is a combination of a complex number of the fundamental frequency component of either a voltage or current phasor, as described in Section 2.1.2, together with the appropriate time stamp. The sample rate of the transmitter output, measured in reports per second, should be adjustable between ten and half of the nominal system frequency, i.e. 25 for the European system.

$$\left. \begin{array}{l} Z = a + jb \\ T = \text{Absolute time stamp} \end{array} \right\} \text{Output to data transmitter} \quad (2-14)$$

The PMU is usually also able to calculate the frequency of the grid, as the property can be derived from the deviation between the voltage angle speed,



and the nominal system frequency. In the Nordic grid, the frequency normally deviates between 49.9 and 50.1 Hz.

The measurement accuracy combines the errors of magnitude, angle and timing into one single value, which is compared to an expected value. This is known as the *total vector error*, *TVE*. There are two levels of accuracy compliance, where both require a TVE of less than 1 %, but are subjected to different difficulties concerning measurement challenges. Transient conditions are not included in these challenges, and therefore different PMUs might produce a different output under such conditions.

Communication between the PMU and the PDC, and between different PDCs internally, is also subject to requirements defined in the IEEE C37.118-2005 standard. The protocol defines five frame types:

**Binary:** One data frame, Two configuration frames, One command frame

**ASCII:** One header frame

The header frame gives information readable for humans, while the two configuration frames are respectively describing the full capability, and the configured capability, of the PMU. These frames are transmitted at system start-up, and whenever requested by the receiving unit (for configuration changes). The command frame is sent from the receiving unit to the PMU, to request start or stop of data transmission, or acquire information about the configurations. This frame might be extended in later revised versions of the standard. When the transmission is active, the measurements are sent continuously through the data frame. It can be formatted as either 16 bits or 32 bits, which allows for different amounts of data transmitted.

These frames can be communicated across several systems, such as serial ports, Ethernet, fibre optic cable, and IP. The latter system, and lower level equivalents, have to be mapped into corresponding protocols, which is described in the Annex I of the standard [Martin et al., 2008, p. 1807].

The difference between this standard and the previous edition, is that the synchrophasor is now defined unambiguously, and several annexes are added to improve the unanimity between different producers.

### 2.3.4 Phasor Data Concentrator

The PDC is a specific software installed on a computer. The PDC behaves like a server service, that receives the data stream from the connected PMUs through the Ethernet, and can transmit configurable output streams to users, mentioned in Section 2.3.2. These output streams can combine or single out the incoming PMU streams in all possible combinations, according to the signals required by

the user. The users can only get the measurement data from the PDC stream, not directly from the PMU itself, because the PMU is restricted to only send its data to a single receiver.

To connect to the PDC output stream, the user needs a program like the *PMU Connection Tester*, which is available for free, and the following parameters:

- IP number
- Port number
- Device ID
- The encoding standard

The IP number and port number are dependent of the PDC stream in question, whereas the device ID and encoding standard are defined by the PMU itself. The most used encoding standard is IEEE C37.118-2005 [Martin et al., 2008], and its capabilities and limitations are described in detail in Section 2.3.3.

To allow the PDC to receive measurements from a PMU, the PDC operator needs the same parameters as mentioned above, but the values are not necessarily the same (for example the IP number will be different).

## **2.4 LabVIEW: A System Design Software**

The system design software named LabVIEW [National Instruments, 2014] was chosen for the application development in this thesis. This is mainly due to the external library presented in Section 2.4.2, because it facilitates the process of acquiring the phasor measurements from the PMU, making them easily available to the application developer. The behaviour and functionality of the LabVIEW software are explained briefly in Section 2.4.1, in order to provide some insight into the application development, and to introduce some important vocabulary terms. Section 2.4.3 outlines important aspects when utilizing the external library in an application.

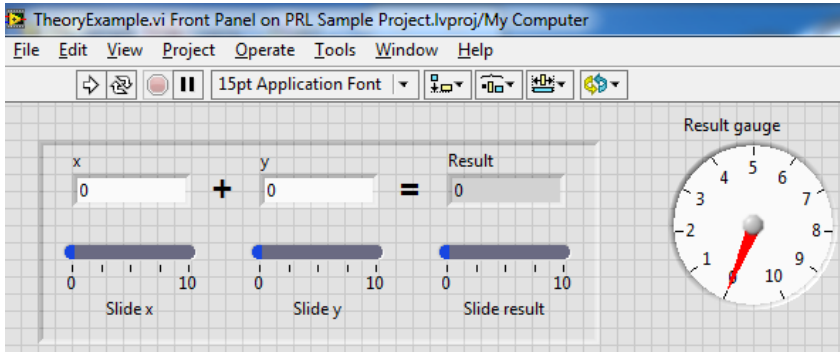
### **2.4.1 Software Structure**

An application created in LabVIEW is called a virtual instrument (VI). For the developer, a VI consists of two different panels; a graphical programming panel, and a visual front panel. The front panel contains buttons and other control components, as well as displays and various indicators, as seen in Figure 2.9(a). The actual calculations are performed in the graphical programming panel, with the front panel control actions as inputs, which is illustrated in Figure 2.9(b). The outputs from the calculations are sent to the front panel indicators for visualization. The front panel is the only visible panel to the user, which makes the applications developed in LabVIEW more user friendly than most.

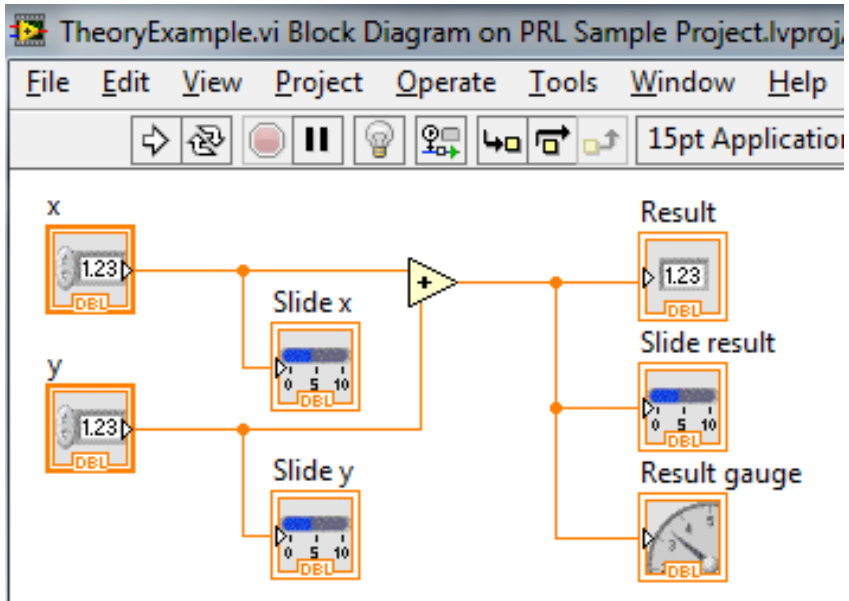
If a project demands large amounts of code, or some part of code is reusable in other places, LabView conveniently allows the developer to extract it into a different secondary virtual instrument (subVI). A subVI is basically an ordinary VI, with the exception that it is intended to be dependent on input, and to result in outputs provided and required from elsewhere. This subVI can be placed and connected where desired in the other VI, in order to perform the part of code it contains. This makes the graphical programming more manageable, as well as allowing easier reassembly of VIs, that only require parts of the original VI. An illustrative comparison is to think of the subVIs as Lego bricks, that constitute the assembled Lego object, which then corresponds to the main VI.

### **2.4.2 PMU Recorder Light**

The PMU Recorder Light (PRL) is a NI LabVIEW program developed in 2013 as part of the STRONGrid project. Its main objective is to simplify the process of receiving the PDC stream, and using this stream in a custom application, without the user having to deal with the data handling details (see Section 2.4.3). In order to do this, the PRL consists of a library that contains several subVIs and some examples of how these might be used in a NI LabVIEW application. To utilize



(a) Front panel containing the different input sections, buttons and display objects.



(b) Block diagram performing calculations on the input, and sending it to the output.

Figure 2.9: An application for adding two numbers, and visualizing the results. The front panel has two input sections accepting a number each, one output section displaying the result, three horizontal slides illustrating the number values, and an additional gauge for displaying the result value. The block diagram performs the addition on the two inputs, and sends each value to its correct display object.

the PRL, the computer must have LabView 2012 installed, and the PRL itself must be run from the "C:\dev\"-folder. A complete documentation of the PRL is given in [Aarstrand, 2013].

An illustrated flow chart for the measurement data is presented in Figure 2.10, as a continuation of the flowchart given for the PMU in Figure 2.6. To the left, the inputs to the PMU are visible, and are transmitted to the PDC, as was described in Section 2.3.2. The measurements are acquired from the PDC by sending commands to the PRL.

The PRL is based on a DLL for efficient data handling, and stores the data in a queue and a buffer. These components are highlighted in green, and the structure they represent, are closed off from direct interference. They are accessible through some *Access Components*, that are highlighted in yellow in the figure, which allows retrieving of data, or sending commands to the PRL. These components can be used in custom NI LabVIEW applications that utilize the PRL functionality.

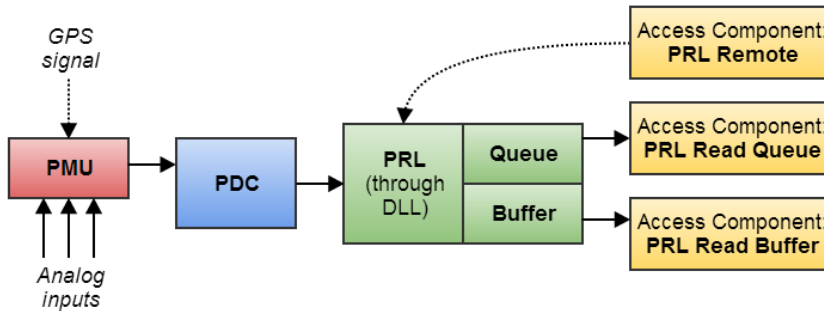


Figure 2.10: A flow chart illustration of the measurement data's path to the user.

The size of the queue and the buffer can be configured through the PRL *Config*-button, which can be seen in Figure 2.11. All the data from the PDC are handled by the DLL, and transferred to the queue and buffer simultaneously, given that the queue is enabled. Otherwise the data is only sent to the buffer. When the queue is enabled, the amount of available data varies due to latency in the application, and the length of the data array is arbitrary. The entire queue content is erased after retrieval, but the buffer is using the principle of FIFO, First-In-First-Out, meaning when the buffer is full, and receives new data, only the oldest data is erased, and the buffer remains full. This behaviour allows for data retrieval in most cases, and the *PRL Read Queue* and *PRL Read Buffer* access components respectively provide the two desired functionalities.

However, before these components can access the stream from the PDC in a custom application, the PRL must be started. This can be done in one of two ways; the PRL application can be run and connected manually, or the *PRL*

*Remote* access component can be used to send the *Run* and *Startup* commands. Figure 2.11 illustrates the PRL application’s screen, which allows for most stream configurations, and provides appropriate amount of information about the received stream.

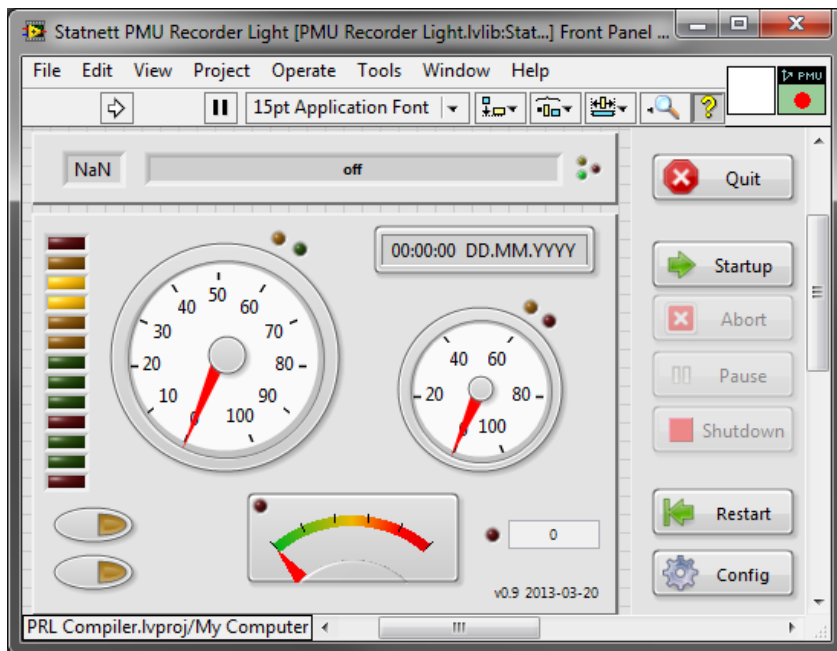


Figure 2.11: A screen shot of the PRL, courtesy of [Aarstrand, 2013, p. 4].

Other important configurations to be made, apart from the queue and buffer sizes, are the parameter inputs described in Section 2.3.4. This, and more, can also be handled by the *Config*-button. The two buttons in the lower left part of Figure 2.11 provide customization options, regarding which PMU signals should be available to the custom application, and which type of signals that are of interest, whether it be the phasors or the frequencies.

### 2.4.3 Custom Application

When a NI LabVIEW application utilizes the PRL functionality, by implementing the access components, it is referred to as a custom application. The components mentioned in Figure 2.10 are illustrated in Figure 2.12, as they appear in a block diagram. Components for other purposes are also included in the PRL library,

such as the *PRL Channel Selector Configuration* illustrated in Figure 2.12(d). Common for all library functions is that they simplify the data stream handling for the custom application developer.

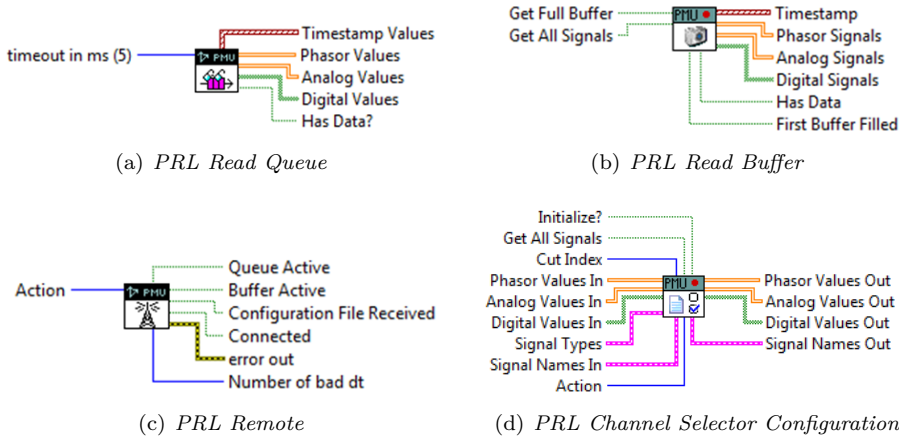


Figure 2.12: *The PRL Read Queue, PRL Read Buffer and PRL Remote access components for usage in a custom NI LabVIEW application that utilizes the PRL functionalities.*

Section 4.3 presents the custom application that was developed for this thesis, visualizing the measurements conducted in the laboratory. A step-by-step approach for developing a similar application, based on the PRL, is outlined below. A block diagram of a custom application template, which follows the described approach, is provided in AppendixA, for the convenience of a potential developer.

1. Send the command **Run** to the *PRL Remote*.
2. Send the command **Startup** to the *PRL Remote*.
3. Send the command **Get Status** to the *PRL Remote*, and wait until both **Configuration File Received** and **Connected** is returned as boolean true.
4. Provide the names, of the chosen signals to acquire, to the *PRL Channel Selector Configuration*, through the input; **Signal Names In**.
5. Use a loop with either the *PRL Read Queue* or the *PRL Read Buffer*, depending on the value of **First Buffer Filled** from the *PRL Read Queue*.

6. During this loop, the PRL control panel can be opened to adjust additional settings by sending the command **Open Panel** to the *PRL Remote*.
7. When the loop is ended, and the custom application is about to terminate, the command **Shutdown** should be sent to the *PRL Remote* to end the connection with the PDC properly.



## References

- Aarstrand, V. H. (2013). *PMU Recorder Light (PRL) - Documentation*. Enfo Technology AS, Lysaker Torg 15 Postbox 374, 3 edition.
- Kosterev, D. and Undrill, J. (2011). *Oscillations in power systems*.
- Machowski, J., Bialek, J. W., and Bumby, J. R. (2012). *Power System Dynamics; Stability and Control*. John Wiley & Sons, Ltd.
- Martin, K., Hamai, D., Adamiak, M., Anderson, S., Begovic, M., Benmouyal, G., Brunello, G., Burger, J., Cai, J. Y., Dickerson, B., Gharpure, V., Kennedy, B., Karlsson, D., Phadke, A., Salj, J., Skendzic, V., Sperr, J., Song, Y., Huntley, C., Kasztenny, B., and Price, E. (2008). Exploring the iee standard c37.118 x2013;2005 synchrophasors for power systems. *Power Delivery, IEEE Transactions on*, 23(4):1805–1811.
- NASPI (2013). North american synchrophasor initiative. Website.
- National Instruments, N. (2014). National instruments. Website.
- Nilsson, J. W. and Riedel, S. A. (2008). *Electric Circuits*. Pearson Education.
- Phadke, A. and Thorp, J. (2008). *Synchronized Phasor Measurements and Their Applications*. Springer US. SN - 9780387765372.
- Saadat, H. (2010). *Power System Analysis*. PSA Publisher.

*REFERENCES*

---

# Chapter 3

## Network Information Systems

As the power production becomes more fluctuating and distributed, and the load characteristics change and increase in magnitude, the need to develop a smarter energy grid for the future has never been greater. A smarter grid involves more measuring devices and more control, which in turn can increase the reliability and optimize both power flow and fault recovery time.

Such a system is referred to as a wide area monitoring system (WAMS). This concept is based on measurement devices strategically installed throughout the power grid. When utilizing PMUs, the provided voltage and current measurements are very accurate. The measurements can then be used to calculate a trustworthy state estimate, that the grid operators can base their operation and mitigation decisions on.

The approach for estimating the current state of the system, is described in Section 3.1, and its many application known to date, based on literature studies, are presented in Section 3.2. The indicators chosen for implementation, in the measurement interface developed in this thesis, are presented in Section 3.3.

### Chapter Contents

---

3.1	Power System State Estimation . . . . .	<b>28</b>
3.2	Synchrophasor Applications . . . . .	<b>31</b>
3.2.1	Background . . . . .	31
3.2.2	Potential . . . . .	31
3.2.3	Pattern Detection . . . . .	33
3.3	System State Visualization Displays . . . . .	<b>39</b>
3.3.1	Phasor Diagram Properties . . . . .	39
3.3.2	System Loadability Limit . . . . .	41

3.3.3	Impedance Stability Index - ISI . . . . .	46
3.3.4	Short-Circuit Capacity Index - $VSI_{SCC}$ . . . . .	47
References	. . . . .	48

---

### 3.1 Power System State Estimation

According to [Machowski et al., 2012, p. 3], a state and its variables can be described as the following:

The system state describes the system’s operating conditions. The state variables are the minimum set of variables  $x_1, x_2, \dots, x_n$  uniquely defining the system state.

This statement results in the relationship presented in Equation 3-1, where  $\mathbf{y}$  is a vector containing the system parameters, and is a function of the state variables,  $\mathbf{x}$ .

$$\mathbf{y} = \mathbf{f}(\mathbf{x}) \tag{3-1}$$

A power system consists of one or more buses, i.e. nodes, and its state is adequately described when the two power flow equations presented in Equation 3-2 and 3-3, have a solution for every node  $i$  in the system:

$$P_i = |U_i| \sum_{j=1}^N |U_j| |Y_{ij}| \cos(\delta_i - \delta_j - \theta_{ij}) \tag{3-2}$$

$$Q_i = |U_i| \sum_{j=1}^N |U_j| |Y_{ij}| \sin(\delta_i - \delta_j - \theta_{ij}) \tag{3-3}$$

Here  $N$  is the total number of nodes in the power system,  $|U_i|$  is the voltage magnitude at bus  $i$ ,  $\delta_i$  is the voltage angle at node  $i$ ,  $|Y_{ij}|$  is the admittance magnitude between node  $i$  and node  $j$ , and  $\theta_{ij}$  is the angle of the admittance between node  $i$  and node  $j$ . This allows for Equation 3-1 to be written as:

$$\begin{aligned} \begin{bmatrix} P_i \\ Q_i \end{bmatrix} &= \mathbf{f}(|\mathbf{U}|, \boldsymbol{\delta}, |\mathbf{Y}|, \boldsymbol{\theta}) \\ &= \mathbf{f}(\vec{\mathbf{U}}, \vec{\mathbf{Y}}) \end{aligned} \tag{3-4}$$

It is assumed that the admittances between each node is known, which entails that the  $2N$  equations contain  $4N$  variables. Since two equations can be solved for two variables, the system state is uniquely defined if two of the following four variables are known for each bus in the system:

$ U_i $	$\delta_i$	$P_i$	$Q_i$
Voltage magnitude at node $i$	Voltage angle at node $i$	Injected active power	Injected reactive power

The two measured variables are thereby the *state variables*, whereas the two others are referred to as *parameters*. They are also known as dependent variables, since they can be calculated based on the state variables and knowledge about the power system topology.

Since Equation 3-2 and 3-3 are non-linear, least-squares calculations must be performed in order to solve them. The resulting expression is the minimum sum of the measurement residuals,  $J(x)$ , as depicted in [Wood and Wollenberg, 1996, p. 472]. This may be expressed as:

$$\min_x J(x) = \sum_{i=1}^{Nm} \frac{[z_i - \mathbf{f}(\mathbf{x})]^2}{\sigma_i^2} \quad (3-5)$$

This formula may have to be calculated several times in order to provide the best solution for the system. Therefore, this type of algorithm, with iterative approach for solving non-linear equations, are dependent on powerful number crunching machines in large server rooms, dedicated to the purpose. The required size will continue to increase proportionally with the increased number of nodes that are measured, which is expected in the future, because the synchrophasor technology is maturing and calls for increased installation scope.

The measurements obtained through PMUs installed throughout the grid, provide both  $|U_i|$  and  $\delta_i$ , more commonly written as  $\vec{U}_i$ , which yield enough information about the power system to calculate a complete overview of its current state. However, this requires pre-knowledge about the system topology, either acquired from possibly outdated manual measurements performed by the grid company itself, or from component data provided by the manufacturer. This will always entail a certain amount of inaccuracy, since both thermal and frequency changes may cause network component data, for both line and transformer impedances, to deviate from the real-time parameter values that are influenced by the effects.

If the PMUs provide more measurements for each node than the  $2N$  already required, for example the current measurement  $I_{ij}$  in the line between node  $i$  and  $j$ , the system admittances can be estimated from Equation 3-6. This allows for more accurate power flow calculations, and creates a hybrid state estimation, where the admittance data is based partly on model data, and partly on measurements.

$$\vec{Y}_{ij} = \frac{\vec{U}_i - \vec{U}_j}{\vec{I}_{ij}} \quad (3-6)$$

With voltage and current measurements performed by PMUs spread across the power grid, the network information systems may grow increasingly accurate, and provide an even better visualization of the current state of the power system. The active power flow in a system is directly influencing many of the planning and operational considerations necessary for a power system, especially in the modern society with high power demands, and strict stability requirements. This is part of the foundation of WAMS, which will be a major component of the smart grids in the future. The impacts of increased accuracy and sample rate for real-time applications, are outlined, and exemplified, in the following section.

## 3.2 Synchrophasor Applications

Even though the utilization of PMU measurements is still partly in its research and development stage, its technology is maturing. Its known applications to date has triggered the production and installation scope shown in Figure 2.7. By installing PMUs i several strategic grid points, the PMU network and its connections to PDCs can influence the stability, control, reliability and overview we have of the grid. In 2009, it was expected that phasor data from synchrophasors would be used for control room decisions, and/or implemented in automated control tools, within a five year time horizon [NASPI, 2009, p. 11]. This reality is closer than ever before, but not yet achieved completely.

### 3.2.1 Background

The technological advances that have made this measurement system possible, are the low cost of high-performance equipment, high-speed measuring devices, customizable communications, and high-volume data storage capabilities. Additionally, the system requires sufficient cyber-security for the data exchange between external, and critical internal, systems. This might be implemented through hardened security buffers, or high-quality data encryption, in order to preserve confidentiality [NASPI, 2009, p. 6, 9].

A PMU is just a device that can perform synchronized phasor measurements. As long as it complies with the requirements listed in [Martin et al., 2008] (a summary is given in Section 2.3.3), it can be referred to as a synchrophasor. Today's digital relays are able to act as a PMU [Chow et al., 2011, p. 3]. They are already performing voltage and current measurements to detect a fault, and contain the hardware needed to act as a synchrophasor. Since these synchrophasors are seen as major part of a future smart grid, and these instruments are already installed on a large scale, it greatly reduces the necessary investment costs for this budget item when it comes to implementing a smart grid.

### 3.2.2 Potential

An example of the difference between the synchrophasor measurements and the signals the grid operators receive today, is shown in Figure 3.1. The SCADA (supervisory control and data acquisition) system does not detect the large voltage drop before the voltage swell, inflicted by a fault-induced delayed voltage recovery event, while the PMU show nearly every detail. The SCADA system also has problems with detecting voltage oscillations, as illustrated in Figure 3.2.

The high resolution and accurate time stamping of the PMU measurements might reveal patterns that indicate transformer saturation, local area oscillations, off-line stabilizers, low damping or imminent equipment failure. The SCADA

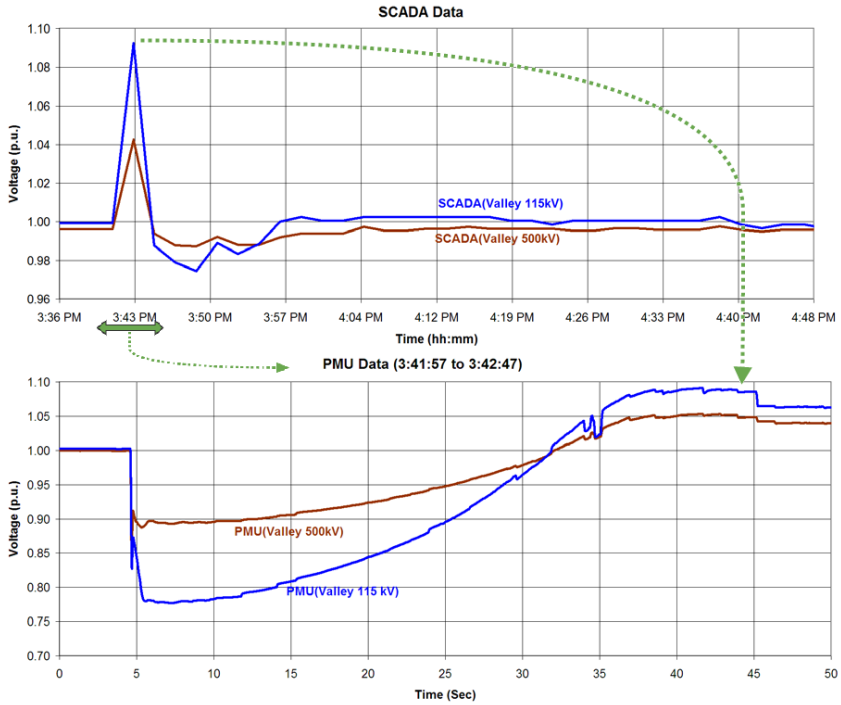


Figure 3.1: *Difference in SCADA and PMU measurements during a fault-induced delayed voltage recovery event, courtesy of [Johnson et al., 2010, p. 5].*

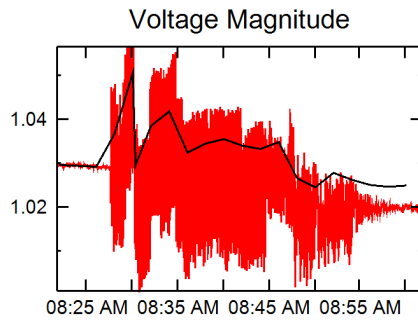


Figure 3.2: *Difference in SCADA (black line) and PMU measurements (red line), during voltage oscillations, courtesy of [White and Chisholm, 2011, p. 21].*



systems used today might not be able to foresee these events, and if they are not identified early enough, the events might have large consequences.

The measurement data can 1) estimate the state of the system, 2) help identify inter-area and local inter-plant modes, 3) provide frequency, voltage and congestion monitoring, and 4) perform actions to protect or control parts of the system. These and additional applications are presented in Table 3.1.

Table 3.1: *Real-time synchrophasor applications, courtesy of [Chow et al., 2011, p. 3] and [NASPI, 2009, p. 3].*

---

<b>Situational awareness</b>	<ul style="list-style-type: none"> <li>• Generating stations (Figure 3.8)</li> <li>• Flowgates and regional transmission interfaces</li> <li>• Separation of islands (Figure 3.3)</li> </ul>
<b>Monitoring</b>	<ul style="list-style-type: none"> <li>• Phasor-data state estimation</li> <li>• Small-signal stability</li> <li>• Voltage stability (Figure 3.1)</li> <li>• Thermal and congestion issues (Figure 3.9)</li> <li>• Event detection and avoidance (Figure 3.5)</li> </ul>
<b>Protection and control</b>	<ul style="list-style-type: none"> <li>• Out-of-step protection</li> <li>• Small-signal stability protection</li> <li>• Long-term stability control</li> <li>• Automated controls (Figure 3.7)</li> <li>• Mode-damping estimates (Figure 3.7)</li> </ul>

---

### 3.2.3 Pattern Detection

The pattern detection that the synchrophasors can provide, will help to identify when to investigate and learn, and when to move to more conservative operations, in time for these mitigations to matter [Bilke, 2011, p. 3-5].

### Voltage Measurements

Patterns, that could be recognised and configured for automated alarm signal to grid operators, include rapidly diverging voltage angles, which might be prior to a system area separation (see Figure 3.3), or a leap in negative sequence current, which might indicate an impending generator failure (see Figure 3.4).

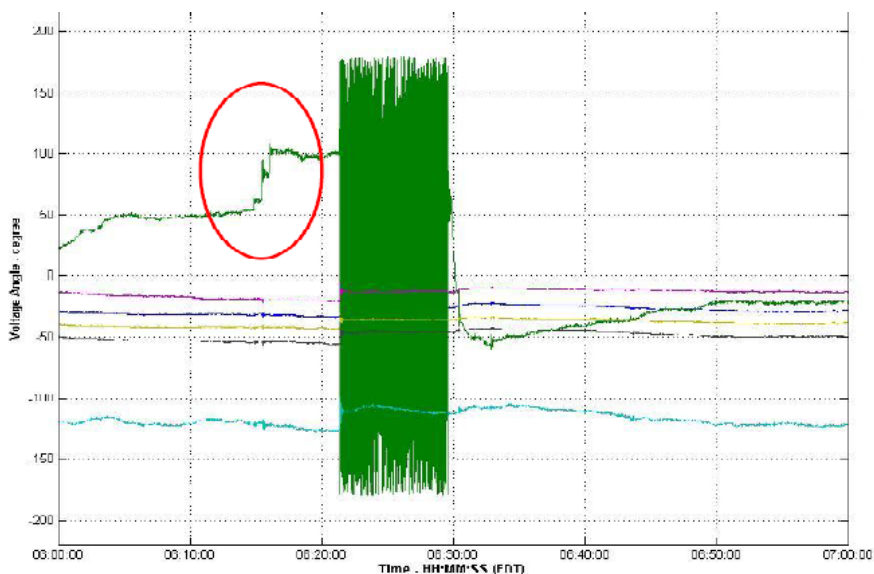


Figure 3.3: *Multiple stressors led to separation, which could be predicted by a noisier path in PMU measured voltage angles five minutes before actual separation. Courtesy of [Bilke, 2011, p. 7].*

### Power Measurements

The voltage measurements can also be used to calculate the power flow between the PMU locations. Figure 3.5 illustrates how the power changed over time as a result of a tripped line. At approximately ten seconds, the line trips and the power flow falls substantially, but the fault does not induce the oscillations. The loss of the tripped line did, however, create an unstable mode of operation, and the rotor angle oscillations built up over time. With the synchrophasor measurements, the severity of the oscillations becomes clear at an early stage, but as illustrated in Figure 3.6, the SCADA measurements could be misinterpreted and lead to wrong, or none, countermeasures being initiated.

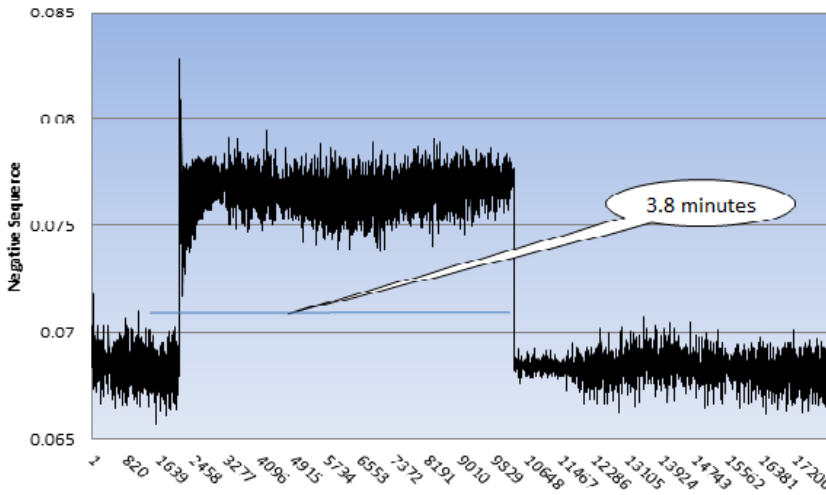


Figure 3.4: Generator failure in Tenaga, Malaysia was detected 3.8 minutes beforehand, through negative sequence current calculations performed by a PMU, located 200 miles away. Courtesy of [Bilke, 2011, p. 9].

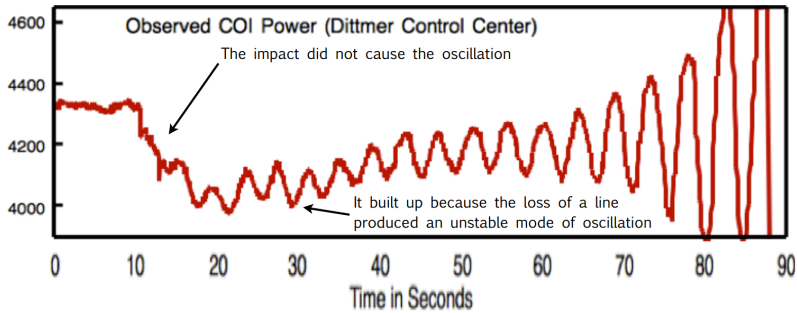


Figure 3.5: A tripped line resulted in an excessive flow on an inter-area transmission path, which created an unstable mode of oscillation, that ultimately led to rotor angle oscillations, and thereby power oscillations. Courtesy of [Kosterev and Undrill, 2011, p. 5].

Not all modes of oscillations are easy to detect with a naked eye, and some automated alarm system, that could provide early warning of potential damping problems from the ambient synchrophasor measurements, would be highly beneficial. A mode meter, as presented in Figure 3.7 could contribute to detecting oscillation modes for local rotor angle motions (in the 1 - 2 Hz range), controller responses (in the 1 - 20 Hz range), shaft torsional motions and subsynchronous oscillations (in the 5 - 40 Hz range), and inter-area power flow oscillations (in the 0.2 - 0.5 Hz range), as shown in Figure 3.5 [Kosterev and Undrill, 2011, p. 3].

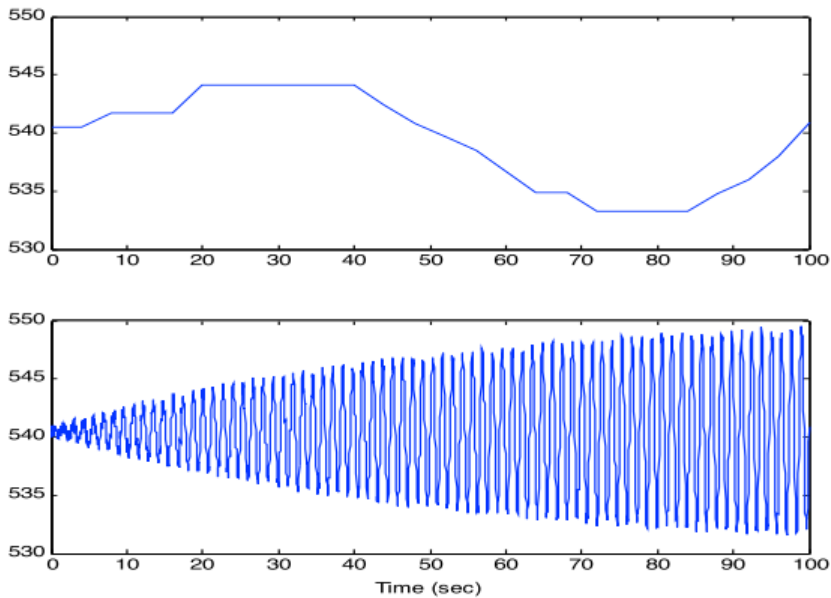


Figure 3.6: *Power oscillation representations with SCADA measurements (upper chart) and with synchrophasor measurements (lower chart), courtesy of [Kosterev and Undrill, 2011, p. 17].*

### Frequency Measurements

As an example of how frequency measurements, and its response pattern, can increase understanding of what type of event is occurring, the performed measurements during a fault on a line segment December 1, 2005 in Norway is presented.

Nordland has a substantial production surplus while Trøndelag consumes more than it produces. A fault on the line segment between these two areas resulted in a disconnection, which separated the frequencies of the two areas,

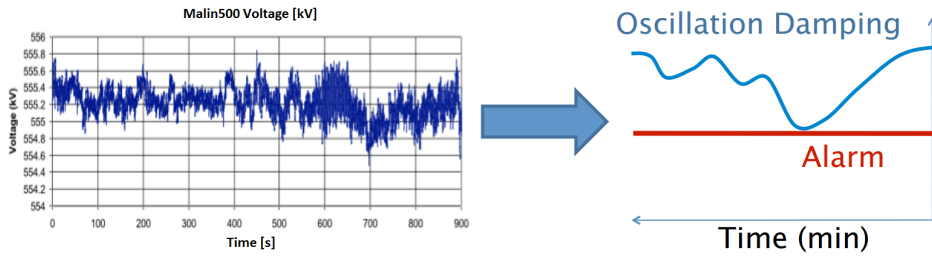


Figure 3.7: A Mode Meter operational tool, extracting early signs of deterioration in oscillation damping from the synchrophasor measurements, courtesy of [Kosterev and Undrill, 2011, p. 20].

as shown in Figure 3.8. The area north of the disconnection, is characterized by small inertia, and at the moment of disconnection the north area frequency is soaring above 53.5 Hz, before some generators shut down, and the frequency drops to  $\sim 51$  Hz, before gradually approaching 50 Hz.

The southern area has a larger inertia and reacts slower to the sudden production deficit. Figure 3.8 shows that the frequency drops to  $\sim 49.25$  Hz after a small delay. This normalizes rapidly, as the power over the Hasle corridor from southern Norway to Sweden, increases substantially, as illustrated by Figure 3.9. The power flowed through Sweden, because of the weak internal grid connections between the southern and northern part of Norway.

The power transfer is usually at 2 200 MW, but during this event, it exceeded this value for about ten minutes. Exceeding the limit for this amount of time should not be possible, due to a number of protection devices set to disconnect in the event of a too high power transfer. Because of the lack of disconnections, and the short duration of exceeding the power transfer limit, this event did not result in major impacts on the system, and normalized within a reasonable amount of time. With synchrophasor measurements, this situation could have been monitored closely and the need for countermeasures evaluated continuously.

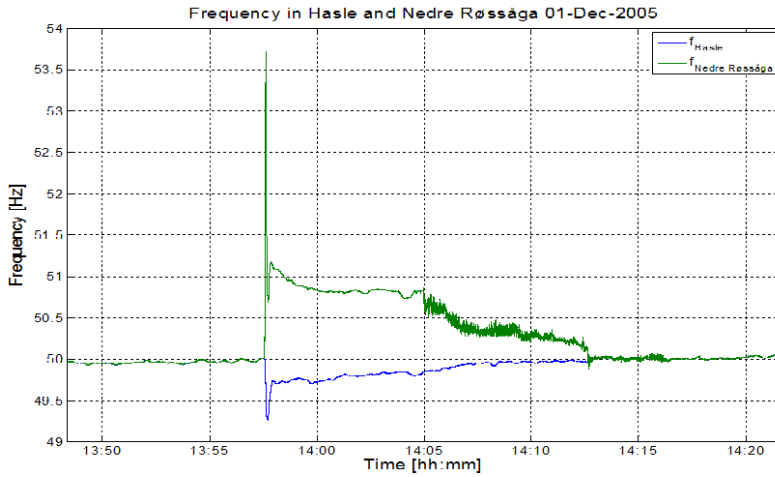


Figure 3.8: The frequency in Nedre Røssåga and Hasle in Norway, representing the north and south area of the line disconnection. Courtesy of [Uhlen, 2013, p. 21].

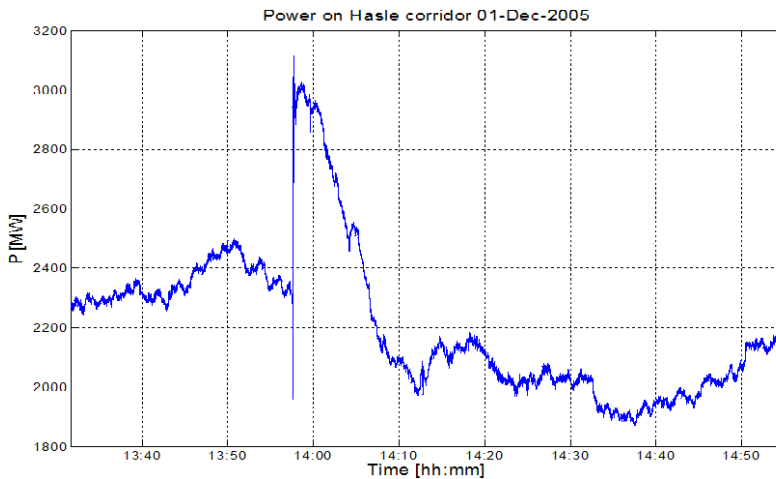


Figure 3.9: The power transfer in Hasle from southern Norway to Sweden during a line disconnection between Trøndelag and Nordland, courtesy of [Uhlen, 2013, p. 18].

### 3.3 System State Visualization Displays

The voltage stability of a power system is defined by the system's ability to regain an equilibrium state after being subjected to a physical disturbance, based on its nodal voltage magnitude [Machowski et al., 2012, p. 9]. There are a variety of stability indices proposed throughout the literature, with varying success of providing a reliable estimate of the distance to a voltage collapse.

One of the main aspects of this thesis is to develop a reasonable accurate network information system, based on state estimation of a specific power system. A visualization of the voltage phasors, current phasors, and voltage drops across the system, would increase the grid operators' understanding of the current state of the system, and an estimation of the voltage-power characteristics might assist them even further. The Impedance Stability Index (ISI) and the Short-Circuit Capacity Index ( $VSI_{SCC}$ ) proposed by Storvann in his thesis, will be implemented in the measurement interface. Those indices are sufficiently reliable, and complements each other, according to [Storvann, 2012, p. 117];

A combination of the indicators ISI and  $VSI_{SCC}$  will give a reasonable, slightly conservative measure of the voltage stability of the system, where  $VSI_{SCC}$  is used to estimate the distance to the maximum power transfer level and ISI determines whether the system is on the stable upper half of the PV curve or not.

First, the basis of the phasor diagram will be outlined in Section 3.3.1. Second, the voltage-power characteristics will be estimated in Section 3.3.2, and last, the theory behind the ISI and  $VSI_{SCC}$  will be detailed in Section 3.3.3 and 3.3.4.

#### 3.3.1 Phasor Diagram Properties

It is known from fundamental electric circuit theory, that the voltage supplied by the source is equal to the voltage drop across the entire circuit. When this principle is applied to the electric circuit illustrated in Figure 3.10, the resulting relationship is depicted in Equation 3-7, where  $\vec{U}_{sys}$  represents the voltage drop across the system. Additionally by inserting Ohm's Law,  $\vec{U} = \vec{Z}\vec{I}$ , the equivalent relationship displayed in Equation 3-8 can be achieved.

$$\vec{E}_{Th} = \vec{U}_{sys} + \vec{U}_{load} \quad (3-7)$$

$$= (R_{sys} + jX_{sys})\vec{I} + (R_{load} + jX_{load})\vec{I} \quad (3-8)$$

Usually, the voltage source and load voltage are measured, because they are relative to the ground potential, and the voltage drop is an unknown system

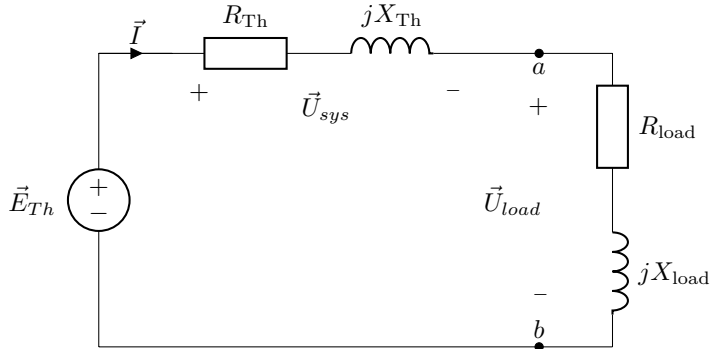


Figure 3.10: *Thévenin equivalent for a system referenced from the terminals of the load.*

parameter. However, the latter voltage can easily be calculated if rearranging Equation 3-7. If these phasors are plotted relative to each other, with respect to real and imaginary values, the impedance ratios inherent in the system, become apparent.

An example of a phasor diagram, is illustrated in Figure 3.11, where the load voltage has been chosen as the reference voltage. The voltage drop phasor  $\vec{U}_{sys}$ , decomposed with respect to its resistive and inductive components, is indicated along with the current phasor. As the figure shows, the resistive voltage drop is parallel to the current, while the reactive voltage drop is orthogonal to the current.

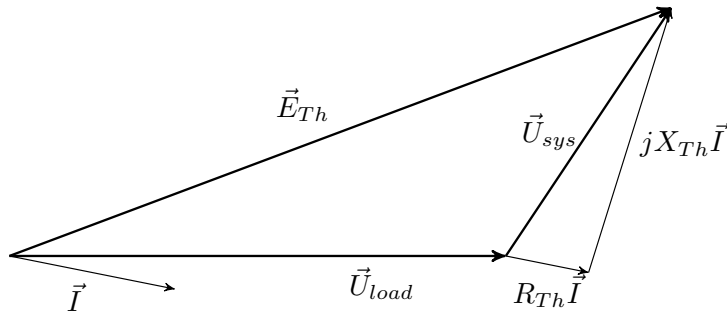


Figure 3.11: *Phasor diagram of the Thévenin equivalent figure, with exemplified impedance ratio.*



### 3.3.2 System Loadability Limit

The total power can either be calculated as a three-phase power, by utilizing line voltage and current (denoted with  $3p$  and  $LL$  respectively in Equation 3-11), or as single-phase, when using phase voltage and current (denoted with  $1p$  and  $\phi$  in Equation 3-10). The three-phase power system may also be represented in a line diagram, in which all voltages and powers will be given in single-phase, thereby giving the single-phase power (Equation 3-9) [Nilsson and Riedel, 2008, p. 403, 447].

$$\vec{S}_{1p} = \vec{U}_\phi \vec{I}^* \quad (3-9)$$

$$\begin{aligned} \vec{S}_{3p} &= 3\vec{S}_{1p} \\ &= 3\vec{U}_\phi \vec{I}^* \end{aligned} \quad (3-10)$$

$$= \sqrt{3}\vec{U}_{LL} \vec{I}^* \quad (3-11)$$

#### 3.3.2.1 Maximum Power Transfer

To be able to estimate the maximum active power that can be delivered to a load, we need to establish a Thévenin equivalent for the system, as seen from the terminals of the load. This will be a single-phase diagram, where all entities will be given as phase quantities. Assuming this has already been achieved (for example by utilizing the source transformation, the node-voltage, or the mesh-current method, as described in [Nilsson and Riedel, 2008, p. 355-361]), we use Figure 3.10 as the starting point.

If we express the voltage source, chosen as the reference voltage with  $\angle 0^\circ$ , and the system and load impedances as complex numbers, we have:

$$\begin{aligned} \vec{E}_{Th} &= |E_{Th}| + j0 \\ \vec{Z}_{Th} &= R_{Th} + jX_{Th} \\ \vec{Z}_{load} &= R_{load} + jX_{load} \end{aligned}$$

In order to calculate the active power delivered to the load, we need either the load voltage or the current. To acquire the current flowing from the Thévenin voltage source to the load, we utilize Ohm's law, and solve for the current:

$$\begin{aligned} \vec{I} &= \frac{\vec{E}_{Th}}{\vec{Z}_{Th} + \vec{Z}_{load}} \\ &= \frac{\vec{E}_{Th}}{(R_{Th} + R_{load}) + j(X_{Th} + X_{load})} \end{aligned} \quad (3-12)$$

By utilizing Ohm's law for the voltage in Equation 3-9 and realizing that a vector multiplied with its complex conjugate is equal to the square of its absolute magnitude, we get the active power consumed by the load:

$$\begin{aligned}
 S_{load} &= \vec{U}_{load} \vec{I}^* \\
 &= \vec{Z}_{load} \vec{I} \vec{I}^* \\
 &= \vec{Z}_{load} |I|^2 \\
 \Re\{S_{load}\} &= \Re\{\vec{Z}_{load}\} |I|^2 \\
 P_{load} &= R_{load} |I|^2
 \end{aligned} \tag{3-13}$$

If inserting the current found in Equation 3-12 into the power expression derived in Equation 3-13, we get the active power consumed by the load, as a function of Thévenin voltage, and system and load impedance:

$$P = \frac{R_{load} |E_{Th}|^2}{(R_{Th} + R_{load})^2 + (X_{Th} + X_{load})^2} \tag{3-14}$$

In order to discern which values of  $R_{load}$  and  $X_{load}$  lead to the maximum power dispatch, the expression in Equation 3-14 must be partial differentiated with respect to the load resistance and reactance.

$$\frac{\partial P}{\partial X_{load}} = \frac{-2R_{load}(X_{Th} + X_{load})|E_{Th}|^2}{[(R_{Th} + R_{load})^2 + (X_{Th} + X_{load})^2]^2} \tag{3-15}$$

$$\frac{\partial P}{\partial R_{load}} = \frac{[(R_{Th} + R_{load})^2 + (X_{Th} + X_{load})^2 - 2R_{load}(R_{Th} + R_{load})]|E_{Th}|^2}{[(R_{Th} + R_{load})^2 + (X_{Th} + X_{load})^2]^2} \tag{3-16}$$

The maximum dispatch is found when Equation 3-15 and Equation 3-16 are both equal to zero. All parts of the two denominators are squared, thereby eliminating the possibility of an infinitely high dispatch. The expressions are zero when the numerators are zero, which results in:

$$\begin{aligned}
 -2R_{load}(X_{Th} + X_{load})|E_{Th}|^2 &= 0 \\
 (X_{Th} + X_{load}) &= 0 \\
 X_{load} &= -X_{Th}
 \end{aligned} \tag{3-17}$$

$$\begin{aligned}
 [(R_{Th} + R_{load})^2 + (X_{Th} + X_{load})^2 - 2R_{load}(R_{Th} + R_{load})]|E_{Th}|^2 &= 0 \\
 (R_{Th} + R_{load})^2 + (X_{Th} + X_{load})^2 - 2R_{load}(R_{Th} + R_{load}) &= 0 \\
 (R_{Th}^2 + 2R_{Th}R_{load} + R_{load}^2) + (X_{Th} + X_{load})^2 - 2R_{Th}R_{load} - 2R_{load}^2 &= 0 \\
 -R_{load}^2 + R_{Th}^2 + (X_{Th} + X_{load})^2 &= 0
 \end{aligned}$$

Solving for  $R_{load}$ , we get:

$$R_{load} = \sqrt{R_{Th}^2 + (X_{Th} + X_{load})^2} \quad (3-18)$$

When inserting Equation 3-17 into Equation 3-18, we get that  $R_{load} = R_{Th}$  when both Equation 3-15 and Equation 3-16 is zero. Evidently, this indicates that the maximum power transfer occurs when:

$$\vec{Z}_{load} = \vec{Z}_{Th}^* = R_{Th} - jX_{Th} \quad (3-19)$$

Provided that these values are within the variable limits of the load. The resulting power can be calculated by inserting Equation 3-19 into Equation 3-14, which results in:

$$\begin{aligned} P_{max} &= \frac{R_{Th}|E_{Th}|^2}{(R_{Th} + R_{Th})^2 + (X_{Th} + (-X_{Th}))^2} \\ &= \frac{R_{Th}|E_{Th}|^2}{4R_{Th}^2 + 0} \\ &= \frac{|E_{Th}|^2}{4R_{Th}} \end{aligned} \quad (3-20)$$

In cases where the maximum power transfer impedance in Equation 3-19 exceeds the maximum load resistance or reactance, first adjust  $X_{load} \rightarrow -X_{Th}$ , then adjust  $R_{load} \rightarrow \sqrt{R_{Th}^2 + (X_{Th} + X_{load})^2}$  to achieve an active power as close to the maximum power transfer limit as possible [Nilsson and Riedel, 2008, p. 410-413].

### 3.3.2.2 Establishing Voltage-Power Characteristics

The parameters utilized in the previous sections are not always known, as they may change over time. To establish the voltage-power characteristics of a system, it is possible to force the system into a state with an almost unstable voltage. However, in an actual power system, with real suppliers and consumers, such an approach would lead to high losses and decreased reliability and credibility. Therefore, the more economic solution would be to estimate it, based on known parameters.

The power voltage characteristics can be based on the measured supply and load voltage, together with the total current flowing through the system, during the current state of the system. The parameters are assumed measured, and thereby known in the following estimation. They are labelled as  $\vec{U}_{gen}$ ,  $\vec{U}_{load}$  and  $\vec{I}$ , corresponding to the parameters illustrated in Figure 3.10, where  $\vec{U}_{gen}$  equals  $\vec{E}_{Th}$ , and  $\vec{Z}_{sys}$  equals  $\vec{Z}_{Th}$ .

Since the system and load impedance is initially unknown, but the respective voltages and current is known, they can be calculated. The system impedance is given by Equation 3-21, when inserting the calculated phasors from the performed measurements.

$$\vec{Z}_{sys} = \frac{\vec{U}_{gen} - \vec{U}_{load}}{\vec{I}} = R_{sys} + jX_{sys} \quad (3-21)$$

The system impedance in the current state, is then assumed to be constant, and independent of the load voltage in the system. When the load voltage is declared as the variable of the equations, the imaginary part of the current flowing through the system is given by Equation 3-22. The current is then conjugated, before being multiplied with the load voltage, in order to calculate the apparent power (Equation 3-9). The active power consumed by the load, being the real part of the before-mentioned calculation, is acquired from Equation 3-23.

$$I(u) = \frac{|U_{gen}| - u}{X_{sys}} \quad (3-22)$$

$$\begin{aligned} P_{load}(u) &= I(u) \cdot u \\ &= \left( \frac{|U_{gen}| - u}{X_{sys}} \right) \cdot u \end{aligned} \quad (3-23)$$

The values of  $u$  between  $|\vec{U}_{gen}|$  and 0 can then established with equal length between the values, and the load power can be calculated. This has been performed i Matlab to illustrate the resulting voltage-power characteristic, and is illustrated in Figure 3.12 as the line called "Best Estimate". Some alternative methods of estimating the voltage-power characteristics are included in the figure, but the one presented in this section performed the best for different sample inputs. The Matlab calculations are documented in Appendix B.

The method described above can not be applied if the supply voltage is unknown, since the exact calculation of the system impedance depends on it. However, the system impedance can be estimated from two consecutive load voltage and current measurements. For the estimation approach, see [Storvann, 2012, p. 26-27].

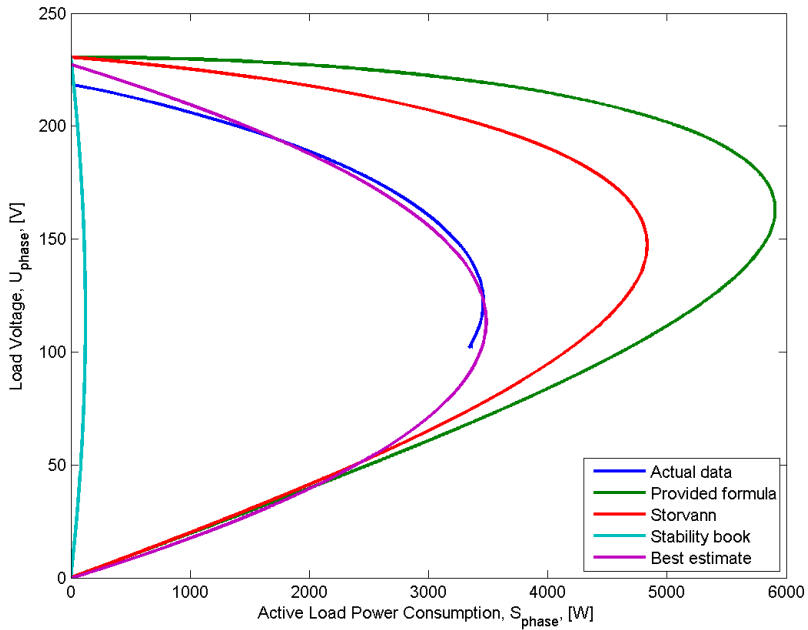


Figure 3.12: Voltage-power characteristic estimations based on a single measurement sample containing generator voltage, load voltage, and current. Actual data stems from simulated voltage-power characteristic of the power system utilized in this thesis, while the other curves are different algorithms for trying to estimate the characteristic.

### 3.3.3 Impedance Stability Index - ISI

As mentioned in Section 3.3.2, the load receives maximum power when  $|\vec{Z}_{load}| = |\vec{Z}_{sys}|$ . As long as  $|\vec{Z}_{load}| > |\vec{Z}_{sys}|$ , the system's voltages are stable, if assuming normal operating conditions (see Figure 3.13 for illustration). The ISI is based on this principle, and is defined as displayed in Equation 3-24, according to [Storvann, 2012, p. 26].

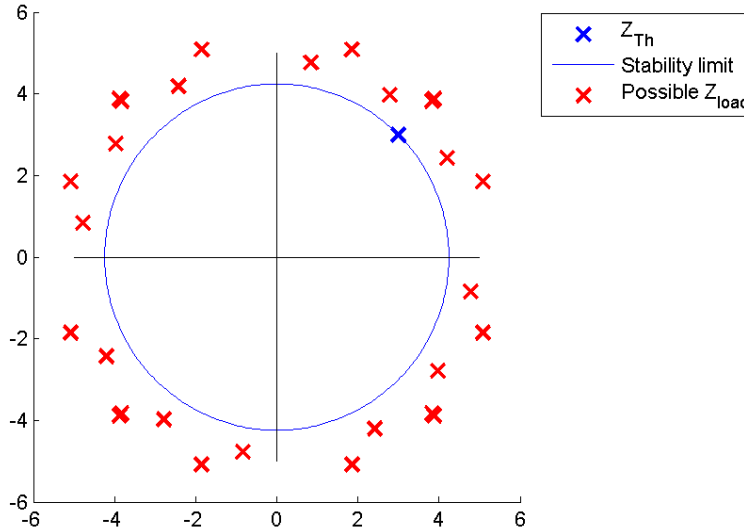


Figure 3.13: *The relationship between the system impedance, the load impedance, and thus the voltage stability limit, based on  $|Z_{load}| \geq |Z_{Th}|$ .*

$$ISI = \frac{|\vec{Z}_{sys}|}{|\vec{Z}_{load}|} \leq 1 \quad (3-24)$$

The load voltage and current must be measured in order for the estimation of the ISI to be possible. These measurements are used directly to calculate the load impedance,  $\vec{Z}_{load}$ , as indicated in Equation 3-25.

$$\vec{Z}_{load} = \frac{\vec{U}_{load}}{\vec{I}} \quad (3-25)$$

The system impedance is acquired through either calculation or estimation, as described in the previous section. Since this thesis concerns a power system set-up

with a single generator and a single load, where the voltages are measured at each end, as well as the current flowing through the system, the system impedance are calculated with the formula presented in Equation 3-21.

### 3.3.4 Short-Circuit Capacity Index - $VSI_{SCC}$

The  $VSI_{SCC}$  also bases its criteria on maximum power flow, by comparing the actual short-circuit capacity of the system with the minimum short-circuit capacity that is required to supply the load [Storvann, 2012, p. 28]. The actual short-circuit capacity should be larger than the minimum short-circuit capacity,  $SCC_{actual} > SCC_{minimum}$ , which results in the voltage stability criteria displayed in Equation 3-26.

$$VSI_{SCC} = \frac{SCC_{minimum}}{SCC_{actual}} \leq 1 \quad (3-26)$$

The actual short-circuit capacity is obtained by applying Equation 3-27 to the measured values of the current system state.

$$SCC_{actual} = \frac{|\vec{U}_{gen}|}{X_{sys}} \quad (3-27)$$

The minimum short-circuit capacity is more demanding to calculate, and assumes the parameters to be equal the maximum power flow conditions. Since the approach for finding maximum power flow in this thesis deviates from the method utilized in [Storvann, 2012], and this voltage stability indicator is of minor importance, the formula derived in [Storvann, 2012, p. 28] is simply presented in Equation 3-28.

$$SCC_{minimum} = \frac{2S_L(1 + \sin \phi)}{|\vec{U}_{sys}|} \quad (3-28)$$

Here,  $S_L$  is defined as the total apparent power transferred when the system reaches its loadability limit,  $\phi$  is the load power factor at the loadability limit, and  $\vec{U}_{sys}$  is the generator voltage measured in the current state.

## References

- Bilke, T. (2011). Naspi update to the nerc operating committee.
- Chow, J. H., Beard, L., Patel, M., Quinn, P., Silverstein, A., Sobajic, D., and Vanfretti, L. (2011). Guidelines for siting phasor measurement units.
- Johnson, A., Bravo, R., and Robles, S. (2010). Operating the grid better with phasor data –understanding fidvr.
- Kosterev, D. and Undrill, J. (2011). Oscillations in power systems.
- Machowski, J., Bialek, J. W., and Bumby, J. R. (2012). *Power System Dynamics; Stability and Control*. John Wiley & Sons, Ltd.
- Martin, K., Hamai, D., Adamiak, M., Anderson, S., Begovic, M., Benmouyal, G., Brunello, G., Burger, J., Cai, J. Y., Dickerson, B., Gharpure, V., Kennedy, B., Karlsson, D., Phadke, A., Salj, J., Skendzic, V., Sperr, J., Song, Y., Huntley, C., Kasztenny, B., and Price, E. (2008). Exploring the ieee standard c37.118 x2013;2005 synchrophasors for power systems. *Power Delivery, IEEE Transactions on*, 23(4):1805–1811.
- NASPI (2009). Synchrophasors and security.
- NASPI (2013). North american synchrophasor initiative. Website.
- Nilsson, J. W. and Riedel, S. A. (2008). *Electric Circuits*. Pearson Education.
- Storvann, V. (2012). Maintaining voltage stability - an analysis of voltage stability indicators and mitigating actions. Master’s thesis, Norwegian University of Science and Technology.
- Uhlen, K. (2013). Wide area monitoring and control systems (WAMS/WACS). Lecture notes.
- White, A. D. and Chisholm, S. E. (2011). Synchrophasor use at OG&E.
- Wood, A. J. and Wollenberg, B. F. (1996). *Power Generation, Operation, and Control*. John Wiley & Sons, Ltd, 2nd edition.



# Chapter 4

## Power System Set-Up Description

The laboratory environment and stationary components, will be presented in Section 4.1. The PMU and PDC utilized for the experiments in this thesis, are documented in Section 4.2. Section 4.3 will outline the various parts constituting the developed measurement interface, clarify the assumptions made in the development process, and provide some examples of possible measurement interface displays. A simulation model of the laboratory is presented in Section 4.4, where the model parameters are calculated.

### Chapter Contents

---

4.1	Stationary Laboratory Components . . . . .	<b>50</b>
4.1.1	Generator . . . . .	52
4.1.2	Line Section . . . . .	52
4.1.3	Substation Unit . . . . .	54
4.1.4	Load Bus . . . . .	54
4.2	Laboratory Measurement Device . . . . .	<b>56</b>
4.2.1	PMU hardware: CompactRIO . . . . .	56
4.2.2	PDC Software: Synchrowave . . . . .	58
4.3	Measurement Interface . . . . .	<b>59</b>
4.3.1	Required Tools and Input Assumptions . . . . .	59
4.3.2	Interface Components . . . . .	61
4.3.3	Examples of Possible Measurement Interfaces . . . . .	74
4.4	Simulation Model in PowerFactory . . . . .	<b>76</b>
	References . . . . .	<b>78</b>

---

## 4.1 Stationary Laboratory Components

Both the simulation model, and the measurement interface assumptions, are based on the distribution network model of the Renewable Energy Laboratory at NTNU, also known as the Smart-Grids Laboratory, which is presented in Appendix C. The laboratory set-up will include the 17 kVA synchronous generator unit, the flexible line equivalent, the substation unit, and a variable load that will be connected at the terminal at the opposite side of the transformer. The *Local grid 1*-bus will be disconnected from the Main bus, and the system will be run isolated from the main grid.

The resulting connections and components of the power system in the laboratory, are presented in Figure 4.1, with normal switching states displayed in Table 4.1.

Table 4.1: *Initial switch states in the laboratory set-up illustrated in Figure 4.1.*

Connection type	Switch label	Switch state
Connection to main grid	S1	Disconnected
Transformer connections	S2, S4	Conducting
	S3	Disconnected
Line equivalent connections	S5, S6	Disconnected
	S7, S8, S9, S10	Conducting
Generator connection	S11	Conducting

Switch states	Switch labels referred to Figure 4.1										
Open	S1	S3	S5	S6							
Closed		S2	S4		S7	S8	S9	S10	S11		

The reference voltage magnitude is chosen to be 400 V, equal to the nominal line-voltage of both generator and transformer, and the reference power will be equal to the three-phase generator rating, 17 kVA. When utilizing the equations for power calculation and Ohm's law, they result in the base value for both the current calculated in Equation 4-1, and the impedance in Equation 4-2. Optionally, the calculations could have been performed with single-phase power and phase-voltage as reference values, which would have given the same results for  $I_{\text{base}}$  and  $Z_{\text{base}}$ . The resulting base values, utilized in the rest of this thesis, are summarized in Table 4.2.

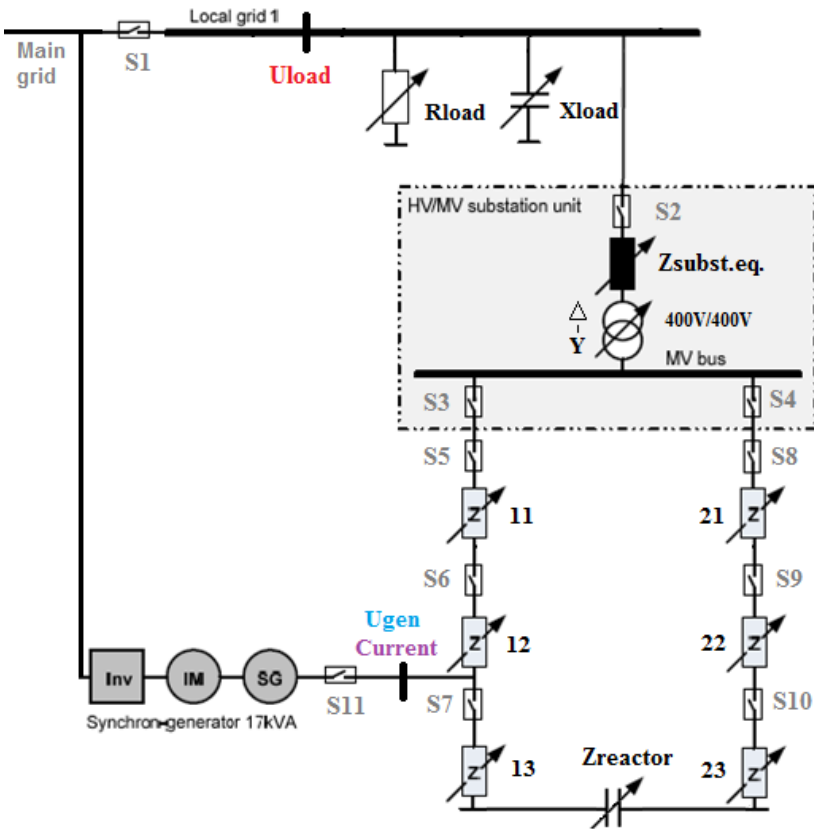


Figure 4.1: A part of the laboratory layout from Appendix C, with irrelevant components removed and the important measurement points and labels included.

$$\begin{aligned}
 S_{\text{base},3\text{p}} &= \sqrt{3}U_{\text{base,LL}}I_{\text{base}} & U_{\text{base,LL}} &= \sqrt{3}Z_{\text{base}}I_{\text{base}} \\
 \Downarrow & & \Downarrow & \\
 I_{\text{base}} &= \frac{S_{\text{base},3\text{p}}}{\sqrt{3}V_{\text{base,LL}}} & Z_{\text{base}} &= \frac{U_{\text{base,LL}}}{\sqrt{3}I_{\text{base}}} \\
 &= \frac{17000 \text{ [VA]}}{\sqrt{3} \cdot 400 \text{ [V]}} & &= \frac{400 \text{ [V]}}{\sqrt{3} \cdot 24.54 \text{ [A]}} \\
 &= \underline{\underline{24.54 \text{ [A]}}} & (4-1) & \quad \quad \quad \underline{\underline{9.41 \text{ [\Omega]}}} & (4-2)
 \end{aligned}$$

Table 4.2: *Base values for calculating pu representations of parameters.*

$$\begin{array}{ll}
 S_{\text{base},3\text{p}} = 17 \text{ kVA} & I_{\text{base}} = 24.54 \text{ A} \\
 U_{\text{base,LL}} = 400 \text{ V} & Z_{\text{base}} = 9.41 \text{ \Omega}
 \end{array}$$

### 4.1.1 Generator

The synchronous generator in the laboratory, models a downscaled version of a small hydropower plant. It generates power from the rotational energy provided by a motor connected to the main grid, as indicated in Figure 4.1. As previously stated, it has a power rating of 17 kVA, and the rest of the parameters significant for this thesis, are displayed in Table 4.3. It is regulated by an automatic voltage regulator (AVR), and the goal of the AVR is to maintain the generator’s terminal voltage at a specified magnitude [Saadat, 2010, p. 594]. It adjusts the terminal voltage of the generator by producing or consuming appropriate amounts of reactive power, and therefore plays an important part of the voltage-power characteristics of the system.

The accessible measurement points are the line-voltages between each phase, and the currents (M1 in Figure 4.2). As only the line-voltages are provided, the measured phasor must be converted into the equivalent phase-voltage, according to the theory detailed in Section 2.2.1, in either [V] or [pu], in order to simplify further calculations of system parameters.

### 4.1.2 Line Section

The flexible line equivalent in the lab is composed of two current paths connected in parallel, where both are connected to the generator terminals at one end, and the two transformer feeders in the other. Each branch consists of several reactors in series (sections 11, 12, 13, 21, 22 and 23 as illustrated in Figure 4.1).

Table 4.3: *Synchronous generator data, courtesy of [Loen, 2014, p. 27].*

Parameters	Values (at 50 Hz)
Serial number	MW25667 10/09
IO class	IP-23
Ambient temperature	40 °C
Rated apparent power	17 kVA
Rated current	24.5 A
Rated voltage	400 V
Rated frequency	50 Hz
Rated power factor	0.8
Number of poles	4
Nominal rotational speed	1500 rpm
Inertia	0.109 kgm <sup>2</sup>

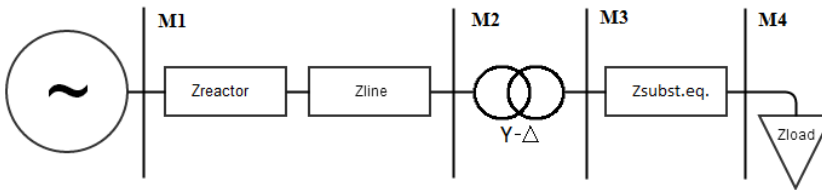


Figure 4.2: *Equivalent line diagram of the power system that is to be studied.*

These individual coils can be bypassed or included, by adjusting the appropriate switches, and thereby changing both the resistance and reactance of the line equivalent. The flexible line equivalent is modelled as a single line impedance,  $Z_{\text{line}}$  in Figure 4.2, in order to simplify the model.

To allow study of the power-voltage characteristics of the system, the load impedance needs to be smaller than the system impedance supplying the load, as stated in Section 3.3.2.2. A variable three-phase reactor,  $Z_{\text{reactor}}$ , may be connected between line-sections 13 and 23, as indicated in Figure 4.1, in order to increase the system impedance, if needed.

### 4.1.3 Substation Unit

The substation unit in the power system set-up, consists of:

- A bus combining the two branches of the flexible line equivalent.
- The 400 V/400 V (line-voltage) Y- $\Delta$ -transformer.
- Another line equivalent, representing the line to the substation in an actual power system, is added, labelled with the impedance  $Z_{\text{subst.eq.}}$ .

There are two measurement locations on the substation unit. M2 is located at the *MV bus* (see Figure 4.1), and M3 between the transformer and the substation line equivalent (see Figure 4.2). The phase-voltages and currents are available for measurements on all phases, in both locations.

Since the transformer is Y- $\Delta$ -connected, it introduces a phase-shift between the two measurement locations, for both the voltage and the current. The connection would also lead to magnitude differences, if the winding ratio of the transformer sides had been equal, but in this case, the ratio is  $a = \sqrt{3}$ , to eliminate this difference from Equation 2-13. The phase-shift can be taken into account by performing a conversion from the side of the measurement to the reference side. In this set-up, the generator side of the transformer is chosen as the reference side, and only measurements performed on locations beyond the  $\Delta$ -side of the transformer must be converted. Section 2.2.2 describes the necessary measures for the conversion.

### 4.1.4 Load Bus

The variable resistive load  $R_{\text{load}}$ , and the variable reactive capacitor  $X_{\text{load}}$ , are connected to the *Local grid 1*-bus, which is supplied by the substation unit.  $X_{\text{load}}$  will not be modified in any way during the laboratory tests, but must be taken into account during the development of both the measurement interface

(Section 4.3), and the simulation model (Section 4.4). These are combined into  $\vec{Z}_{load} = R_{load} + jX_{load}$  in Figure 4.2.

The measurement location M4, is located on the *Local grid 1*-bus. It provides access to the three line-voltages, and the currents flowing through each of the feeders connected to the bus. The currents measured at this point, will be either  $\vec{I}_{R_{load}}$ , or  $\vec{I}_{X_{load}}$ . Since the number of input sockets of the measurement device (detailed in Section 4.2.1) is limited, and the required current measurement is of the current flowing through the entire test system, M4 is unsuited to provide the current measurement. For the voltage measurement, both the line-to-phase-voltage-conversion and the  $\Delta$ -to- $Y$ -transformer-conversion are required when utilizing this measurement location.

It is appropriate to measure the voltage at the generator terminals (M1) and at the load terminals (M4). Because of the system topology with one source and one sink, the measurement location of the current is of less importance, but is chosen to be measured at M1. The chosen measurement points for the PMU connections are listed below:

- M1, Generator voltage,  $U_{gen}$ : Line-voltage output at generator control panel.
- M4, Load voltage,  $U_{load}$ : Line-voltage output at local grid 1 connection panel.
- M1, Current,  $I$ : Current at the generator control panel.

## 4.2 Laboratory Measurement Device

A PMU was utilized as the measurement device during the experiments, and it consists of both hardware and software. Their properties are outlined below, before describing the tests that will be performed in the laboratory.

### 4.2.1 PMU hardware: CompactRIO

The CompactRIO (cRIO) is a programmable hardware for the programming language NI LabVIEW, which was developed by National Instruments. This language specializes in creating *virtual instruments*, and can emulate many kinds of measurements, and use them to exercise control in a system. It is a graphical language, with building blocks, structures and *wires*, that represents functions, loops and variables of textual languages.

The hardware of the cRIO consists of three main components according to [National Instruments, 2011, p. 1-6]:

- The chassis that contains the other elements (NI 9076)
- Real-Time Controller and FPGA
- In/Out Modules

The *In modules* are acquiring the measurements, such as voltages, currents, temperatures, motions, resistances, GPS signals, or sounds (microphones). These modules can be installed independently of each other, and then have the cRIO reprogrammed to take these measurements into account. The controller possesses the ability to stream the output from the program to a receiver/PDC, through Ethernet or other methods, and thereby allowing human or automatic reaction to the measurements.

The In/Out Modules are directly connected to the field-programmable gate array (FPGA). The FPGA component in general is an integrated circuit that contains programmable logic, which can be modified by languages such as Verilog or VHDL [National Instruments, 2013, p. 1]. Any code in the NI LabVIEW language can be compiled to a format suitable for FPGA, which greatly simplifies the development while still being very configurable, since Verilog and VHDL are complicated languages, both to learn, and to write, sufficiently. Additionally, the LabVIEW library already contains many pre-made examples, which simplifies the connection process to the cRIO even further.

The Real-Time Controller is connected to the FPGA through a high speed PCI bus, which transfers great amounts of pre-processed measurement data to process it further, according to the directions given by the custom application,



## CompactRIO Programming Model

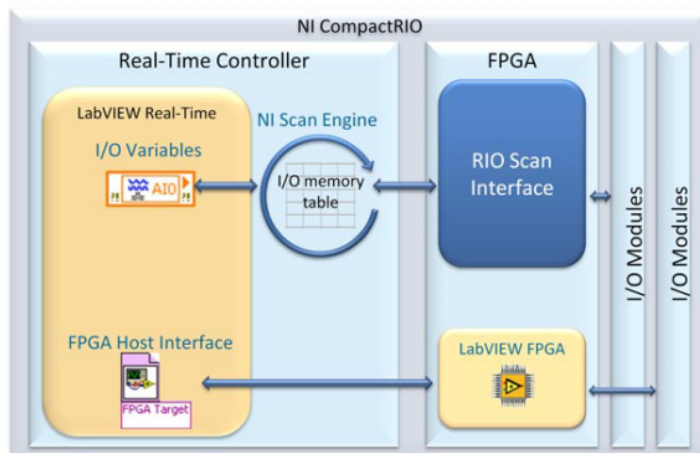


Figure 4.3: *CompactRIO Programming Model*, courtesy of [National Instruments, 2011, p. 5].

which is programmed into the FPGA. This connection supports multithreading, and simplifies the programming process through its built-in functions, and C/C++ compatibility.

The two cRIO's that are used at NTNU, are running a program developed for NTNU by Ph.D. student Dinh Thuc Duong. This program transforms the cRIO in question, into a PMU that is able to measure frequency, voltage and current phasors, and to output the data to a local PDC.

One of the before-mentioned PMUs, is installed in the Renewable Energy Laboratory at NTNU. It measures the voltage at the secondary side of the main supply directly, and takes part in the Nordic STRONGrid project [STRONGrid, 2013]. The second PMU does not have a fixed installation, and was utilized in this experiment to measure voltages and currents at desirable locations in the power system. Its available in-/out-modules are listed below, as seen from left to right in Figure 4.4. The low voltage input module was utilized for the measurements performed in this thesis.

- Voltage (NI 9225)
- Current (NI 9227)

- Low Voltage (NI 9239)
- GPS signal (NI 9467)



Figure 4.4: *The compactRIO, programmed as a PMU, utilized for performing measurements. The chassis is containing the controller, power supply, and Ethernet connection on the left; the voltage, current and low voltage input modules in the middle; and the GPS module at the right.*

#### 4.2.2 PDC Software: Synchronwave

There are several PDC software products on the market, and often the different PMU suppliers have developed their own software. Because of the IEEE standard described in Section 2.3.3, all PMUs and PDCs must communicate with the same encoding, and do not depend on having the same hardware/software supplier. There even exists an open source PDC software called *OpenPDC* available for free download.

At NTNU the *Synchronwave PDC Software*, called SEL-5073 from *Schweitzer Engineering Laboratories, Inc* (SEL), is used. The PDC software is connected to the PMU at NTNU, and passes the measurements on to the output stream recipients, as depicted in Section 2.3.

## 4.3 Measurement Interface

The measurements gathered by the measurement device described in Section 4.2, must be processed and visualized, in order to become useful results. In this thesis, NI LabVIEW, National Instrument's programming language and software, has been chosen for this purpose. Section 2.4.1 explains the structure of application development, including the abbreviations VI and subVI, and the difference between the front panel and the block diagram. The external library *PRL* [Aarstrand, 2013], required for obtaining measurements, is also described in the before-mentioned section.

The application developed in this section will be referred to as the *measurement interface*, and is the main VI of this thesis. It consists of several subVIs, breaking down the amount of code into related categories, which also simplifies the process of the reassembling other VIs (measurement interfaces). The measurement interface and its subVIs were designed specifically to suit the laboratory set-up described in Section 4.1. This basis entails certain assumptions regarding the measurement inputs, required parameter outputs, and desired output formats, which leads to restrictions on the measurement interface usage. This can be expanded on by someone with a basic understanding of LabVIEW programming.

Section 4.3.1 will elaborate on the tools needed to develop the measurement interface, and to connect it to the measurement device, as well as describing the input measurements and their format. Section 4.3.2 will address the power system parameters, calculated from the measurement input signals, and how they can be visualized in various interface components. An example of a measurement interface is presented in Section 4.3.3.

### 4.3.1 Required Tools and Input Assumptions

The measurements are acquired by a PMU, that transmits its data to a PDC (see Section 2.3 for further details on the topic). The measurements will be available through the use of a PDC, by utilizing the external LabView library called *PRL* (described in Section 2.4.2).

#### 4.3.1.1 Measurement Input

The visible terminals in Figure 4.2 illustrate the measurement points that are available in the laboratory set-up. In order to estimate the system state and power flow, the application needs access to at least two voltage measurements and one current measurement. The measurement interface supports voltage connection to any of the points in the figure, but assumes current measurements to be performed at the Y-side of the transformer.

The measurement points located in the laboratory are downscaled in mV, compared to the actual voltages and currents present in the system. The voltages might also be given as either line-voltage or phase-voltage. The properties of the different measurement points are summarized in Table 4.4.

Table 4.4: *The properties of the different measurement points in the laboratory, referred to the labels given in Figure 4.1. The input columns indicate the measured values when the parameter is equal to 1 pu.*

Location	Voltage			Current	
	Type	Scale [mV/V]	Input [V]	Scale [mV/A]	Input [V]
M1	Line	10	4.00	40	0.98
M2	Phase	10	2.30	80	1.96
M3	Phase	10	2.30	80	1.96
M4	Line	10	4.00	20	0.49

To be able to compare the instantaneous values, the voltages must be converted to the same type of measurements. Because the phase-voltage is more convenient to use during calculations, the measured line-voltage of the generator should be converted to a phase-voltage, and the theory described in Section 2.2.1 must be applied. This involves both a magnitude decrease with a factor of  $\sqrt{3}$ , and a negative phase shift of  $30^\circ$ , compared to the line-voltage phasor, as stated in Equation 2-11.

The Y- $\Delta$ -transformer is also introducing a phase shift between the measurements, as was presented in Section 2.2.2. This has to be taken into account in the interface calculations, together with the measurement scale coefficients presented in Table 4.4. Since the Y- $\Delta$ -transformer is known to have a winding ratio of  $a = \sqrt{3}$ , the magnitude difference that could have been introduced by the transformer, is eliminated, and therefore not considered in the implementation of this subVI.

Both here and for the rest of the interface components, the measurements are assumed to consist of three signals in the following order:

1. Generator voltage
2. Load voltage
3. Current

The time tag signal is treated separately, but is of course paired to each of the measurement signals enumerated above, as stated in Equation 2-14. The order of the three signals is of significance, because the application can not distinguish one from the other, merely based on their values. It assumes this order, and

treats each signal as voltage or current, according to its position in the acquired measurement array, containing the signals.

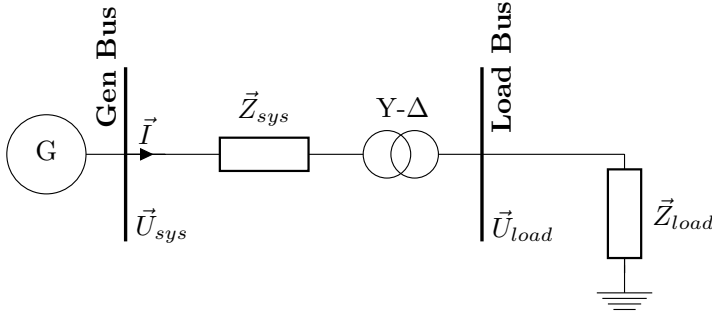


Figure 4.5: *Illustration of the simplified laboratory set-up, utilized as basis for the measurement interface calculations.*

### 4.3.2 Interface Components

To achieve the capabilities of the measurement interface presented in this section, the interface is dependent on a variety of subVIs. Some of them work mainly behind the scenes, and contribute with convenient functionality, as those presented in Section 4.3.2.1. Other subVIs focus on calculating new parameters from the measurements, and preparing them for visualization in the front panel. These will be examined in the rest of this section.

When the appearance of the subVI in the block diagram is presented, the input and output connections of the subVI is visible. The name of the input/output is written in either bold, normal or grey font, which conveys information about whether that particular connection is, respectively, mandatory, recommended or optional. If the subVI contains mandatory inputs, it does not work until these have been supplied with the correct data connections. The subVI can be executed without the recommended or optional connections, but they may add additional functionality, or customization options, regarding the output.

#### 4.3.2.1 Conversion and Auxiliary Functions

**Line diagram conversion:** As stated in Section 4.3.1, the measurement signals must be converted according to the chosen measurement points in the laboratory. To achieve this dynamically, the converting controls are available to the user from the front panel (Figure 4.6). The control includes options for measured

line-voltage vs. phase-voltage for both the generator and the load, and whether the measurement point of the load voltage is located before or after the transformer (which includes a phase-shift of the voltage). Another control allows for input of the measurement scale coefficients, given in  $\text{mV}/\text{V}$  for the voltages and  $\text{mV}/\text{A}$  for the current, as presented in Table 4.4.

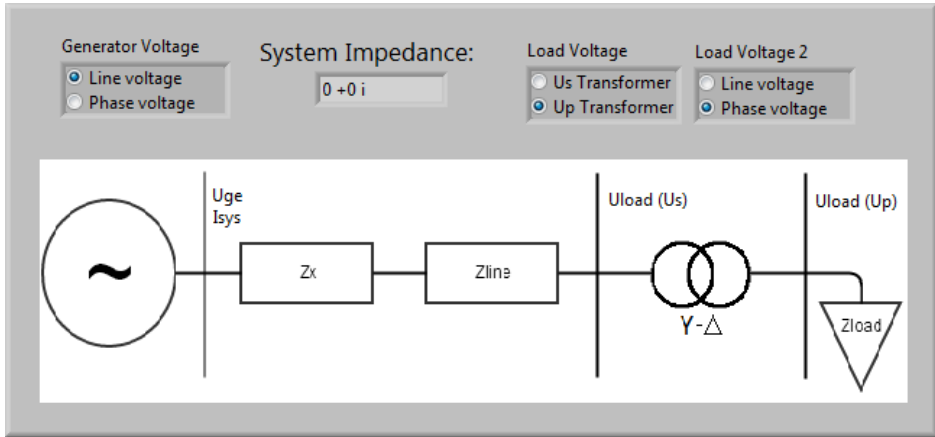


Figure 4.6: The control display for the Signal Converting Choices of the subVI named *LabMeasurementConverter*.

A subVI named *LabMeasurementConverter* takes all of these controls as input, along with the PMU measurements, and transforms the measured signals to actual power system phase-voltages referred to the generator side of the transformer. Its appearance in a block diagram is illustrated in Figure 4.7. All other subVIs that have phasors as inputs, have assumed that this conversion has taken place.

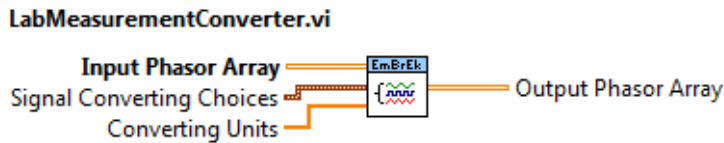


Figure 4.7: Inputs and outputs of the subVI named *LabMeasurementConverter*, used for converting and phase-shifting the measured phasors to suit a line-diagram referred to the generator side of the power system set-up.

**Saving and loading measurements:** In addition to the converting controls for the measurement input signals, the interface also includes controls for stopping the application, opening the control panel of the PRL, saving the received measurement data, and loading the saved data to replay the calculations as outlined in Section 2.4.3. The two latter functionalities are implemented in a subVI named *SaveLoadMeasurementData*, and its inputs and outputs are illustrated in Figure 4.8. They are automatically saved as text files with the extension *.lvm* in a folder named *SavedMeasurements*, which is also the default folder when loading the measurements.

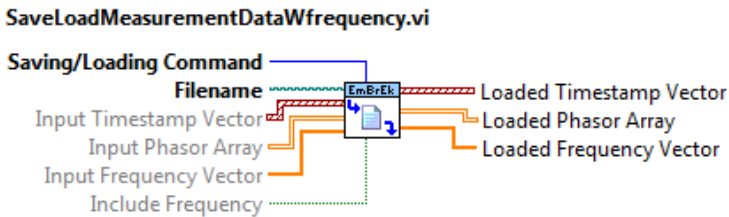


Figure 4.8: *Inputs and outputs of the subVI named SaveLoadMeasurementData, used for either saving the received measurements, or for loading already saved measurements in order to replay the experiment with the device off-line.*

**Buffer indices:** Before the first PRL buffer has been filled, the program creates and maintains its own buffer. In this buffer, the phasors with the most recent time stamp is located at the end of the buffer, column number  $n - 1$  where  $n$  is the number of time frames in the buffer. This index calculation had to be done a large number of times, and was extracted into its own subVI in order to decrease repetition of code and avoid careless mistakes. The subVI named *FindingMostRecentIndex* is illustrated in Figure 4.9, which accepts the buffer containing the measured phasors as inputs, and outputs the index of the most recently measured  $\vec{U}_{gen}$ ,  $\vec{U}_{load}$  and  $\vec{I}$ .

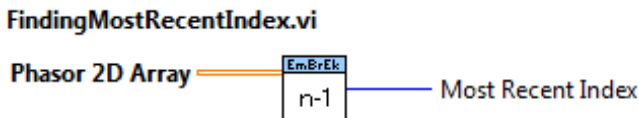


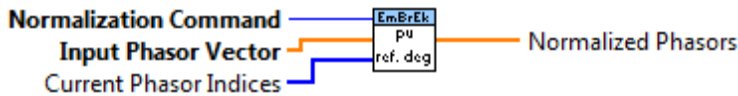
Figure 4.9: *Inputs and outputs of the subVI named FindingMostRecentIndex, used for returning index  $n - 1$  in order to extract the measured phasors with the most recent time stamp from the buffer.*

**Instant visualization:** The PMU usually has a sample rate of the same number of nominal sinusoidal voltage waves per second, which translates to the nominal frequency of 50 Hz in Europe. When the actual frequency deviates from this, which it usually does, the absolute angles are always changing. The result of displaying the absolute voltage angles in an array is mildly distracting, as the angles are rapidly changing and without obvious correlation.

To amend this issue, the values in the array can be calculated as angles relative to a reference angle. For this particular laboratory set-up, the measured load voltage is chosen as the reference, and thus has an angle of  $0^\circ$ . This is beneficial for several of the visualizations described later in this chapter, especially the phasor diagram. A separate subVI was developed for this purpose, named *Normalizer1D*, and is illustrated in Figure 4.10(a). It takes the instantaneous measured phasors as input, and a command input for choosing what kind of normalizing should take place. The choices are *Convert to pu*, *Reference Angle*, or performing both conversions simultaneously.

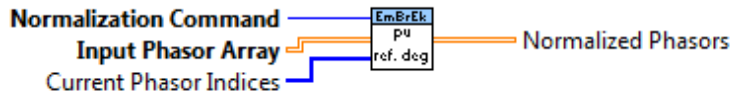
A second subVI, named *Normalizer2D*, takes measurement phasors over a time period as input, instead of only the most recently measured phasors, and forwards each time sample to *Normalizer1D* for conversion. Figure 4.10(b) illustrates the inputs and outputs of the *Normalizer2D*.

**Normalizer1D.vi**



(a) Inputs and outputs of the subVI named *Normalizer1D*

**Normalizer2D.vi**



(b) Inputs and outputs of the subVI named *Normalizer2D*

Figure 4.10: Inputs and outputs of the normalizer subVIs used for either converting a vector or an array of phasors (single or multiple time frame(s)) from SI units to pu, let all phasor angles be calculated relative to the load voltage angle, or both.



**Historical visualization:** Some of the parameters calculated in the subVIs presented in the subsequent sections can best be visualized in a trend curve showing the historical changes in values over a time period. The subVI named *GraphPlotter* converts the time stamps and an array containing the calculated parameter values into the data-type required by the trend curve object in LabVIEW, which is referred to as a *waveform chart*. A reference to the waveform chart is required in order for this subVI to operate, but the Y Scale Limits and Signal Names are optional to supply, as indicated in Figure 4.11.

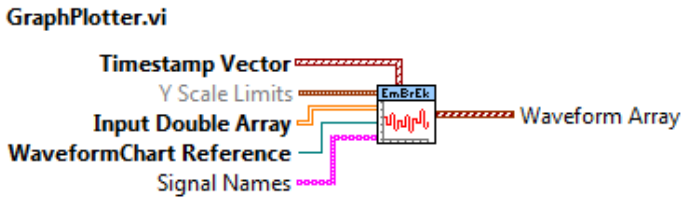


Figure 4.11: Inputs and outputs of the subVI named *GraphPlotter*, used for creating waveform chart data from time stamps and calculated parameters, in order to visualize the historical changes in values over a time period.

The input array in this case can not be complex numbers, they need to be decimal values. One of the resulting graphs can be seen in Figure 4.12, where the real and imaginary parts of the calculated impedances in the power system have been separated before being used as input for the *GraphPlotter*.

#### 4.3.2.2 Impedances

The impedances in a power system is often paramount to further analyses. Several of the subsequent sections will require either the system impedance, the load impedance, or both. These calculations have therefore been extracted to their own subVIs, available wherever they are needed. They are therefore taking both instantaneous phasors and phasors measured over a time period as input. Accordingly, they can output both the instantaneous impedance value and the impedance calculated over a time period, as illustrated in Figure 4.13 and Figure 4.14.

The calculations performed in the two subVIs is based on Equation 3-21 and Equation 3-25, which is acquired from fundamental electric circuit theory applied to the system model in Figure 4.5.

Although the AVR of the generator controls the generator voltage, it does not control the frequency of the generator, which will deviate when the generator is operated in island mode. The frequency will influence the inductances

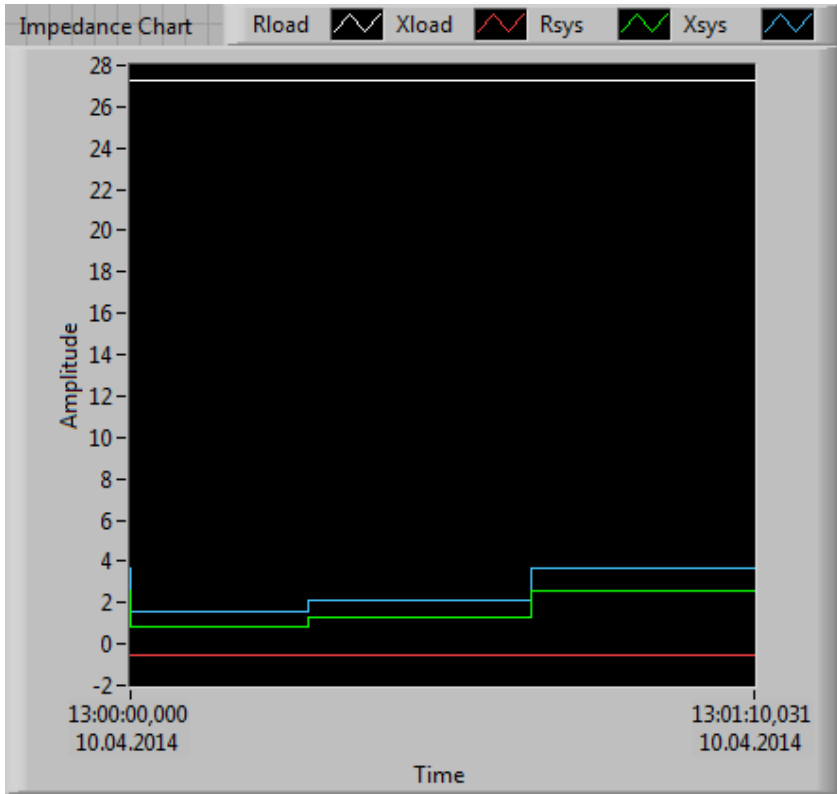


Figure 4.12: Waveform chart of the calculated impedances during an increased load power event performed on the system model in PowerFactory.

#### CalculateImpedanceSystem.vi

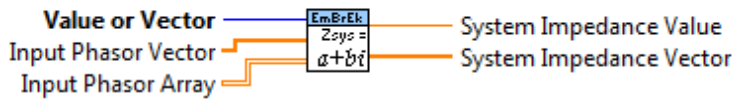


Figure 4.13: Inputs and outputs of the subVI named CalculateImpedanceSystem, used for calculating the impedance between the two voltage measurement points.

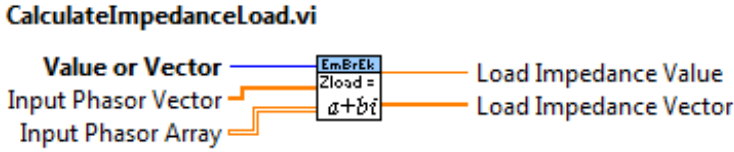


Figure 4.14: Inputs and outputs of the subVI named *CalculateImpedanceLoad*, used for calculating the load impedance.

and capacitances in the system, and is taken into account in the subVI *CalculateImpedanceSystemWfrequency* illustrated in Figure 4.15.

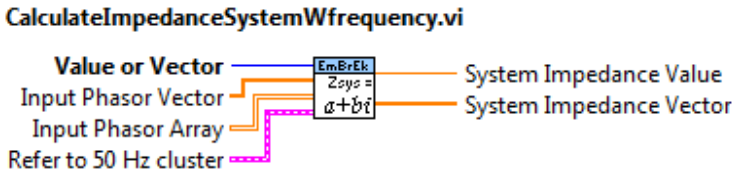


Figure 4.15: Inputs and outputs of the subVI named *CalculateImpedanceSystemWfrequency*, used for calculating the system impedance referred to 50 Hz.

It performs the same calculations as the *CalculateImpedanceSystem* subVI, but it normalizes the  $X_{\text{sys}}$  with respect to a system of 50 Hz, before outputting the calculated reactance. From  $\vec{Z}_{\text{sys}} = R_{\text{sys}} + j\omega_s L$ , it is apparent that only the reactance is dependent on the frequency, since  $\omega = 2\pi f$ . If the actual system frequency is denoted with the subscript  $s$  and the nominal frequency with  $n$ , while recognising that the inductance  $L$  is independent of frequency, the resulting relationship between the calculated and normalized reactance becomes:

$$\begin{aligned}
 L &= \frac{X_s}{j\omega_s} = \frac{X_n}{j\omega_n} && \text{Then solve for } X_n \\
 X_n &= \frac{\omega_n}{\omega_s} X_s \\
 &= \frac{2\pi f_n}{2\pi f_s} X_s && \omega = 2\pi f \\
 &= \frac{f_n}{f_s} X_s && (4-3)
 \end{aligned}$$

Here  $X_s$  is the calculated system reactance based on measured voltages and currents,  $f_s$  is the measured system frequency, and  $f_n$  is the nominal system

frequency, 50 Hz.

### 4.3.2.3 Voltage and Current Phasors

The measurements themselves are acquired and processed as complex numbers. In order to convey the information they possess in a more intuitive format, they may be represented in numeric polar coordinates, as stated in Equation ??, or be graphically displayed as vectors in a diagram, as illustrated in Figure 3.11.

The subVI named *CalculatePhasorRepresentations* takes the three most recently measured signals as inputs. The voltage drops between the voltage measurement points, and over the load, are calculated based on the following equations, which is derived by following the principles outlined in Section 3.3.1:

$$\vec{U}_{drop} = \vec{Z}_{sys}\vec{I} \quad \vec{U}_{load} = \vec{Z}_{load}\vec{I} \quad (4-4)$$

The impedances  $\vec{Z}_{sys}$  and  $\vec{Z}_{load}$  are acquired by utilizing the subVIs from Section 4.3.2.2. If the generator reactance is supplied, the generator emf with its voltage drop to the terminal voltage is estimated from Equation 4-5.

$$\Delta\vec{U}_{gen} = jX_{gen}\vec{I} \quad \vec{E}_{emf} = \vec{U}_{gen} + \Delta\vec{U}_{gen} \quad (4-5)$$

Together with the three measurement signals, these calculated parameters are outputted as polar representations in an array and in two different phasor diagrams, as shown in Figure 4.16.

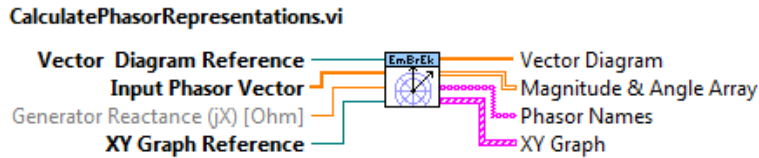


Figure 4.16: *Inputs and outputs of the subVI named CalculatePhasorRepresentations, used for displaying instantaneous phasors as vectors in a vector diagram, as numeric polar coordinates in an array, or as phasors combined with the voltage drops in a phasor diagram. It can use the generator reactance as input to estimate the internal emf and voltage drop in the generator.*

**Array:** An array is a basic way to represent any data, but not all types of information are suited to be displayed in an array. When it comes to PMU measurements, the values measured in the next time frame is approximately the same as those measured in the current time frame. Voltage and current phasors

have amplitudes that may differ significantly from each other, but are somewhat stable from one time frame to the next. The same applies to their angles, if calculated relative to a chosen reference angle. The phasors are therefore suited for this display format.

Figure 4.17 exemplifies how an array can connect names of the PMU signals to their measured voltage and current magnitudes and angles. The third column has utilized the normalization subVI to display the pu magnitudes for the phasors, while the fourth column applied the reference angle command to the same subVI to achieve relative angles, instead of their absolute counterparts that are constantly changing.





V & I - Phasors		[V]/[A]	[pu]	[deg]
	Generator voltage	238,13	1,04	6,24
	Load voltage	196,14	0,85	0
	Voltage drop	48,14	0,21	32,55
	Current	9,07	0,37	-15,24

Figure 4.17: The array outputted from the subVI named *CalculatePhasorRepresentations*, displaying the voltage and current magnitudes in both SI units and pu, and their angle in degrees.

In addition to only displaying measurement values, the array rows are assigned a coloured label unique to each of the received signals. It thereby acts as a legend for the vector diagram, and increases its overall readability and visualization ability.

**Phasor diagram:** A phasor diagram is a more visual display object than the array, and the user needs only one quick glance at it to evaluate whether the angles are as expected. In order to distinguish the different voltage signals from each other, colouring the different phasors according to a legend as shown in Figure 4.17 increases its readability.

The phasor diagram plots all voltage signals for each time frame, and the result is a phasor cluster where each phasor remain almost constant relative to the other phasors, while the system is in steady state. As with the array, the phasor diagram only shows the measured voltages within this time frame, but the phasor diagram is suited to show how the voltage angles are changing according to the frequency. As mentioned in the previous paragraph, the absolute voltage angles are constantly changing while the amplitudes are reasonably stable during steady state.

The whole cluster is rotating clockwise if the frequency is less than 50 Hz. This also applies for the other way around, and with increasing frequency deviation the cluster rotates faster. If it is desired, the phasor diagram could be plotted relative to a reference angle as well, as in this case, which would keep the phasor cluster from rotating and concentrate the phasors around the chosen reference phasor.

Figure 4.18 illustrates the built-in vector diagram provided by LabVIEW. It is easy to use, and automatically performs the necessary scaling of the phasors, so that the length of the largest voltage phasor reaches the outer circle. However, it is accompanied with certain restrictions, such as the inability to let individual phasors have a different starting point than the origin. The voltage drop phasors (the phasors with cyan and green colouring) should be located at the end of their corresponding voltage phasor in order to act as a phasor diagram. Additionally, it dynamically changes the pu base in its visualization of the phasors, and their absolute lengths do not indicate the magnitude of the voltages and currents in the power system.

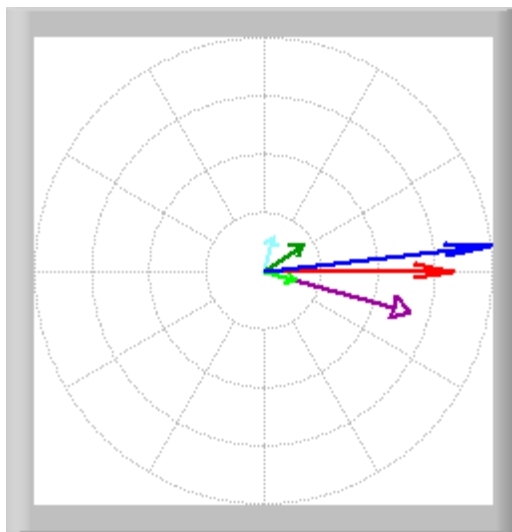


Figure 4.18: *The built-in vector diagram provided by LabView, which presents the different phasors with the origin as the starting point.*

These current LabView deficiencies have been corrected in this thesis by developing a new phasor diagram. Figure 4.19 presents the implemented phasor diagram functionality, complete with its own legend. It utilizes an XY Graph with real and imaginary parts of the phasors in pu as the x and y axis, respec-

tively. The generator voltage, load voltage, current and estimated internal emf phasor (electromagnetic force) use the origin as their starting points. The real, imaginary and complex voltage drop phasors have the end of the load voltage as their starting point, while the internal voltage drop phasor uses the end of the generator voltage phasor as its starting point.

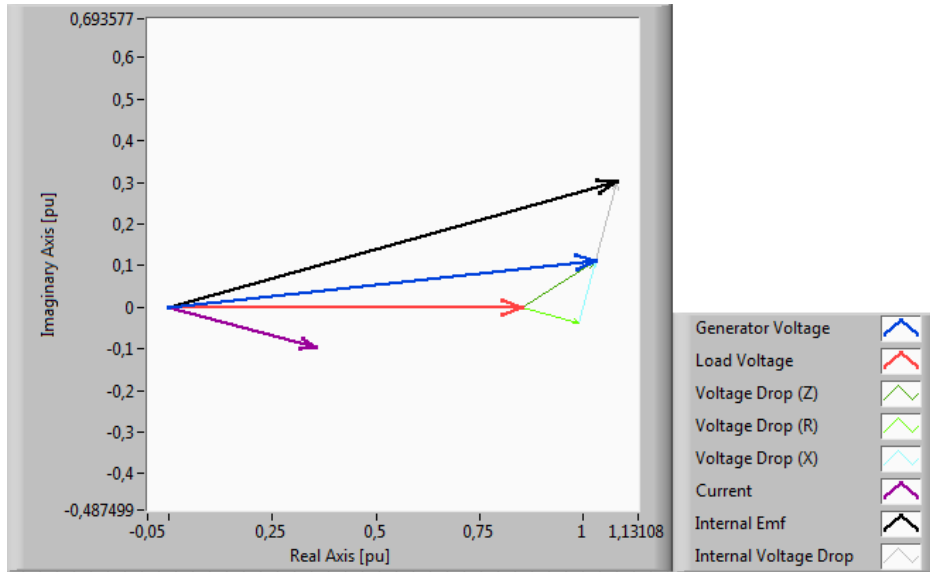


Figure 4.19: *The phasor diagram developed for this thesis, with the voltage drop phasors using the corresponding voltage phasor end points as starting points.*

An automated scaling had to be implemented, guaranteeing the correctness of the relative angles and lengths of the phasors, while also assuring that the whole phasor diagram is in view at all times, without it only occupying a fraction of the available chart display. This was performed by adding a padding of predefined magnitude around the start and end points of the phasors, and positioning the phasor cluster in the middle of the object screen. This functionality also supports different ratios between the x and y axis, in contrast to the square built-in vector diagram in Figure 4.18.

Initially, the phasors in Figure 4.19 were only simple straight lines without any form of start or end point identification. To improve its readability, a subVI named *CreatePhasorArrows* was developed to add an arrow head at the end of each phasor.

#### 4.3.2.4 Active and Reactive Power

The generated and consumed apparent powers can be calculated by multiplying the two voltages separately with the complex conjugated current, as indicated in Section 3.3.2. This is indicated in Equation 4-6, and Equation 4-7 displays the method for acquiring the active and reactive powers separately.

$$\begin{aligned}\vec{S} &= \vec{U}\vec{I}^* \\ &= P + jQ\end{aligned}\tag{4-6}$$

$$\begin{aligned}P &= \Re\{\vec{S}\} & Q &= \Im\{\vec{S}\} \\ P &= |U||I| \cos(\delta_u - \delta_i) & Q &= |U||I| \sin(\delta_u - \delta_i)\end{aligned}\tag{4-7}$$

When the equations above are applied to the system considered in Figure 4.5, the result is:

$$\begin{aligned}\vec{S}_{generated} &= \vec{U}_{gen}\vec{I}^* & \vec{S}_{consumed} &= \vec{U}_{load}\vec{I}^* \\ \vec{S}_{generated} &= P_{gen.} + jQ_{gen.} & \vec{S}_{consumed} &= P_{cons.} + jQ_{cons.}\end{aligned}\tag{4-8}$$

The subVI named *CalculatePowerFlow* applies the equations above to the measured voltages and currents, and outputs an array with the generated and consumed active and reactive power. Another input to the subVI is indicated in Figure 4.20, which allows the user to indicate whether the outputted array should be given as three-phase or single-phase values, and whether the units should be in [W]/[VAr] or [kW]/[kVAr].

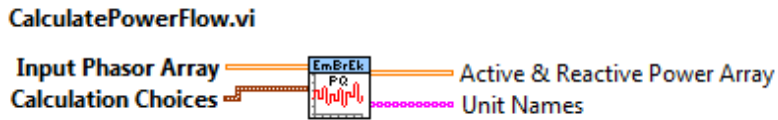


Figure 4.20: *Inputs and outputs of the subVI named CalculatePowerFlow, used for calculating the generated and consumed active and reactive powers at the generator and at the load.*

#### 4.3.2.5 Indicators

There are several system parameters that can be calculated in order to be used as indicators for voltage stability, where some of them have previously been described in Section 3.3. Three of the indicators have been implemented in the measurement interface (MI), and are presented in the following paragraphs.



**PV-Curve:** The voltage-power capability curve was established by defining a one dimensional load voltage vector ranging from the absolute value of the measured generator voltage, to zero, and then calculating the resulting  $P_{load}$  from Equation 3-23. The required  $X_{sys}$  was obtained by utilizing the subVI *CalculateImpedanceSystem*. The current state is indicated on the PV-curve by plotting the instantaneous  $|\vec{U}_{load}|$  against the active power consumed (retrieved by executing the formula for active power, previously presented in Equation 4-7.

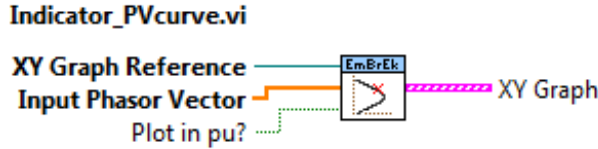


Figure 4.21: *Inputs and outputs of the subVI named Indicator\_PVcurve, used for estimating the voltage-power-characteristics in real-time based on theoretic maximum power transfer.*

**ISI:** The ISI also utilizes the subVIs presented in Section 4.3.2.2, *CalculateImpedanceSystem* and *CalculateImpedanceLoad*, to calculate the system and load impedances respectively. The indicator value itself was calculated from Equation 3-24, by dividing the absolute value of the system impedance by the absolute value of the load impedance. Figure 4.22 illustrates the inputs and outputs of the subVI, where *ISI Indicator and Limit* is an array with the first row containing the calculated ISI, and the second row featuring only the voltage stability limit value for the indicator, which in this case is value 1. This simplifies the plotting of the results with the *GraphPlotter*, since the *WaveformChart* is the most convenient display object for these results.

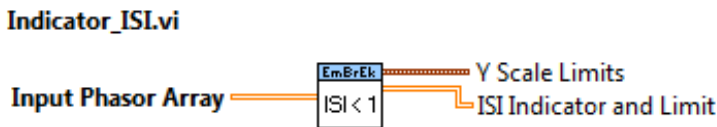


Figure 4.22: *Inputs and outputs of the subVI named Indicator\_ISI, where the value is based on the ratio between the system and the load impedance.*

**VSI<sub>SCC</sub>**: The indicator value was calculated from Equation 3-26 by dividing the minimum short-circuit capacity of the system which is required to supply the load, by the actual short-circuit capacity during the current state of the system. Figure 4.23 illustrates the inputs and outputs of the subVI, where *VSI<sub>SCC</sub> Indicator and Limit* is an array with the first row containing the calculated indicator, and the second row filled with the voltage stability limit value, 1. This serves the same purpose as described for the ISI indicator.

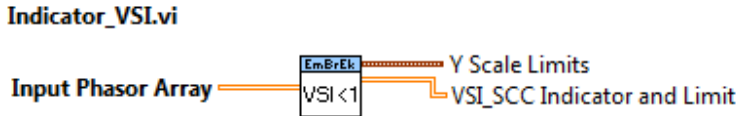


Figure 4.23: Inputs and outputs of the subVI named *Indicator\_VSI*, where the value is based on the ratio between the minimum short-circuit capacity needed to supply the load, and the actual short-circuit capacity.

### 4.3.3 Examples of Possible Measurement Interfaces

An example of a possible measurement interface utilizing the subVIs presented above, is provided in Figure 4.24. It consists of the *LabMeasurementConverter* in the upper right corner, the *CalculatePhasorRepresentations* in the large white area to the left, and the active and reactive powers acquired from the *CalculatePowerFlow* results are visualized with the *GraphPlotter* in their separate trend curves displayed in the bottom right corner. The control tabs located in the middle at the top of the interface contains options for scaling coefficients, stopping the application, opening the *PRL* control panel, or saving the measured data.

An overview of all the different subVIs, provided in the developed measurement interface library, is presented in Appendix D. It is included, as a convenience for any fellow developer, wanting to utilize the subVIs presented in this section, or expanding the existing library.

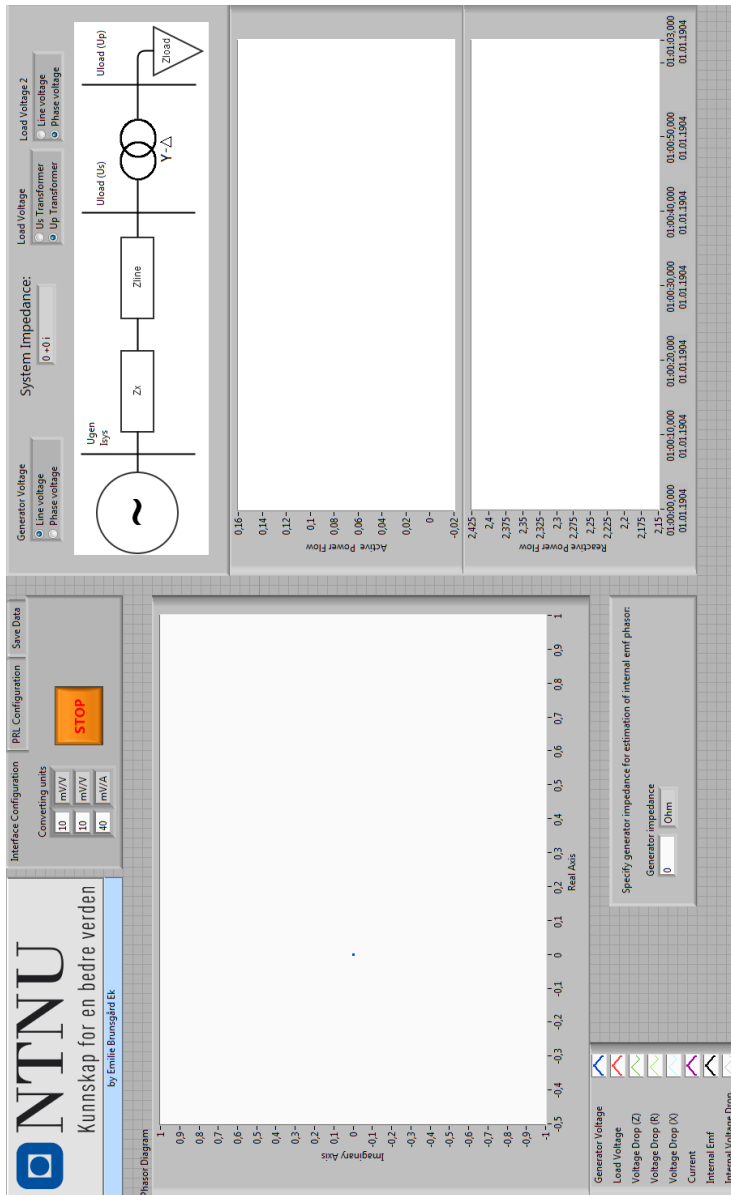


Figure 4.24: Example of a measurement interface utilizing the library developed through the work with this thesis.

## 4.4 Simulation Model in PowerFactory

It is important to be aware of the theoretical behaviour of the system, when subjected to events, before doing laboratory tests. A simulation model was developed in DIgSILENT PowerFactory 14.1 for this reason, and this section elaborates on its components, which are based on the stationary laboratory components described in Section 4.1.

The synchronous generator in the laboratory, was modelled with the "synchronous machine"-component within PowerFactory. It was defined with 17 kVA nominal apparent power, 400 V nominal line-voltage, and a power factor of 0.8. The internal reactance of the generator model is of little relevance, due to the AVR applied on the laboratory generator. An AVR, of the type named SEXS, was defined for the generator in the simulation model to imitate the laboratory regulator. The model regulator constants have not been initialized to those of the laboratory regulator, and thus some deviations between the model results and laboratory results are expected.

In order to perform the scenarios described in Section 5.3.1, the simulation model has split its line component into three equal lines, connected in parallel, between the generator bus and the MV bus, as illustrated in Figure 4.25. The power is then transferred through the transformer line equivalent, containing the theoretical transformer impedance, and finally supplying the load.

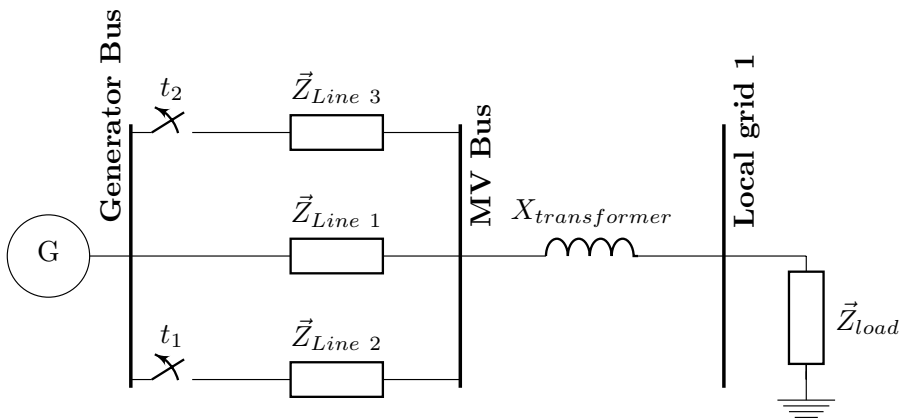


Figure 4.25: *Simulation model developed in PowerFactory for event simulations and validation of the measurement interface.*

With the measured line equivalent impedance values presented in Appendix E,

it is possible to calculate a theoretical value for the maximum line impedance of the model. By choosing the equivalent line lengths and cross-sections that result in the largest combined impedance, we get the values presented in Table 4.5. The section numbers correspond to the labels indicated in the laboratory set-up displayed in Figure 4.1.

Table 4.5: Impedance in  $[\Omega]$  and  $[pu]$  of the flexible line equivalent sections, that result in the combined largest line impedance.

Section #	Impedance	
	$[\Omega]$	$[pu]$
21	$0.326 + j0.780$	$0.0346 + j0.0829$
22	$0.781 + j0.780$	$0.0830 + j0.0829$
23	$0.751 + j0.780$	$0.0798 + j0.0829$
13	$0.751 + j0.780$	$0.0798 + j0.0829$
<b>In total</b>	<b><math>2.609 + j3.120</math></b>	<b><math>0.2772 + j0.3315</math></b>

The reactance of the substation unit is the sum of the internal reactance of the transformer, and its substation equivalent connection to the local grid. The internal reactance is assumed to be  $j0.05 \Omega$ , and the substation equivalent connection can be chosen to be either 0.4, 0.8 or 1.6 mH. Its reactance can be calculated by using the equation  $X = j\omega L = j2\pi fL$ , where  $L$  is the inductance and  $f$  the system frequency. With a system frequency of 50 Hz, the corresponding reactances is calculated to be:

$$\vec{X} = j2\pi \cdot 50 \text{ [Hz]} \cdot \begin{bmatrix} 0.4 \\ 0.8 \\ 1.6 \end{bmatrix} \cdot 10^{-3} \text{ [H]} = j \begin{bmatrix} 0.12 \\ 0.25 \\ 0.50 \end{bmatrix} \text{ [\Omega]} \quad (4-9)$$

In order to achieve maximum system impedance, the reactance of the substation equivalent is chosen to be  $j0.50 \Omega$ , with an inductance of 1.6 mH, which results in  $X_{\text{transformer}} = X_{\text{internal}} + X_{\text{subst.eq.}} = j0.55 \Omega$ .

## References

- Aarstrand, V. H. (2013). *PMU Recorder Light (PRL) - Documentation*. Enfo Technology AS, Lysaker Torg 15 Postbox 374, 3 edition.
- Loen, I. L. (2014). Stability analysis of small hydro power plants. Master's thesis, Norwegian University of Science and Technology.
- National Instruments, N. (2011). *Hands-On: CompactRIO Part I: Programming with LabVIEW Real-Time*. National Instruments. Technical Symposium.
- National Instruments, N. (2013). Getting started with compactrio - performing basic control. Website.
- Saadat, H. (2010). *Power System Analysis*. PSA Publisher.
- STRONGrid (2013). Smart transmission grid operation and control. Website.

# Chapter 5

## Case Studies and Results

This chapter will present and discuss the test descriptions, based on the simulation model and laboratory set-up described in Chapter 4, as well as the obtained results. The results acquired from the simulation model, will be displayed in Section 5.1. Section 5.2 will examine the response of the measurement interface, when based on the voltage and current values extracted from some of the model simulations, and when compared to the parameter values displayed in the various measurement panels, located in the laboratory. Finally, the test descriptions and corresponding results from the laboratory experiments will be presented in Section 5.3.

### Chapter Contents

---

5.1	Model Simulations . . . . .	<b>80</b>
5.1.1	Simulation Event Descriptions . . . . .	80
5.1.2	Increasing Load Power Demand Results . . . . .	83
5.1.3	Increased Line Impedance Results . . . . .	91
5.2	Measurement Interface Validation . . . . .	<b>98</b>
5.2.1	Recreating Simulation Results . . . . .	98
5.2.2	Measurement Location Error Estimations . . . . .	103
5.2.3	Comparisons with Laboratory Measurement Panels	105
5.3	Laboratory Experiments . . . . .	<b>108</b>
5.3.1	Test Descriptions . . . . .	108
5.3.2	Increasing Load Power Demand Results . . . . .	109
5.3.3	Varying System Impedance Results . . . . .	114

---

## 5.1 Model Simulations

The simulation results concern two different events applied to the model described in Section 4.4. The course and component settings of the events are outlined in Section 5.1.1, and an overview of the parameter changes between the various simulations events is displayed in Table 5.3. The results from the respective events are presented in Section 5.1.2 and 5.1.3, where some of the important component values in each simulation, are repeated in order to increase the readability.

### 5.1.1 Simulation Event Descriptions

The simulation model events described below, are based on the experiments that are to be performed in the laboratory, which will be outlined in Section 5.3.1. Because of the differences in nature between the power system set-up in the laboratory and simulation model, some modifications from the laboratory test descriptions had to be implemented in the simulation events. The simulation model was based on the power system illustration displayed in Figure 4.25, and the parameter names refer to this figure.

#### 5.1.1.1 Increasing Load Power Demand Event

In order to study how the power system state changes during an increased load power demand, a continually increasing load power demand event was defined for the variable load component. The details of the event configurations are presented in Table 5.1. Line 2 and 3 in the simulation model are disconnected during this particular event, with only *Line 1* supplying the load.

Table 5.1: *Parameters for the increased load power demand event.*

Event Parameters	Values
Ramp start time	5 s
Ramp duration	30 s
Simulation duration	40 s
Proportional active power step	50 000 %
Proportional reactive power step	0 %

This scenario was performed with three different values for the system impedance, to better simulate the laboratory environments. First, the theoretical value of  $Z_{\text{sys}}$ , calculated in Table 4.5 in the previous chapter, was applied to *Line 1*;  $Z_{\text{line}} = 2.61 + j3.12 \Omega$ . Then the system impedance estimated by the measurement interface, during initial start-up, from laboratory measurements was used;  $Z_{\text{line}} = 3.67 + j5.22 \Omega$ . Finally, the average of the estimated system impedances



during an increased load power demand experiment, performed in the laboratory, was utilized;  $Z_{\text{line}} = 3.36 + j3.54 \Omega$ . These scenarios are respectively referred to as *Load: Theoretical*, *Load: Lab-start* and *Load: Lab-average*.

The calculated impedances originally included the transformer impedance, due to the chosen measurement points in the laboratory set-up. The theoretical transformer impedance of  $j0.55 \Omega$  was therefore subtracted, since the frequency deviations in the simulation model, was too small to have any influence on the reactance. The resulting line impedances are displayed in the scenario overview presented in Table 5.3.

During these three simulations, the load power had an initial value of  $S_{\text{load}} = 0.1 + j2.2 \text{ kVA}$ . This was chosen in order to better simulate the increased load power demand response of the laboratory set-up, since this  $S_{\text{load}}$  was equal to the load power measured during initial power system operation in the laboratory.

### 5.1.1.2 Line Impedance Increase Event

A direct line impedance increase event is neither realistic in the real world, except for thermal changes, nor possible to apply in PowerFactory. The effects of an increased system impedance are applied by starting the simulation with three equal lines connected in parallel to supply the load. The resulting line impedance will vary with how many of the lines are connected simultaneously, since they share the power flow supplying the load equally. Their combined impedance is reduced with each added identical line, which is supported by Equation 5-1.

$$\begin{aligned} Z_{\text{eq}} &= \frac{1}{\frac{1}{Z_1} + \dots + \frac{1}{Z_n}} && \text{With } Z_n = \dots = Z_1 \\ &= \frac{1}{n/Z_1} && \text{Where } n \text{ is the number of lines in parallel} \\ &= \frac{Z_1}{n} && (5-1) \end{aligned}$$

The lines were chosen to have equal impedance, because of simplified theoretical calculations of the equivalent impedance, and because the direct comparability with the experiment performed in the laboratory for this scenario, is of limited relevance. The number of switches for the flexible line equivalent, required to be changed simultaneously in order to achieve a predefined theoretical impedance, is too great to be implemented realistically.

The single line impedance is chosen to be the theoretical maximum line impedance calculated in Table 4.5,  $Z_{\text{line}} = 2.61 + j3.12 \Omega$ . Equation 5-1 provides the resulting impedances of the parallel connections, of two and three lines respectively, which are calculated in Equations 5-2 and 5-3.

$$Z_{\text{lineEq3}} = \frac{Z_{\text{line}}}{3} = 0.87 + j1.04 \Omega \quad (5-2)$$

$$Z_{\text{lineEq2}} = \frac{Z_{\text{line}}}{2} = 1.305 + j1.56 \Omega \quad (5-3)$$

As previously stated, the simulations start with all three lines connected. Then two switch events will occur after two time intervals of different lengths. After the first event, one of the lines is disconnected, leaving only two lines supplying the load. After the second event, a second line is disconnected, and only one line supplies the load. The details of the event configurations and the resulting line impedances are presented in Table 5.2. A load flow calculation was applied to the system before starting the dynamic event simulations, in order to avoid large transient behaviour in the beginning of the simulation period.

Table 5.2: *Parameters for the line impedance increase event.*

Time intervals		Resulting line impedance	
0-20	seconds	$Z_{\text{lineEq3}}$	$0.870 + j1.04 \Omega$
20-45	seconds	$Z_{\text{lineEq2}}$	$1.305 + j1.56 \Omega$
45-60	seconds	$Z_{\text{lineEq}}$	$2.610 + j3.12 \Omega$

This scenario was performed with two different values of the load power demand, to illustrate its effect during an increased system impedance event. First, the load power during initial power system operation in the laboratory was used, with the value of  $S_{\text{load}} = 0.1 + j2.2$  kVA. Then the active power demand was increased significantly, setting the apparent power demand to be  $S_{\text{load}} = 7.5 + j2.2$  kVA. They are respectively referred to as *System: Lab-start*, and *System: Arbitrary*.

Table 5.3: *Overview of the changed settings in the different scenarios.*

Scenario	Changed parameter	Impedance/Power	
		$[\Omega]/[\text{kVA}]$	[pu]
<i>Load: Theoretical</i>		$2.61 + j3.12$	$0.2772 + j0.3315$
<i>Load: Lab-start</i>	$Z_{\text{line}}$	$3.67 + j5.22$	$0.3899 + j0.5546$
<i>Load: Lab-average</i>		$3.36 + j3.54$	$0.3570 + j0.3761$
<i>System: Lab-start</i>	$S_{\text{load}}$	$0.1 + j2.2$	$0.0059 + j0.1294$
<i>System: Arbitrary</i>		$7.5 + j2.2$	$0.4412 + j0.1294$

## 5.1.2 Increasing Load Power Demand Results

The increased load power demand event was performed with three different settings for the line impedance; theoretical value, measured value during initial laboratory operation, and averaged value during an increased load power demand test performed in the laboratory. The simulation event was described in Section 5.1.1.1, and the results are presented in Section 5.1.2.1, 5.1.2.2 and 5.1.2.3.

### 5.1.2.1 Load: Theoretical

During this simulation,  $Z_{\text{line}} = 2.61 + j3.12 \Omega$ ,  $Z_{\text{transformer}} = j0.55 \Omega$  and  $S_{\text{load}} = 0.1 + j2.2 \text{ kVA}$ . The load power started increasing five seconds into the simulation, and stabilized after increasing for thirty seconds. The load power demand at the end of the event was defined to be 500 times higher than at the start of the simulation, which corresponds with  $S_{\text{load}} = 50 + j2.2 \text{ kVA}$ . Table 5.1 contains a detailed overview of the event configuration.

The resulting voltage and current magnitudes and angles during the simulation are rendered in Figure 5.1 and Figure 5.2. The plot of the generated and consumed active and reactive three-phase power by the synchronous machine and variable load is presented in Figure 5.3. Figure 5.4 illustrates the voltage-power characteristics of the system by plotting the simulated load phase-voltage along the y-axis and the simulated active three-phase power consumed by the load along the x-axis during the simulation.

From Figure 5.1 we see that the load voltage decreased to under half of its initial value, while the current increased proportionally. This led to an increased active load power, and thereby an even larger active generator power, as illustrated in Figure 5.3. The PV-curve displayed in Figure 5.4 exhibits how the system state barely exceeds the peak of the voltage-power characteristics, i.e. the loadability limit, and that the system is not able to supply a larger load than 10.379 kW. When the load demand continued to increase, the voltage dropped below 122,42 V, and the supplied load power started to decrease.

The difference between the load voltage angle and the current angle, decreased during the start of the event, but started to increase again after a short period of time (see Figure 5.2). This is consistent with the reactive load compared to the active load being relatively high in the beginning, in contrast to the very high active load and the unchanged reactive load in the end of the simulation. The load reactance is small compared to the load resistance, and thus resulting in a small angle difference between the load voltage and the current. The difference stems from the small load reactance remaining.

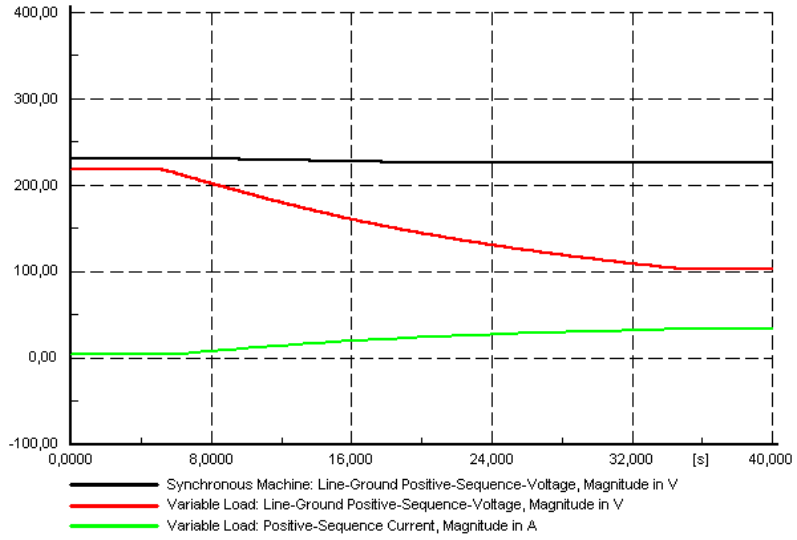


Figure 5.1: *The simulated phase-voltage [V] and current [A] magnitudes during scenario Load: Theoretical.*

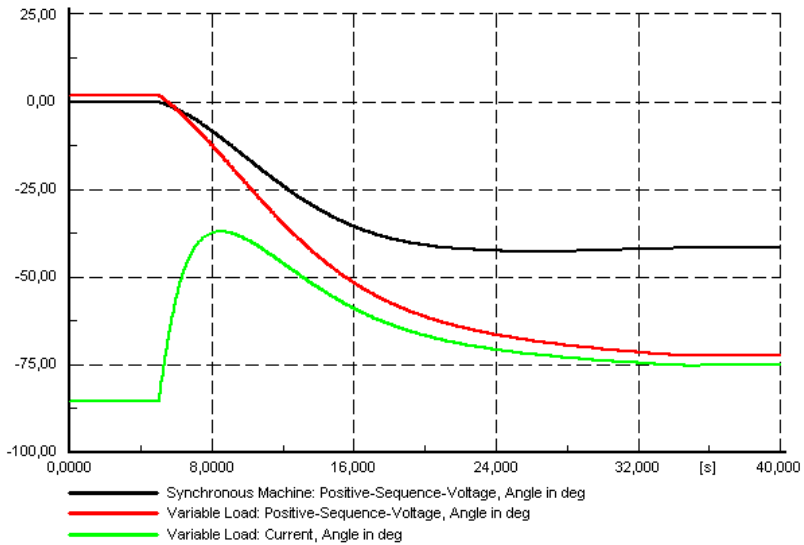


Figure 5.2: *The simulated phase-voltage and current angles [deg] during scenario Load: Theoretical.*

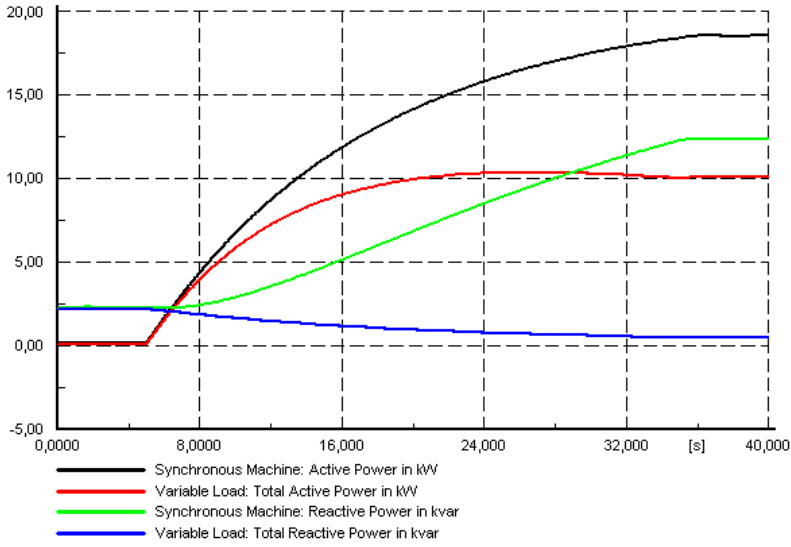


Figure 5.3: *The simulated three-phase power flows during scenario Load: Theoretical.*

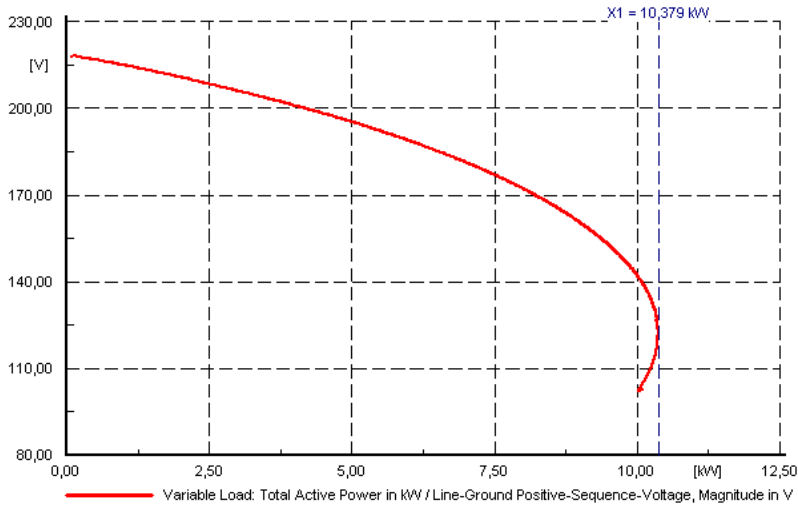


Figure 5.4: *The simulated voltage-power characteristics, given as phase-voltage versus three-phase power, during scenario Load: Theoretical.*

### 5.1.2.2 Load: Lab-start

During this simulation,  $Z_{\text{line}} = 3.67 + j5.22 \Omega$  is the only changed parameter.  $Z_{\text{transformer}} = j0.55 \Omega$  and  $S_{\text{load}} = 0.1 + j2.2 \text{ kVA}$  are unchanged from the previous simulation, and the load power increase follows the same pattern as previously described.

Figure 5.5 and Figure 5.6 illustrates the voltage and current magnitudes and angles during the course of this simulation, and Figure 5.7 displays the generated and consumed active and reactive power throughout the simulated event. The resulting voltage-power characteristic can be studied in Figure 5.8.

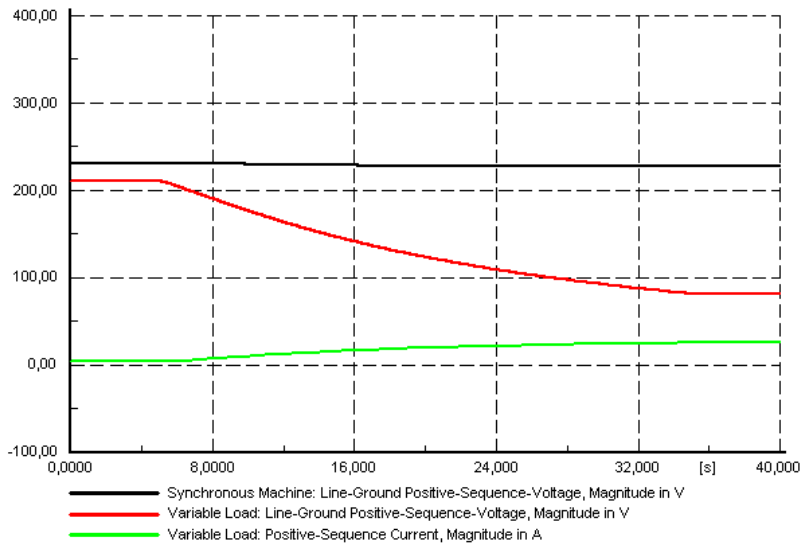


Figure 5.5: *The simulated phase-voltage [V] and current [A] magnitudes during scenario Load: Lab-start.*

The general course of the different parameters are not particularly different from the previous simulation, only their magnitudes have changed. The most notable difference being the maximum supplied load power, which have decreased from the theoretical value of 10.379 kW to 6.949 kW. This loadability limit of the power system is reached when the absolute magnitude of the load phase-voltage is equal to 119.142 V, according to Figure 5.8. This corresponds to the case when the system impedance measured in the laboratory during initial operating conditions, is being constant throughout the entire increasing load power demand scenario. Since the system impedance actually changes based on frequency and connected components, this result is probably not very realistic.

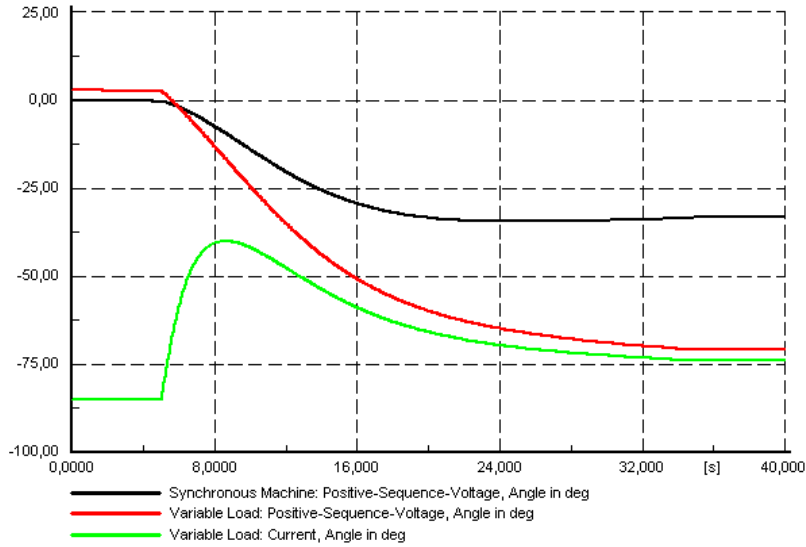


Figure 5.6: *The simulated phase-voltage and current angles [deg] during scenario Load: Lab-start.*

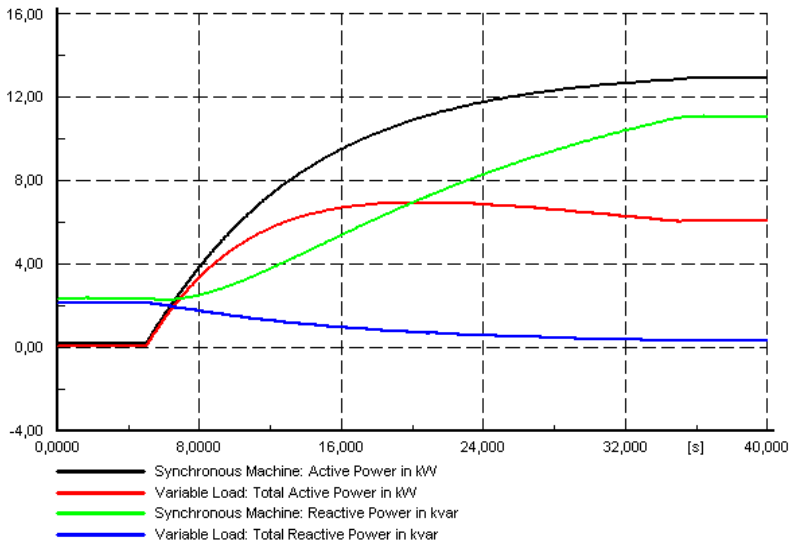


Figure 5.7: *The simulated three-phase power flows during scenario Load: Lab-start.*

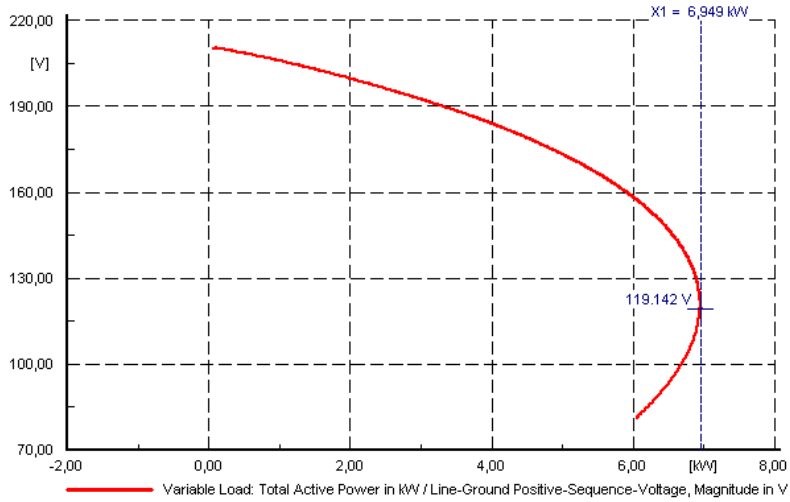


Figure 5.8: *The simulated voltage-power characteristics, given as phase-voltage versus three-phase power, during scenario Load: Lab-start.*

### 5.1.2.3 Load: Lab-average

During this simulation,  $Z_{\text{line}} = 3.36 + j3.54 \Omega$  is the only changed parameter, and the load power increase follows the same pattern as described in Section 5.1.2.1.

The magnitudes and angles of the phase-voltages and currents are presented in Figure 5.9 and 5.10, whereas the three-phase powers produced and consumed in the system are plotted in Figure 5.11. The active power consumed in the load is paired with the load voltage in the same power system state, and then plotted in Figure 5.12 as the voltage-power characteristics of the system.

The load voltage magnitude has decreased to below 100 V at the end of this simulation, while this was not the case in Section 5.1.2.1. This is also illustrated in Figure 5.12, since the PV-curve, i.e. the voltage-power characteristics, extends further down below the point where the maximum active power is delivered to the load. This state corresponds to  $P_{\text{load}} = 8.545 \text{ kW}$  and  $U_{\text{load}} = 120.149 \text{ V}$ .

The change in the resistance component of the line impedance is almost negligible compared to the previous case, but the reactance is greatly reduced. This change has had a large impact on the maximum active power being delivered to the load,  $\Delta P_{\text{load},3-2} = 1.596 \text{ kW}$ . However, the difference in active power delivered between the first simulation and the current one, is  $\Delta P_{\text{load},1-3} = 1.834 \text{ kW}$ . The change in resistance was greatest between the first and the current simulation, instead of the reactance being the greatest, as was the case relative to the



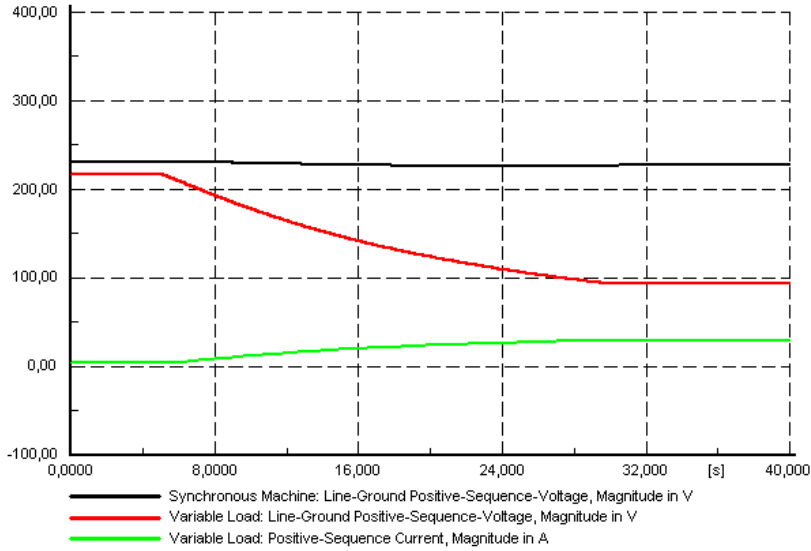


Figure 5.9: *The simulated phase-voltage [V] and current [A] magnitudes during scenario Load: Lab-average.*

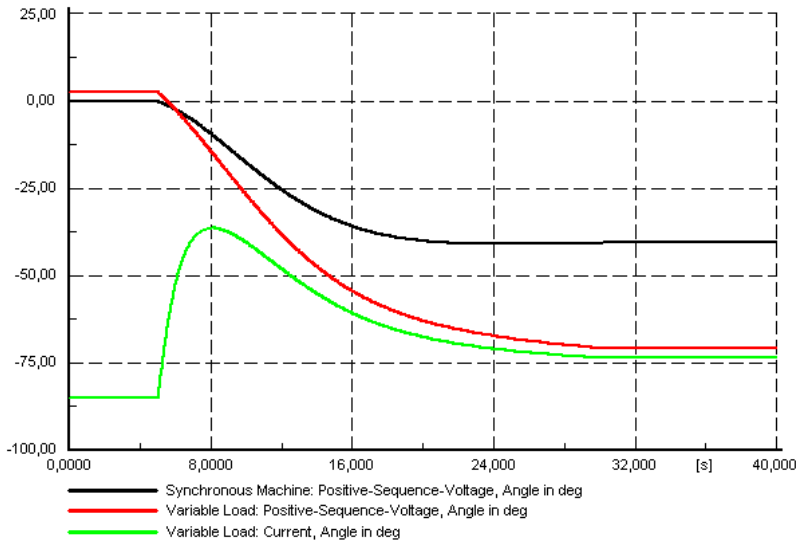


Figure 5.10: *The simulated phase-voltage and current angles [deg] during scenario Load: Lab-average.*

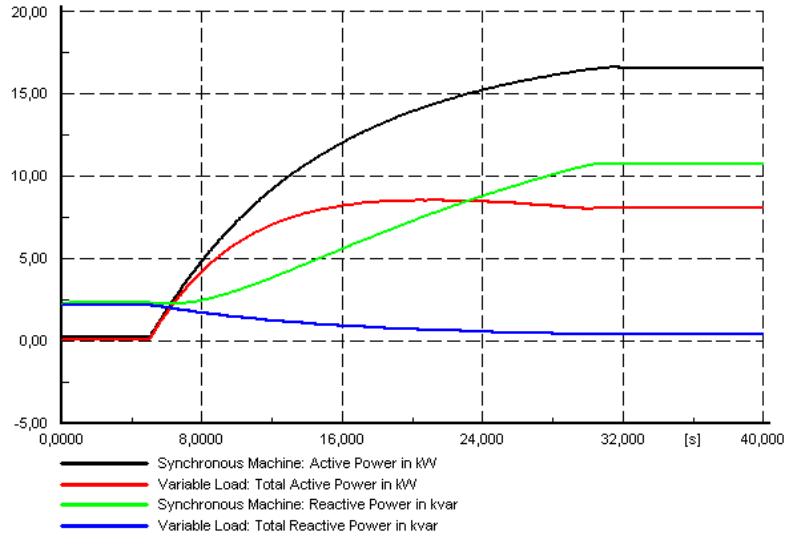


Figure 5.11: The simulated three-phase power flows during scenario Load: Lab-average.

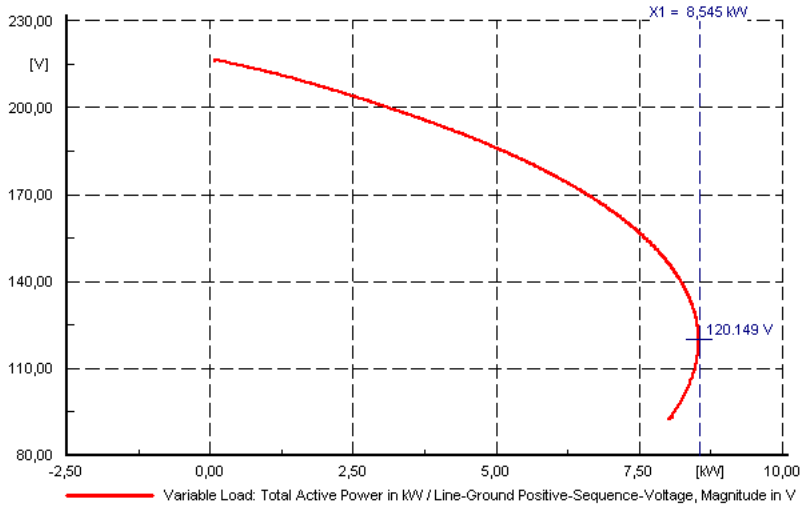


Figure 5.12: The simulated voltage-power characteristics, given as phase-voltage versus three-phase power, during scenario Load: Lab-average.

second simulation. It is apparent that both the resistance and the reactance of the system impedance is of significant importance when it comes to maximum active power being delivered to the load.

### 5.1.3 Increased Line Impedance Results

The increased line impedance event was performed with two different load power demands; measured value during initial laboratory operation, and a larger arbitrary active power load to better illustrate the behaviour of the system during such an event. Section 5.1.1.2 outlines the simulation event, and the results are exhibited in Section 5.1.3.1 and 5.1.3.2.

#### 5.1.3.1 System: Lab-start

During this simulation,  $S_{\text{load}} = 0.1 + j2.2$  kVA,  $Z_{\text{transformer}} = j0.55 \Omega$  and  $Z_{\text{line}} = 2.61 + j3.12 \Omega$ . For the first twenty seconds, the load was supplied by the three lines connected in parallel. The first switch event occurred at the twentieth second of the simulation, leaving just two lines in parallel to supply the load. Twenty-five seconds later, at the forty-fifth second, the second switch event is executed. The result is that only one line remains to supply the load, which lasts until the end of the simulation (with a duration of 60 seconds). Table 5.2 presents an overview of the equivalent system impedances during the different time intervals.

The simulated voltage and current magnitudes and angles are illustrated in Figure 5.13 and 5.14. The plot of the generated and consumed active and reactive three-phase power is presented in Figure 5.15. Figure 5.16 illustrates how the voltage-power relationship for the load changes depending on the system impedance.

When the load was supplied by the three lines connected in parallel, it divided the current and decreased the voltage drop across the system. Figure 5.13 illustrates the small deviation between the absolute values of the voltages. After the first line tripped, the system impedance was effectively increased, which increased the voltage drop across the system and thereby decreased the load voltage. The result of the second line tripping was that only one line remained to supply the load,. This increased the voltage drop even further, and increased the angle difference between the two voltages (see Figure 5.14). The angle of the current is very different from the voltage angles because the reactive load is significantly larger than the active load during the entire simulation, while the current being so small it introduces an insignificant voltage drop across the system impedance.

The generated and consumed powers are also influenced by the changed line impedance, as indicated by Figure 5.15. The active powers are increasing, while the reactive powers are decreasing, but both pairs of powers are deviating. The

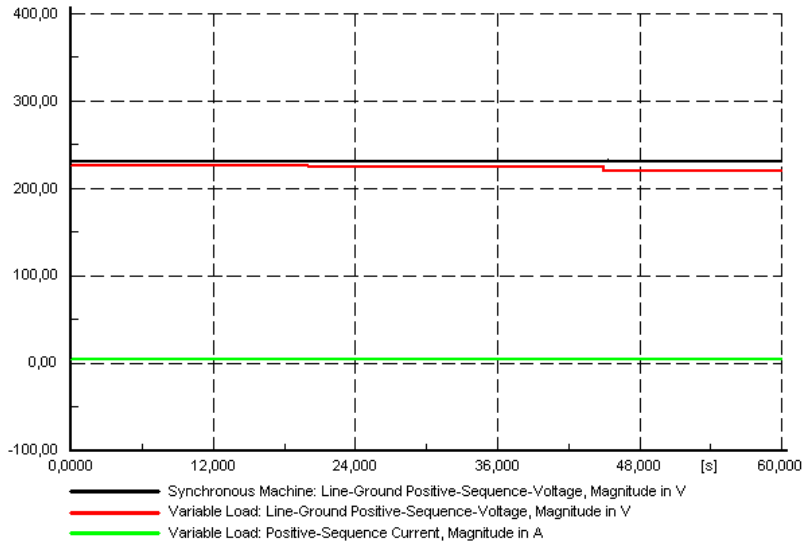


Figure 5.13: *The simulated phase-voltage [V] and current [A] magnitudes during scenario System: Lab-start.*

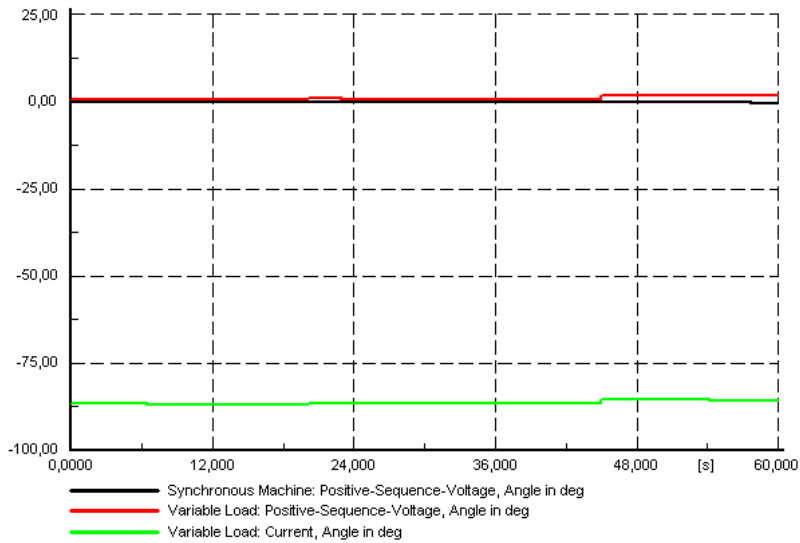


Figure 5.14: *The simulated phase-voltage and current angles [deg] during scenario System: Lab-start.*

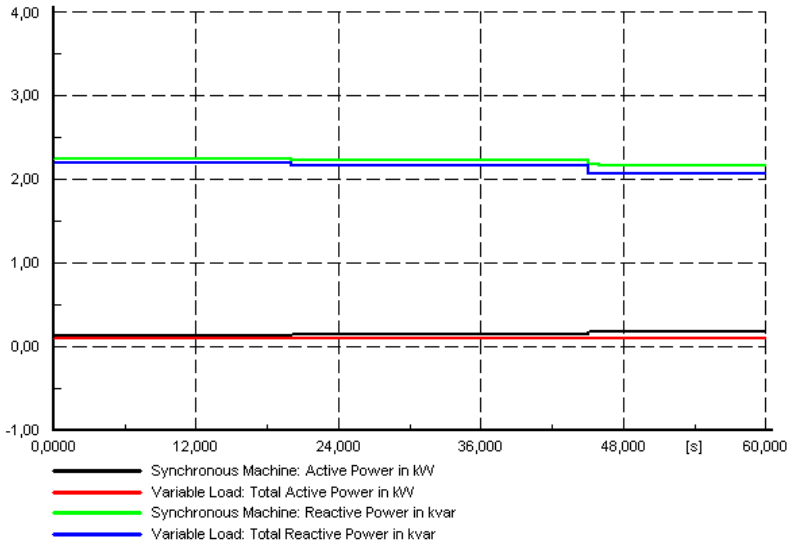


Figure 5.15: *The simulated three-phase power flows during scenario System: Lab-start.*

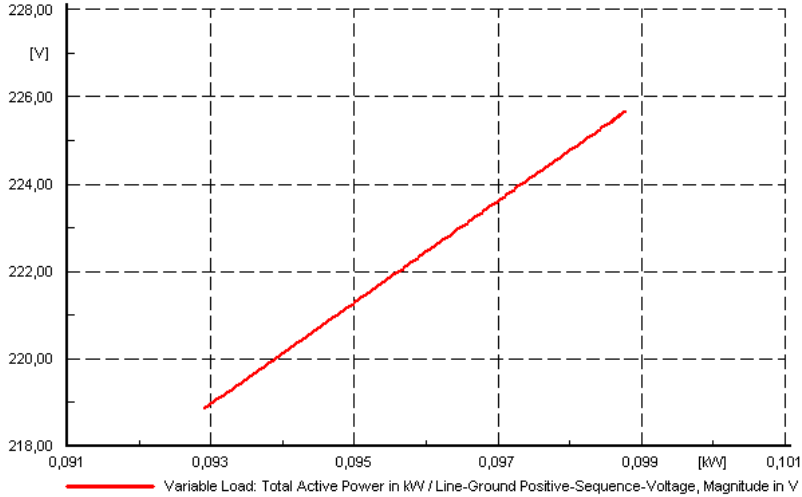


Figure 5.16: *The changed relationship between the phase-voltage and three-phase power during during scenario System: Lab-start.*

voltage-power characteristic is also changed by the line impedance difference, according to Figure 5.16. The figure displays only a single line marking the simulated phase-voltage versus the three-phase power delivered to the load because the load power demand has been constant throughout this entire simulation. The system state has been changed from  $U_{\text{load,start}} = 225.47$  V and  $P_{\text{load,start}} = 0.0986$  kW to  $U_{\text{load,end}} = 218.90$  V and  $P_{\text{load,end}} = 0.0929$  kW. The line indicates that the PV-curve has been decreased, i.e. the maximum active load power available to be delivered to the load has been decreased.

Overall, the magnitude changes of the different parameters during the simulation are very small. To better illustrate the behaviours, and to illuminate the effect of the load power magnitude, the event was also simulated with an increased load power. This was performed in the next section.

### 5.1.3.2 System: Arbitrary

During this simulation,  $S_{\text{load}}$  was chosen to be  $= 7.5 + j2.2$  kVA, while  $Z_{\text{transformer}}$  and  $Z_{\text{line}}$  remain constant from the previous simulation. The time intervals between the switch state changes are also equal to those presented in Section 5.1.3.1, as are the equivalent line impedances calculated in Table 5.2.

The simulated voltage and current magnitudes and angles are illustrated in Figure 5.17 and 5.18. The plot of the generated and consumed active and reactive three-phase power is presented in Figure 5.19. Figure 5.20 illustrates how the voltage-power relationship for the load changes depending on the system impedance.

When the system supplies a higher load and is subjected to increased system impedance, the system voltages, currents and powers are influenced considerably if compared to the case where it was supplying a smaller load. The load voltage magnitude decreased more than before, because a higher load power leads to an initially larger current, which in turn increased the voltage drop over the system impedance proportionally.

The voltage angle and currents experience some transient behaviour before returning to pre-change steady state values. Only the generator voltage angle maintains an increased value after every switch event, which may be related to the increasing reactive power generated.

Now that the parameter magnitudes are larger, the voltage-power characteristic can be estimated relatively accurate for the system, both in the start and the end of the simulation. The two states are marked by the ends of the line displayed in Figure 5.20, which corresponds to the following values;  $U_{\text{load,start}} = 213.14$  V and  $P_{\text{load,start}} = 7.25$  kW, to  $U_{\text{load,end}} = 191.66$  V and  $P_{\text{load,end}} = 5.87$  kW. The estimated characteristics are illustrated as curves in Figure 5.21, and the two voltage-power relationships given above are marked with X's in the figure. The line from Figure 5.20 fits between the two points.

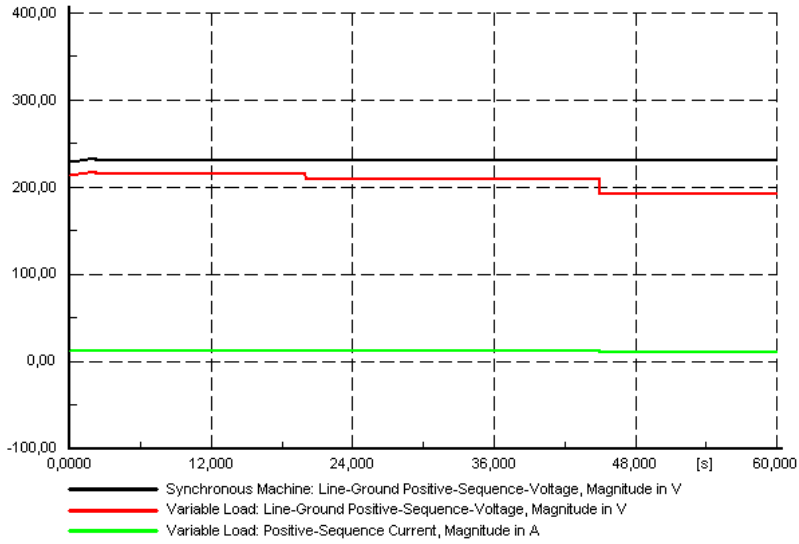


Figure 5.17: *The simulated phase-voltage [V] and current [A] magnitudes during scenario System: Arbitrary.*

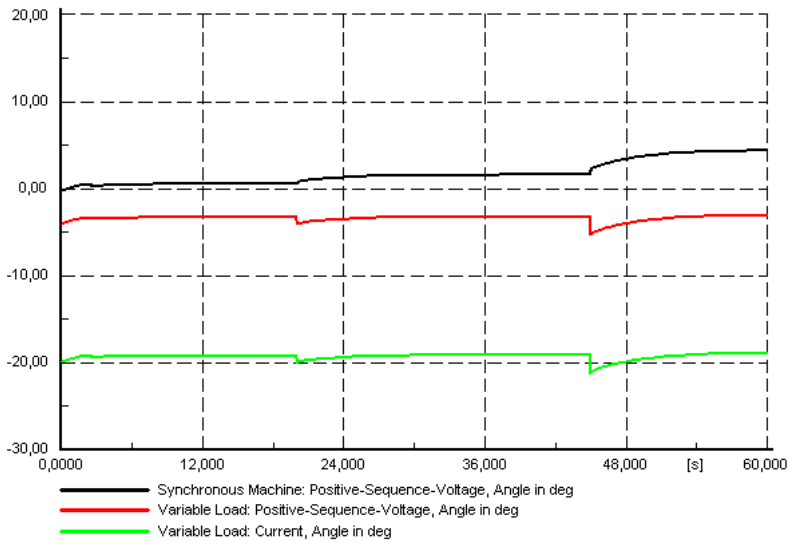


Figure 5.18: *The simulated phase-voltage and current angles [deg] during scenario System: Arbitrary.*

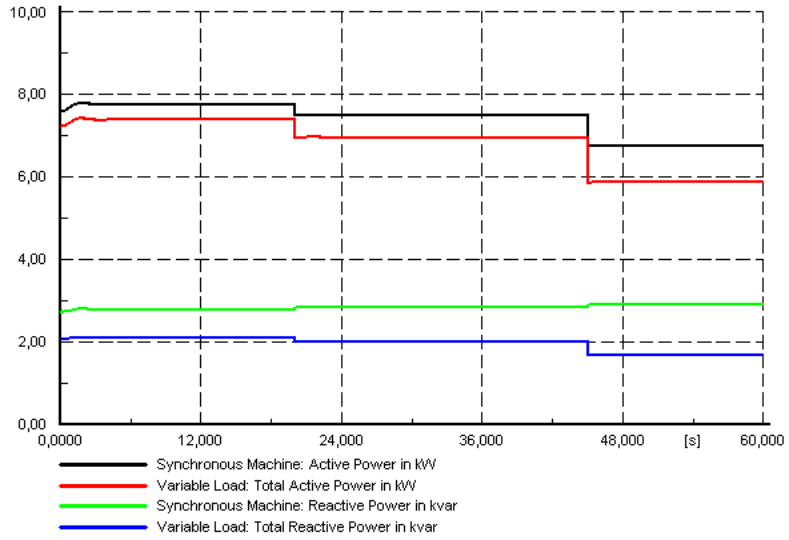


Figure 5.19: *The simulated three-phase power flows during scenario System: Arbitrary.*

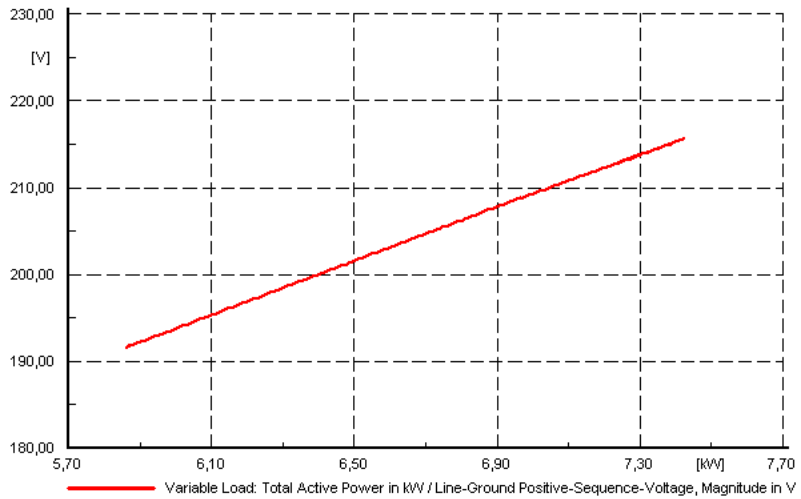


Figure 5.20: *The changed relationship between the phase-voltage and three-phase power during during scenario System: Arbitrary.*



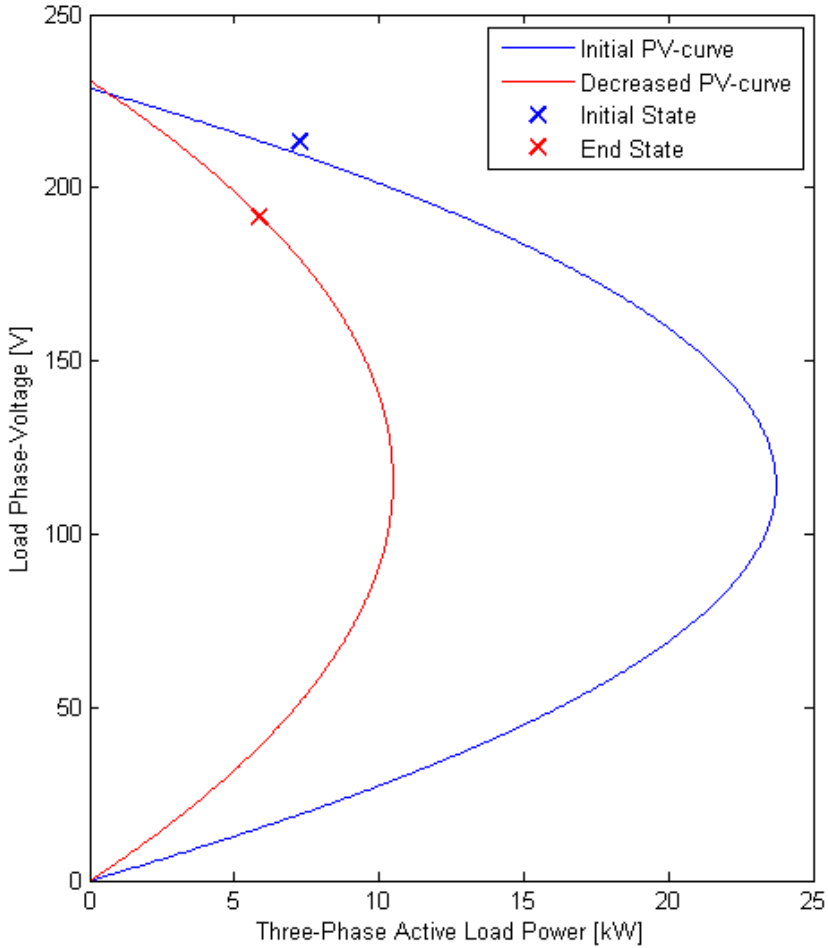


Figure 5.21: Illustration of the reduced voltage-power characteristic as a result of increased system impedance. Curves are based on the voltage-power characteristic estimation utilized in the measurement interface (described in Section 3.3.2.2), and markers indicates each end of the line displayed in Figure 5.20.

## 5.2 Measurement Interface Validation

A major objective of this thesis was to develop a credible measurement interface (MI), that calculates a series of parameters, with high validity. When receiving measurements performed in the lab, there are various sources of error that could alter the results.

### 5.2.1 Recreating Simulation Results

In order to test the developed MI, while excluding the possible errors introduced by real-time measurements, the voltage and current magnitudes and angles from the model simulations, were used as input for the MI. A separate MI was developed, in order to use other inputs than real-time measurements. This application supports both loading of previously saved measurements, and loading of phasor magnitudes and angles exported from PowerFactory. The only changed concept of the application, is where the inputs are acquired from. The subVIs calculating the power system parameters, are identical to the ones used in the real-time MI.

The calculated parameters from the MI was first exported from LabView, and then imported into MatLab, together with the PowerFactory data. Table 5.4 shows which PowerFactory datasets were used as input for the measurement interface, and which could be directly compared to results from the MI.

Table 5.4: *Model simulation results used as input for the measurement interface.*

Test Scenario	Figure reference		Dataset
Load: Lab-average	<i>Input</i>	5.9	Phasor magnitudes
	<i>Input</i>	5.10	Phasor angles
	<i>Comparing</i>	5.11	Power flows

After having performed the *Load: Lab-average* scenario in PowerFactory, the phasor magnitudes and angles were exported into their own separate text files. These were loaded into the MI, and the subVIs calculated and visualized the system state during the simulation.

#### 5.2.1.1 Power Flow

Figure 5.22 illustrates the estimated voltage-power characteristics, and the simulated power flow, as they appear in the MI. The power flow display is almost identical to PowerFactory power flow illustrated in Figure 5.11. The deviations in power flow calculations from each time frame, was obtained with MatLab, after importing both the PowerFactory simulations, and the MI calculations. These

deviations are plotted in Figure F.1, found in Appendix F, and the maximum deviation for active power generated and consumed, and reactive power generated and consumed, are summarized in Table 5.5.

The shape of the estimated voltage-power-characteristics in the MI, seems reasonable accurate. The parameter values in the maximum power transfer state in the simulation (see Figure 5.11) was  $U_{\text{load}} = 120.149 \text{ V}$  and  $P_{\text{load}} = 8.545 \text{ kW}$ . The PV-curve displayed in Figure 5.22, is given as phase-voltage versus single-phase power. It should have been provided as three-phase power in order to be compared directly, but a multiplication with three is easily performed in retrospect.

The peak of the PV-curve exceeds the 3 000 W mark, tending towards 3 100 W. This equals an estimated maximum power flow of almost 9 300 W, i.e. 9.3 kW. According to the power flows simulated, this is unobtainable, since the load power starts to decrease again after reaching 8.545 kW. The difference might lie in the assumptions made for estimating the maximum power. The utilized estimation is described in Section 3.3.2.2, which does not take restrictions on the load power factor as input. Since the only changing variable was the variable load, the load impedance will have difficulty reaching the complex conjugate of the system impedance. This illustrates the difference between the maximum power transfer, and the system's loadability limit.

### 5.2.1.2 Impedances

Some of the parameters calculated in the measurement interface were not possible to extract from PowerFactory directly, but were calculated in MatLab from the phasor magnitudes and angles, by utilizing previously derived equations (Equation 3-21 and 3-25). The resulting plot is provided in Figure F.2 in Appendix F, and the visualization performed by the MI, is displayed in Figure 5.23. The differences between the to calculations are plotted in Figure F.3, and the maximum deviations in each parameter are summarized in Table 5.5.

Table 5.5: *Maximum deviations in parameter calculation, between PowerFactory and LabView, during scenario Load: Lab-average.*

<b>Power deviations:</b>		<b>Impedance deviations:</b>	
Active produced	$9.900 \cdot 10^{-5} \text{ W}$	$R_{\text{load}}$	$5.032 \cdot 10^{-5} \Omega$
Active consumed	$5.000 \cdot 10^{-6} \text{ W}$	$X_{\text{load}}$	$4.981 \cdot 10^{-5} \Omega$
Reactive produced	$5.700 \cdot 10^{-5} \text{ VAr}$	$R_{\text{sys}}$	$5.011 \cdot 10^{-6} \Omega$
Reactive consumed	$5.000 \cdot 10^{-6} \text{ VAr}$	$X_{\text{sys}}$	$5.164 \cdot 10^{-6} \Omega$

The deviations between PowerFactory and the MI is all in the range of  $10^{-5}$  or smaller. This precision is sufficiently accurate for most studies of the real-time

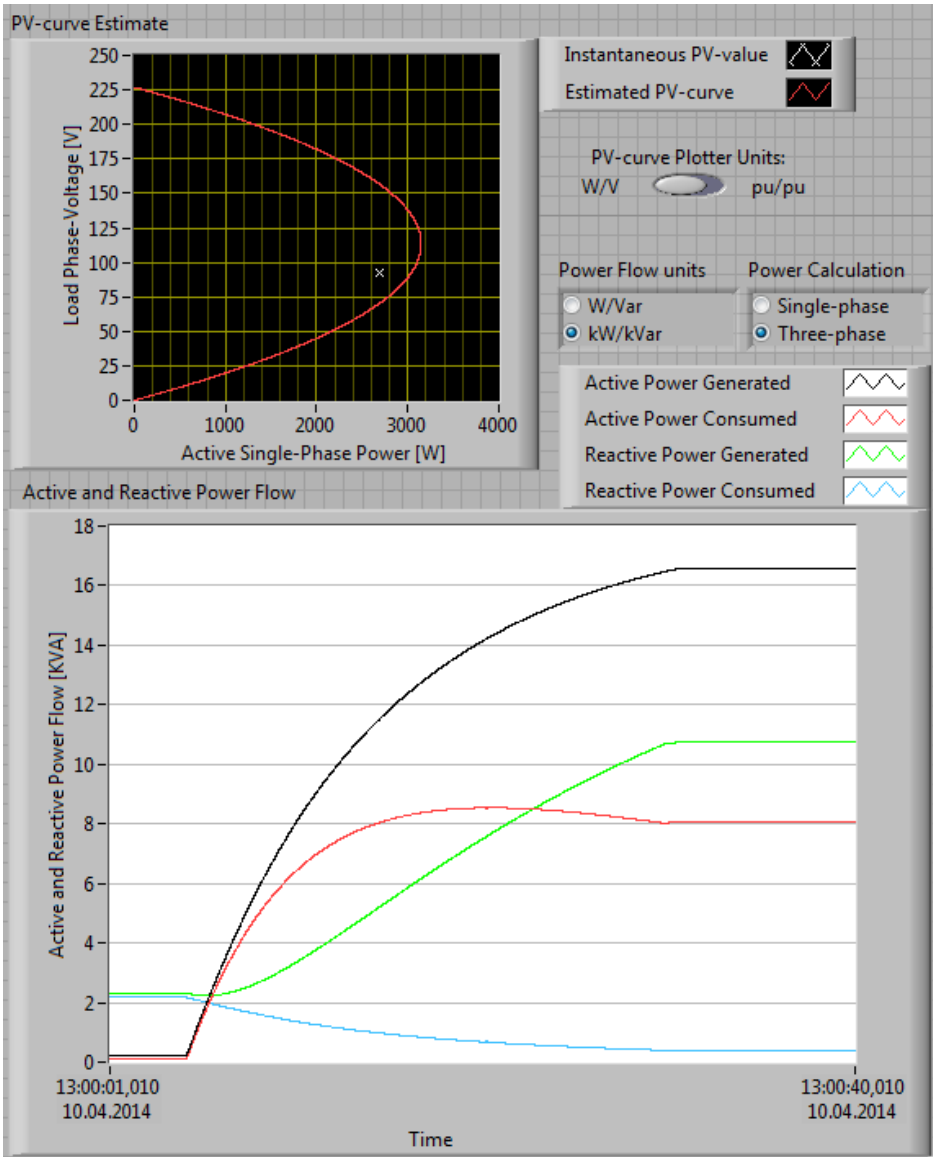


Figure 5.22: The estimated voltage-power characteristics and the generated and consumed active and reactive powers calculated by the measurement interface, based on the PowerFactory simulation of voltage and current magnitudes and angles as input.

power system state.

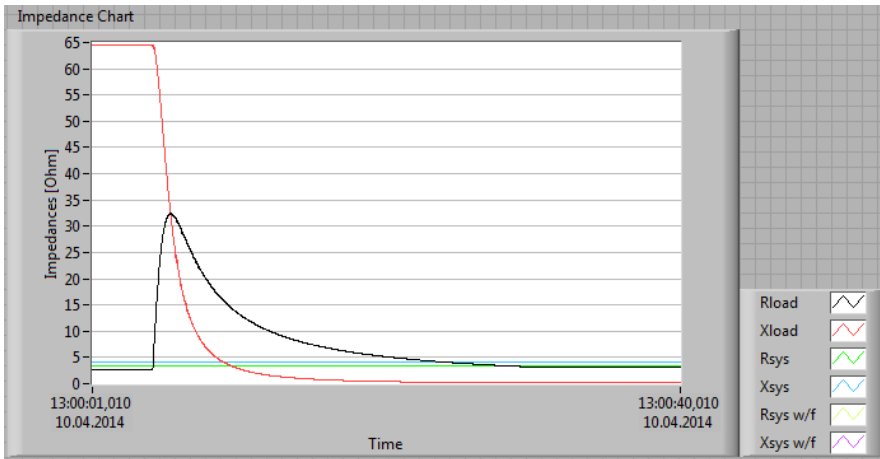


Figure 5.23: *The estimated system and load impedances split up in their resistance and reactance components, based on the PowerFactory simulation of voltage and current magnitudes and angles as input.*

### 5.2.1.3 Voltage Stability Indices

The stability indicators presented in Section 3.3.3 and 3.3.4 was implemented in the MI, by the subVIs described in Section 4.3.2.5 and 4.3.2.5. What remains to discover, is whether the indicators actually yield correct information regarding imminent voltage instability. Figure 5.25 illustrates the indicator values during the increased load power scenario. The black line is the ISI indicator, the red line is the  $VSI_{SCC}$  indicator, and the green line indicates the limit, which both indicators should be less than.

The ISI crosses the limit at the same point as the load power in the PV-curve and power flow plot starts to decrease. An ISI larger than the limit indicates voltage instability, assuming normal operating conditions, while the VSI can only indicate the distance to the instability point. From the figure, it appears it reaches its maximum value at the correct time. However, the magnitude of the maximum point is too small, since it should be closer to the limit before decreasing again.

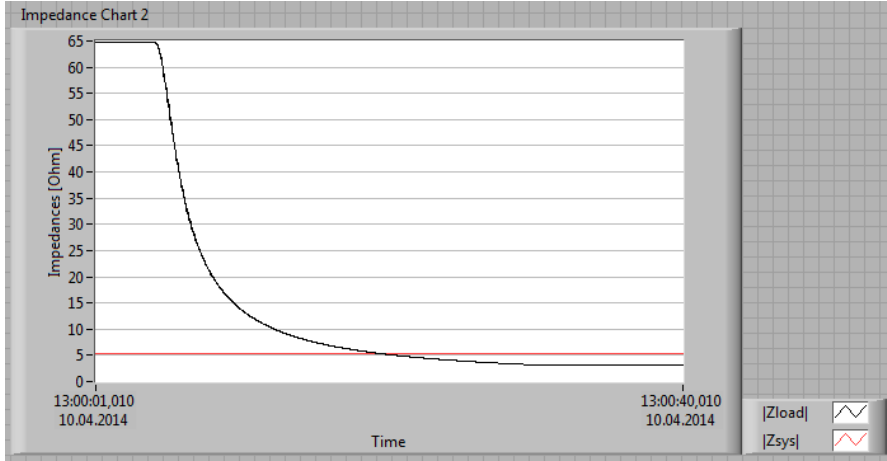


Figure 5.24: The estimated system and load impedances visualized as their absolute values, based on the PowerFactory simulation of voltage and current magnitudes and angles as input.

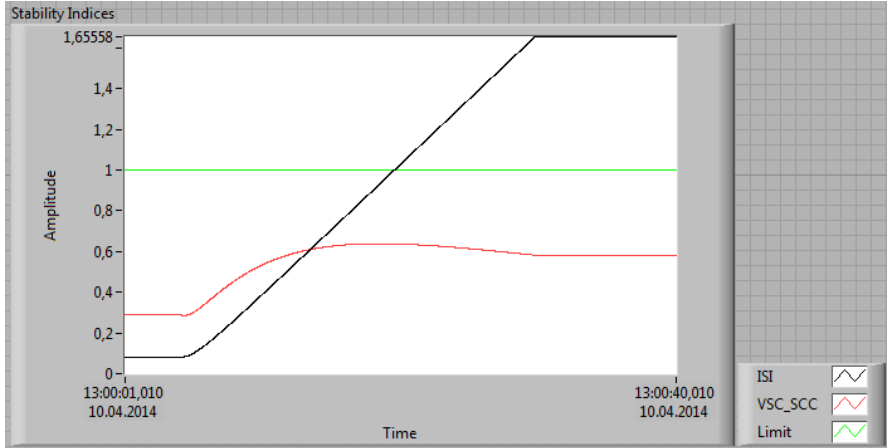


Figure 5.25: The voltage stability indicator values calculated by the measurement interface, based on the PowerFactory simulation of voltage and current magnitudes and angles as input.

#### 5.2.1.4 Phasors

The phasor visualizations presented in Section 4.3.2.3 may yield intuitive information about the state of the power system. Five instant states of the phasor diagrams are provided in Appendix G, illustrating the changing phasors when the load power demand is being increased. The phasors at the end for the simulation is presented in Figure 5.26.

The figure shows that the current is increased, which lead to larger voltage drop across the system, which again increased the angular and magnitude differences between the generator and load voltage. These phasor diagrams supplies the grid operators with this information instantaneously, and are very suited for measurement interfaces. The phasors illustrated are credible, and complies with both theory and manual calculations based on the PowerFactory datasets (of voltage and current magnitudes and angles).

### 5.2.2 Measurement Location Error Estimations

Validation of the MI must also be performed with respect to performed and transmitted measurements from the laboratory. There are a number of measurement errors that could influence the results. Some of them are:

- The sinusoidal-to-phasor conversion in the PMU may be flawed.
- One or more of the PMU input channels may be inaccurate.
- The different phases may be unsymmetrical at different locations in the power system set-up .
- The measurement outlet itself, or the measurement signal transformer, may introduce faults.

As many as possible of these plausible error sources have been eliminated by performing extensive tests. All PMU input channels where connected to the same phase in the same measurement location in order to reveal inaccuracies between the different input channels. The values was obtained from readout of the PRL interface directly, without any influence from the MI developed in this thesis.

A PMU channel was also connected simultaneously with an oscilloscope channel, to uncover the possible inaccuracy of the PMU inputs, and transmitting functionality, overall. This is also a reasonable test to perform, although the oscilloscope is prone to human readout error. Additionally, all three phases at several measurement locations where measured by the three PMU input channels in order to discover any unsymmetrical behaviour between the phases.

The data and details of these tests, are provided in Appendix H. The most important discovery was that the magnitudes of the voltages were uneven, with

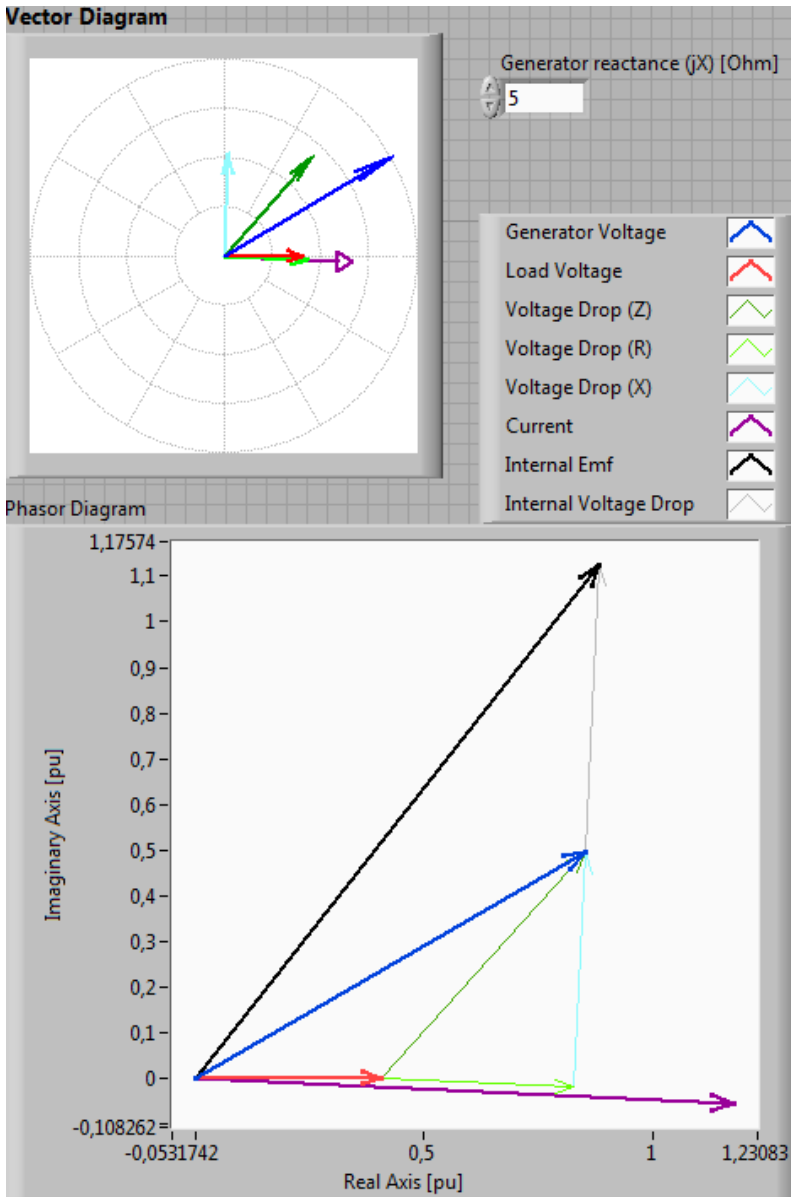


Figure 5.26: The phasor visualization at the end of scenario Load: Lab-average, calculated by the measurement interface based on the PowerFactory simulation of voltage and current magnitudes and angles as input.



the R-to-S-line-voltage being the largest (equivalent to A-B-line-voltage). Since this is the voltage measured, it will influence the calculated consumed power and phase diagrams. The three input channels of the PMU were found to give exactly the same phasor value to the PRL, when connected to the same phase in a measurement location simultaneously. The peak-to-peak magnitudes of the signals measured by the oscilloscope, was also consistent with the PMU phasor value, when converted into rms-value.

### **5.2.3 Comparisons with Laboratory Measurement Panels**

In addition to compare the MI calculations with the simulation data, they were also directly compared to the values given by the laboratory measurement panels during different load power demands. The parameters and their values for four different load power demands were noted, and are documented in Table 5.6.

The voltage measured at the generator did not change for either the laboratory panels or the measurement interface during the various load power demands, and were therefore not included in the table. The laboratory panel showed a line-voltage of 398 V, while the MI displayed a phase-voltage of 232 V. When multiplied with the square root of three, it corresponds to a line-voltage of 401.84 V, which deviates with 3.84 V from the panel value. This may be due to either lack of documented decimals of the phase-voltage from the MI, or inaccurate readout of the gauge display at the generator panel. It is assumed that the laboratory panels are correct, but human readout might influence the accuracy and correctness of the laboratory measurements.

The load voltage panel clearly showed different magnitudes for the different line voltages, and with the measured phase coincidentally having the largest magnitude, this deviation is reflected in Table 5.6. This difference between load voltage phases indicates that the power system set-up has some unsymmetrical properties. The maximum documented deviation was 1.3 V. The current appears more accurate, with maximum deviation of 0.54 A, but when compared percentage this was not the case. The error source originating from gauge readouts may be relevant in this aspect.

When the frequency measured by the PMU was compared to the value displayed at the generator display, the maximum deviation was 0.23 Hz. Since the frequency display at the generator was digital as well, the gauge readout was not influencing the deviation. However, decimals of both displays varied during steady state, and a synchronized documentation of instantaneous values was difficult to perform.

The system impedance, calculated by the MI, was the only parameter to change significantly with respect to changed frequency. This is linked to the

equation for estimating reactance from an inductance,  $X = j2\pi fH$ . The subVI performed fairly well when taking this into account.

When the generated active and reactive power calculated by the MI was compared to the value displayed at the laboratory panel, it was found to deviate with a value of 0.3 kVA for each. Although most of this might be due to human difficulty performing exact readouts from gauges, some of the deviation may also be due to only measuring a single phase at each measurement point in a three-phase system, and extrapolate the calculated single-phase power. This is a likely source, since the voltages were shown to not be perfectly symmetrical.

Table 5.6: Power system parameters calculated by the MI during four different load power demands directly compared to the values given by the laboratory measurement panels. *N/A* indicates "not applicable", since the laboratory obviously does not possess a panel estimating the system impedance.

Readout location	$P_{\text{gen}}$ [kW]	$Q_{\text{gen}}$ [kVAr]	$f$ [Hz]	$U_{\text{load}}$ [V]	$I$ [A]	$Z_{\text{sys}}$ [ $\Omega$ ]
Lab. panels	10.6	3.75	46.95	290	16	<i>N/A</i>
	10.5	3.70	50.00	290	16	
MI	10.5	3.60	46.75	290.98	15.94	$3.23 + j3.66$
	10.5	3.59	50.16	290.98	15.92	$3.24 + j3.91$
Deviations	0.1	0.15	0.2	-0.98	0.06	<i>N/A</i>
	0	0.11	-0.16	-0.98	0.08	
Lab. panels	8.80	3.0	47.50	307	12.6	<i>N/A</i>
	8.75	3.0	50.00	307	12.5	
MI	8.63	2.95	48.00	308.31	13.00	$3.34 + j3.74$
	8.60	2.81	49.91	308.31	13.04	$3.34 + j3.91$
Deviations	0.17	0.05	-0.097	-1.3	-0.4	<i>N/A</i>
	0.15	0.19	0.091	-1.3	-0.54	
Lab. panels	6.0	2.0	50.00	330	8.5	<i>N/A</i>
	6.0	2.0	48.00	330	8.5	
MI	5.7	2.15	50.23	330.82	8.8	$3.60 + j3.97$
	5.7	2.15	47.77	330.82	8.8	$3.61 + j3.82$
Deviations	0.3	-0.15	-0.23	-0.82	-0.3	<i>N/A</i>
	0.3	-0.15	0.23	-0.82	-0.3	
Lab. panels	3.2	2.0	48.00	353	5	<i>N/A</i>
	3.2	2.0	50.00	353	5	
MI	2.7	2.3	47.97	353	4.86	$4.08 + j4.23$
	2.7	2.3	49.94	353	4.86	$4.133 + j4.35$
Deviations	0.5	-0.3	0.031	0	-0.1	<i>N/A</i>
	0.5	-0.3	0.059	0	0.14	

## 5.3 Laboratory Experiments

The motivation, and initial approach, for the experiments performed in the laboratory, are described in detail in Section 5.3.1. The results obtained during the two tests, increased load power demand and varying system impedance, are presented in Section 5.3.2 and 5.3.3 respectively.

### 5.3.1 Test Descriptions

The test scenarios that are of interest, involves increased load power demand, and varying system impedance. The former scenario represents peak-demand-periods in a supply grid, and illustrates how the load voltage and overall system behave until a voltage collapse occurs, or the system is brought back into a more stable state. The latter scenario illustrates the system behaviour if one or more of the power lines, supplying the load, are disconnected. For example, a tree falling over the line, or for maintenance purposes. The following sections will go into detail on how to perform these scenarios, as experiments, in the laboratory.

#### 5.3.1.1 Gradually Increasing Load Power Demand

During this scenario, it is interesting to see how close to the unstable operating point the system can get. That would allow the stability indicators, presented in Section 3.3, to illustrate their reliability, or to discover their flaws during real-time operation.

In order to reach this loadability limit, the system impedance needs to be as large as possible, letting the load impedance be the smallest of the two (see Figure 3.13). To achieve this, sections 11 and 12 of the flexible line equivalent will be disconnected, and the sections 21, 22, 23 and 13 will be set to maximum impedance, as calculated in Table 4.5. A three-phase variable reactor may be added to the set-up, if the maximum impedance of the line was proved to be insufficient.

The initial condition of the variable load, is not connected. While performing the increased load power demand scenario, the variable resistance is first connected with its maximum value, and then manually decreased stepwise every fifth second. The measurements are logged by the measurement interface, and saved for later reruns.

#### 5.3.1.2 Varying System Impedance

The system impedance in the lab was only changed by switching the amount of series-connected reactors in the flexible line equivalent.

Another scenario of almost the same purpose was also performed, in order to validate the measurement interface's calculations. The important parameters from both the laboratory panels, and the measurement interface, were documented for a number of different system impedance states. The states were kept at steady state during the readout, and the load power demand was kept constant throughout the experiment. The parameters taken into consideration are:

- Generator voltage
- Load voltage
- Active and reactive power, produced by the generator
- System frequency
- Calculated system impedance (no counterpart in the laboratory displays)

### 5.3.2 Increasing Load Power Demand Results

The scenario approach provided in Section 5.3.1.1 was conducted as described. The voltage and current magnitudes, and angles, measured in the laboratory, are displayed in Figure 5.27 and 5.28. The signals start out very linear, before changing, which represents the initial state before any load changes to the system were made. The resistance was disconnected, while the capacitor was connected, and the current angle was approximately  $-90^\circ$ .

Then the load power demand was increased manually every fifth second, which results in a larger current. This increased the voltage drop across the system impedance, and thus decreased the load voltage simultaneously. Some ripples were formed by the action of load impedance switching, but they were not significantly influencing the measurements. The current angle was approaching the load voltage angle, while the generator voltage angle was increasing, and diverging from the load voltage angle.

The generator voltage magnitude was fairly constant throughout the entire test, except in a confined period during the latter half of the experiment. The load voltage magnitude was also suddenly changing its stepwise decreasing path. Both of these came as a result of the generator reaching its maximum generation of power, which is apparent from Figure 5.29. Right before the sudden decrease of power, the generator was supplying  $S_{\text{gen}} = 14 + j5.4$  kVA, which is equivalent to 15.00 kVA in apparent power, while the load was consuming 9.7 kW active power. The frequency of the power system had decreased to below 46 Hz, and the generator could not supply a larger load (see Figure 5.30).

The load impedance was kept at this level a bit longer than five seconds, to see if the system stabilized itself. When it did, the load was decreased another

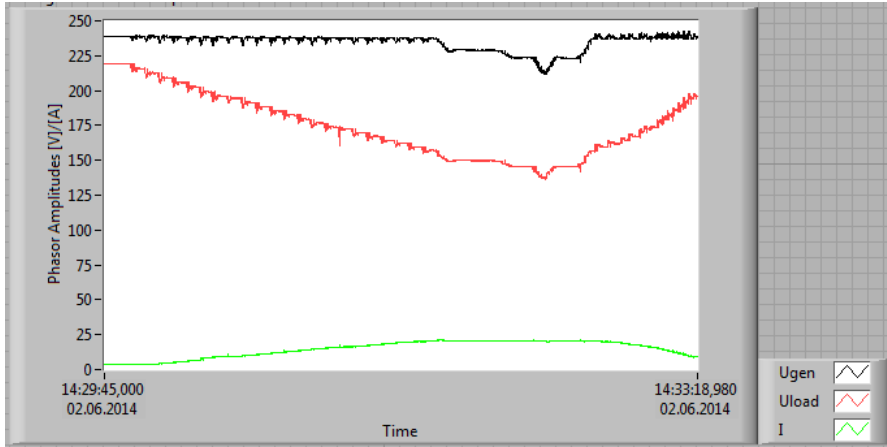


Figure 5.27: *The measured voltage and current magnitudes during increasing load power demand in the laboratory.*

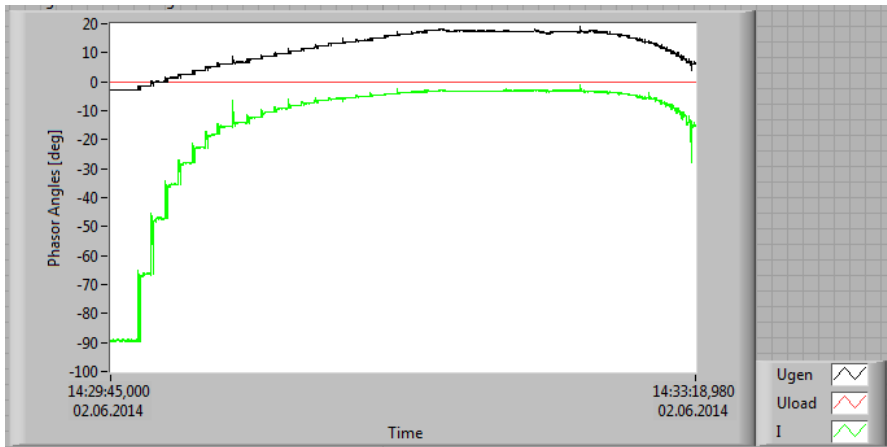


Figure 5.28: *The measured voltage and current angles during increasing load power demand in the laboratory.*

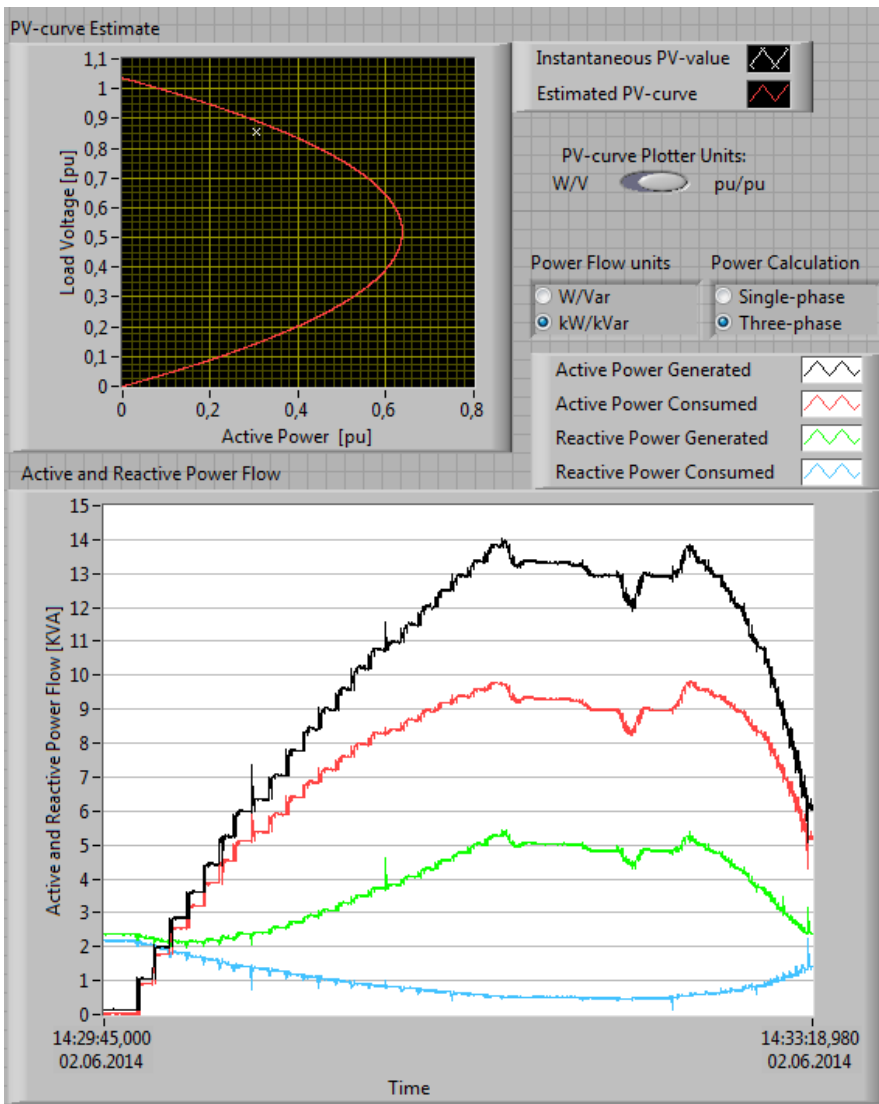


Figure 5.29: The estimated voltage-power characteristics at the end of the saved scenario, and the generated and consumed active and reactive power calculated during an increasing load power demand in the laboratory.

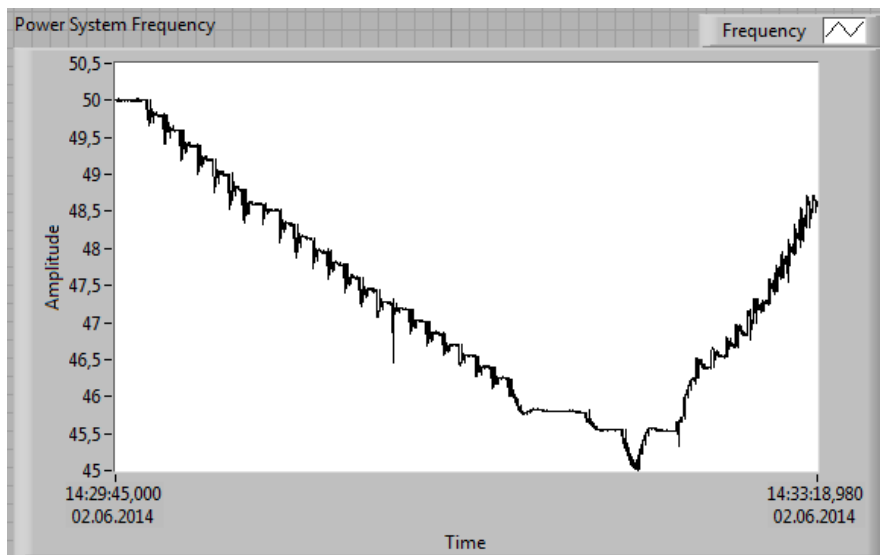


Figure 5.30: *The measured power system frequency during an increasing load power demand in the laboratory.*

level, but quickly increased again to avoid voltage collapse (see Figure 5.31). To end the test, the load impedance was gradually increased until its maximum was reached. The saved data from the measurements ended during this load power decrease. As seen in Figure 5.32, the absolute value of the load impedance was never decreased below the absolute value of the system impedance. This indicates that the loadability limit was not reached during this experiment.

The voltage-power characteristic, also displayed in Figure 5.29, corresponds to the end of the saved measurements, during the mentioned load impedance increase. The current voltage-power level almost coincides with the estimated PV-curve, which it did during most of the test. The greatest exception occurred in the beginning of the test, just when the load impedance started to decrease. This change lead to a relatively large difference in estimated system impedance, from  $Z_{\text{sys}} = 3.67 + j5.77 \Omega$  to  $Z_{\text{sys}} = 3.36 + j3.93 \Omega$ . Since the maximum active power transfer is estimated based on the system impedance, this changed the magnitude of the peak of the PV-curve, as the previously mentioned exception indicates. The estimation formula is also based on that the maximum loadability is reached when  $Z_{\text{load}} = Z_{\text{sys}}^*$ , which is unobtainable when only changing the variable resistor. The loadability limit is therefore less than the maximum power transfer limit.



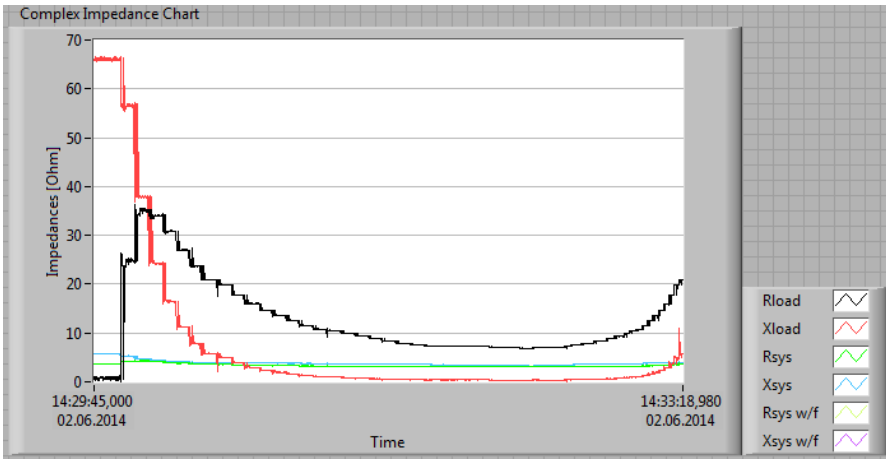


Figure 5.31: *The estimated load and system impedances split up in their resistance and reactance components during increasing load power demand in the laboratory.*

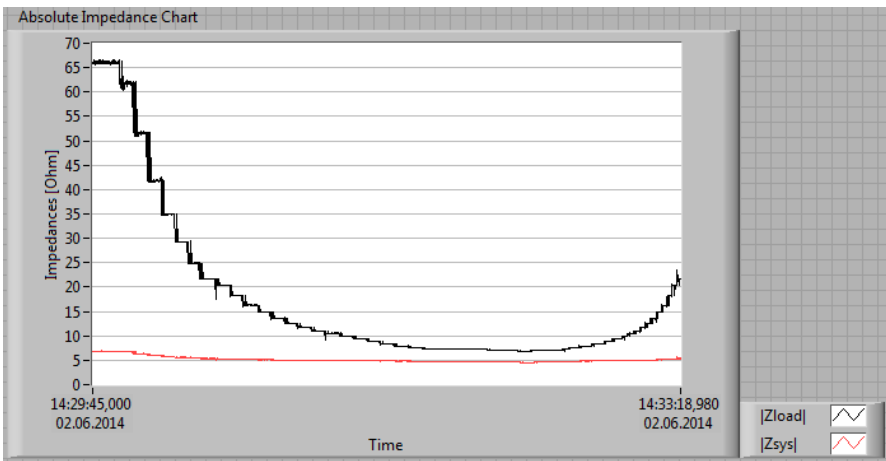


Figure 5.32: *The estimated load and system impedances visualized as their absolute values during increasing load power demand in the laboratory.*

The phasor diagram at the maximum load power demand is presented in Figure 5.33. It shows an increasingly large voltage angle divergence between the reference load voltage angle, and the generator voltage angle. The estimated electromagnetic force (emf) in the generator is even higher. However, according to both the impedances in Figure 5.32 and the ISI indicator displayed in Figure 5.34, the point of voltage instability has not been reached. The absolute magnitude of the load impedance was never less than the absolute value of the system impedance. Since the ISI indicator was validated in the previous section, we can conclude that  $|Z_{\text{load}}| \simeq 1.43|Z_{\text{sys}}|$ , based on the  $\frac{|Z_{\text{sys}}|}{|Z_{\text{load}}|} \simeq 0.7$  readout of Figure 5.34. To reach the voltage instability, and experience the ISI indicator result in a value greater than one, the system impedance should have been higher during the experiment.

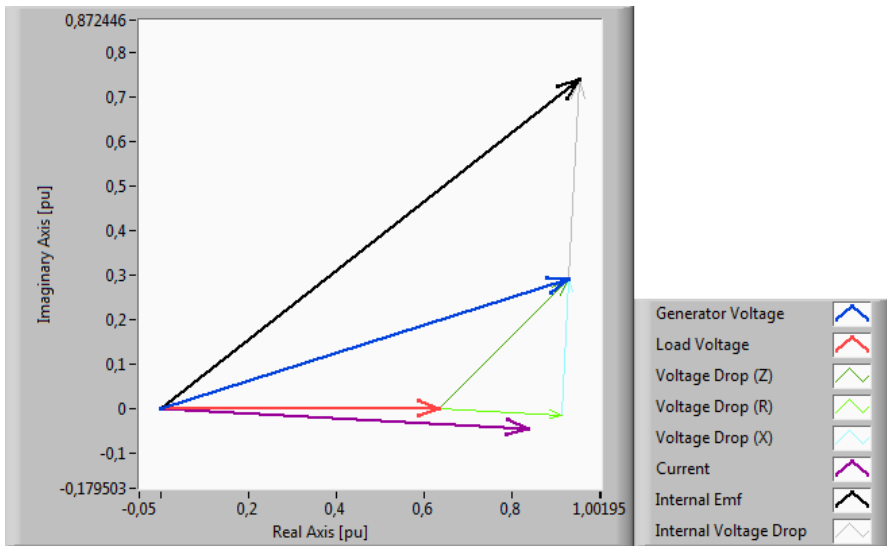


Figure 5.33: *The visualized phasor diagram at the maximum load power demand measured in the laboratory.*

### 5.3.3 Varying System Impedance Results

The system impedance was varied in random direction, in order to measure the differences in voltages, currents, powers and impedances. The load impedance was kept at its highest value, meaning that the load power demand was set to its smallest possible setting. The detailed description is provided in Section 5.3.1.2.

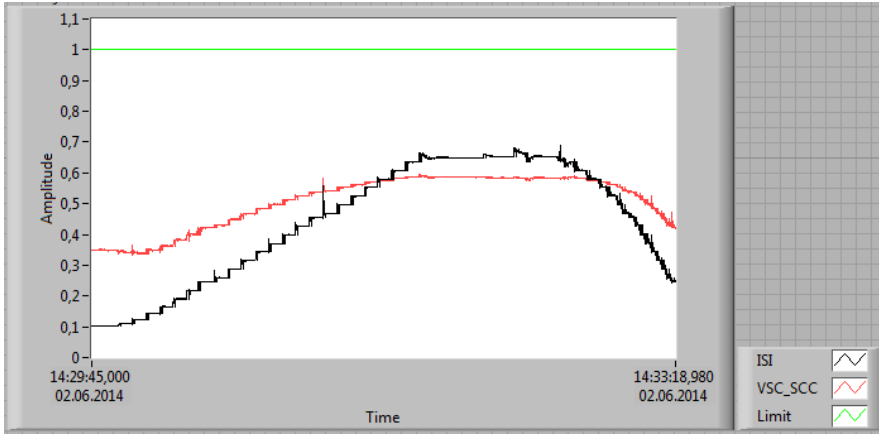


Figure 5.34: *The voltage stability indicator values calculated during increasing load power demand in the laboratory.*

All the trend curves displayed for this test showed very high disturbances when the system impedance was changed. Since this change was implemented physically by turning switches that either short-circuited a series-reactor, or included it, it effectively resulted in an open circuit when the switch transitioned, which make the high disturbances in load voltage and current reasonable. Each switch only implies a small change in system impedance, which make the changes in voltage and current magnitudes, and angles, at the different settings, small, as seen in Figure 5.35 and 5.36. The disturbances have been filtered out in later figures, emphasizing the steady state magnitude changes, which was the objective of this particular experiment.

When the system impedance was changed, Figure 5.37 shows that the active power generated and consumed are barely influenced. The reactive powers on the other hand, varies between 2.67 and 2.35 kVAR for the generated power, and between 2.45 and 2.18 kVAR for the consumed power. This is related to the impedance estimations, visualized in Figure 5.38, where the load reactance was the most influenced parameter. This is clearly governing the changes in generated and consumed reactive power, and is linked with the change in load voltage. Since the system impedance changes, the voltage drop across it changes, and this influences both magnitude and angle of the load voltage, which in turn influences the load impedance in cooperation with the current. Since the load resistance is so small (being not connected during the experiment), the absolute magnitude of the impedance is almost equal to its reactance, which is displayed in Figure 5.39.

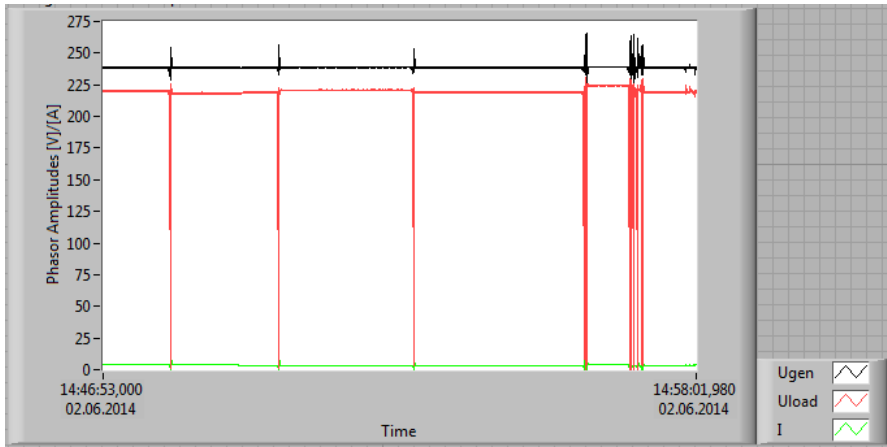


Figure 5.35: *The measured voltage and current magnitudes during varying system impedance in the laboratory.*

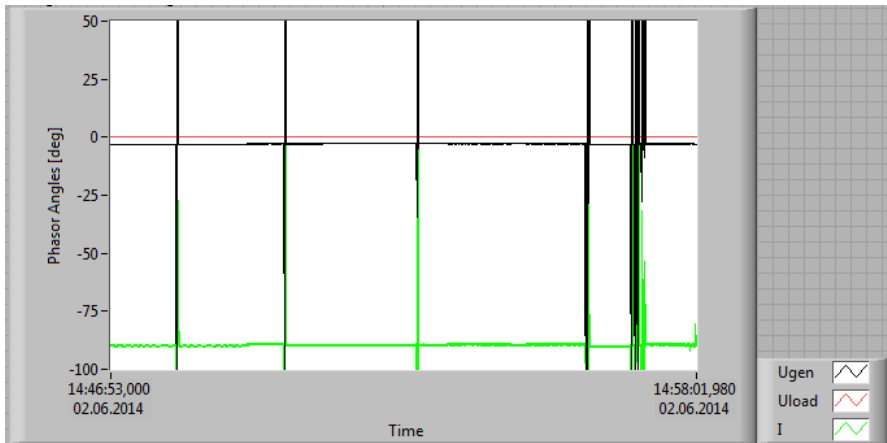


Figure 5.36: *The measured voltage and current angles during varying system impedance in the laboratory.*

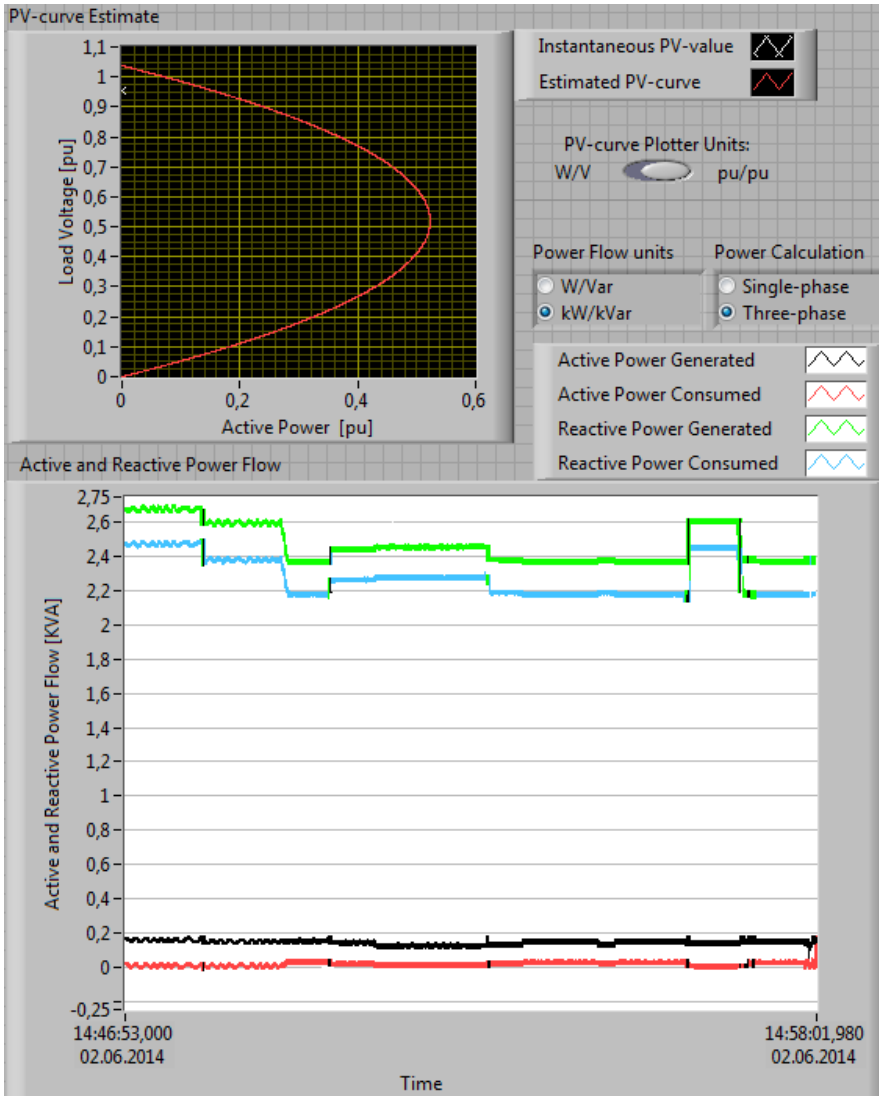


Figure 5.37: The estimated voltage-power characteristics at the end of the saved scenario, and the generated and consumed active and reactive power calculated during varying system impedance in the laboratory, filtered with respect to switching transients.

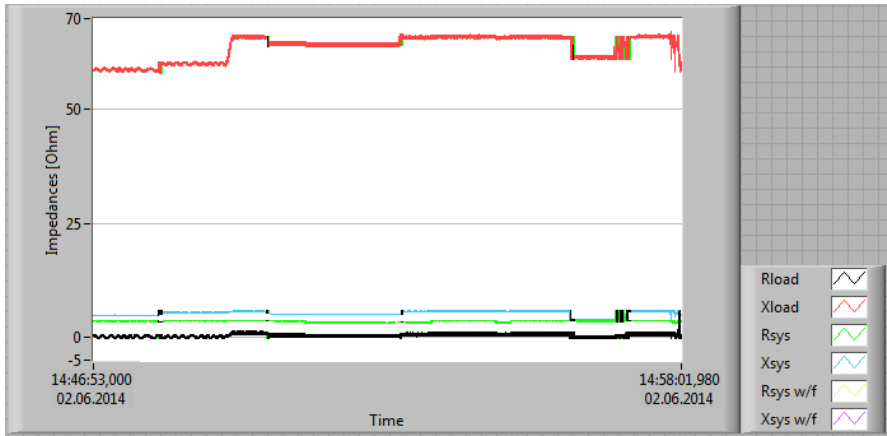


Figure 5.38: The estimated load and system impedances split up in their resistance and reactance components during varying system impedance in the laboratory, filtered with respect to switching transients.

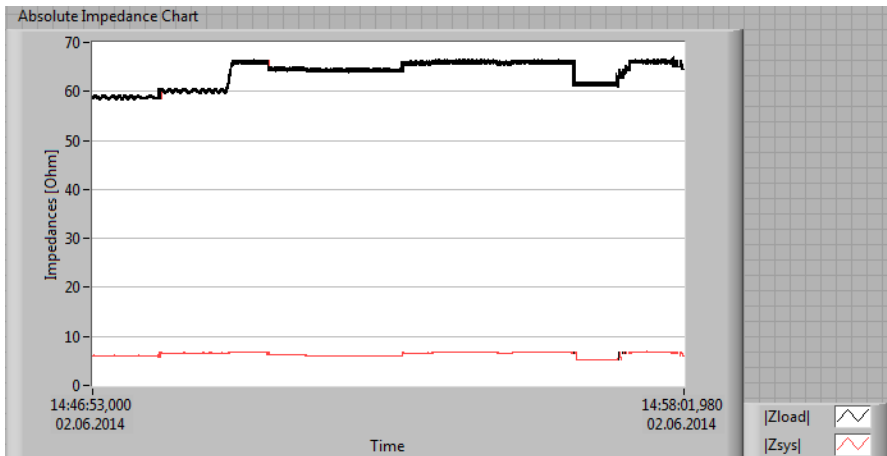


Figure 5.39: The estimated load and system impedances visualized as their absolute values during varying system impedance in the laboratory, filtered with respect to switching transients.

# Chapter 6

## Discussion

Most of the important observations were discussed in the previous chapter. However, they must be brought into context with the overall objective of this thesis, which is to investigate the abilities of a general network information system (NIS), based on PMU measurements. The specific measurement interface (MI), that was developed during this research, has tried to possess the features and accuracy necessary to behave as a NIS, for utilization in a grid operator control room.

### 6.1 Network Information System

By orienting through the state of the art research on synchrophasor measurements, it has become clear that their applications are diverse, and numerous. Among the real-time applications are situational awareness for grid operators a main issue, and tools to aid them in their decision making constitutes the majority of the research papers. Response pattern detection of voltage, frequency and power measurements have been emphasized, and the possibility of developing automated alarm systems based on these patterns, with the objective of increasing system protection and reliability, has been the centre of attention.

The high resolution, and accurate time stamps, inherent in the measurements, make the synchrophasors superior to the SCADA systems used today, and it enables unique possibilities for state estimations, and the before-mentioned pattern detection. They can assist the grid operators by 1) predicting impending system area separations by detecting diverging voltage angles and frequency signals, 2) giving an early warning of power oscillations in the system, created by an

emerging unstable mode, 3) monitoring actual power flow, as well as voltage angle differences, between areas, to discover real-time thermal or congestion issues, and 4) alerting of imminent generator failure, through detecting a leap in the negative sequence current.

## 6.2 Network Information System Abilities

The measurement interface, developed in this thesis, contains a number of these parameters, which are visualized in various ways. All parameters are derived from the voltage and current phasor measurements, conducted by a PMU measuring either a single phase-voltage, a single line-voltage, or a single phase current, at three different measurement points.

### 6.2.1 Voltage and Current Phasor Measurements

The voltage phasors are visual by nature, and a phasor diagram presenting the phasors' amplitudes and angles has a high readability, and improves understanding of the state estimate. Given that the topology of the power system is accounted for when comparing the angles, i.e. transformer phase-shifts, this phasor diagram can indicate the power flow between the various areas as well. The amplitudes can be illustrated with both SI units and pu, but the latter option will include the ability to evaluate whether the voltage level at the location, is within its nominal limits.

Since the phasor diagram only illustrates the instantaneous state of the power system, the voltage amplitude and angle are plotted in their own respective trend curves, where the dimension of time is added, and their stability over time can be evaluated. This type of information might also aid a grid operator with responsibility of many power system monitors simultaneously.

### 6.2.2 Frequency Measurements

The frequency measurements was not very relevant for such a small power system, and has therefore not been devoted much time during this thesis. However, it is possible to follow how the difference between demand and supply changes the system frequency compared to the nominal value, and the measured frequency may be taken into account when estimating reactance in the system. It can also be used to verify the turbine governor response, and investigate the speed drop characteristic, for a given generator node in the system.



### 6.2.3 Impedance Calculations

Sine the current phasor was provided together with the voltage phasors from the generator and load, the impedances can be calculated. These values are best presented in a trend curve as their resistance and reactance, or as their absolute magnitude, with corresponding trend curve for their angles. The system impedance can be utilized in estimations concerning the maximum loadability of the system, to calculate the voltage drop, or to find the grid losses.

### 6.2.4 Power Calculations

The active and reactive power, generated or consumed, at a certain point in the power system, is always of interest to the grid operator. Such data determines whether the system is stable or not, during long-term steady state, but are dependent of the measured state of the system, as well as some prior knowledge of the line impedances. If the PMUs measure voltage phasors at every node in the power system, the generated and consumed powers can be derived, and the state estimation is complete. With some additionally measured current phasors, the impedances in the system can be estimated, and the network information system becomes even more accurate, than when the system impedances are based on manual measurements, or manufacturer data, that does not take the current temperature into consideration.

The estimation of the voltage-power characteristics of the system, can almost be treated as a voltage stability indicator. During normal operating conditions, the voltage-power relationship of the load should be located on the upper half of the (nose-)curve, and preferably further away from the peak than the origin. This is the stable side of the characteristics, and decreased power is met with increased voltage. If the load power demand is increased beyond the maximum loadability of the system, both the voltage and supplied power is decreased further, which would likely lead to a voltage collapse in an actual power grid. The estimation of this characteristic provides the grid operators with a clear, and intuitive, illustration of the distance from the current power system state, to a possibly unstable state.

### 6.2.5 Voltage Stability Indicators

Two dedicated voltage stability indicators were implemented in this NIS; the impedance stability index (ISI) and the short-circuit capacity index ( $VSI_{SCC}$ ). The first index one is based on the ratio between the absolute magnitude of the system impedance, and the load impedance. While  $|Z_{load}| \geq |Z_{sys}|$ , the ISI is less than one, and indicates a stable power system state, given normal operating conditions. If it becomes greater than one, the voltage-power relationship of the

load is located on the lower part of the PV-curve, and the power system operation is at risk of an imminent voltage collapse.

The latter index is somewhat more extensive, and is based on the ratio between the minimum short-circuit capacity, compared to the actual short-circuit capacity in the current state of the system.  $VSI_{SCC}$  yields information about the distance until the system state reaches its maximum loadability, but not whether the system is on the stable or unstable side of the power-voltage characteristics. Therefore, the index should not be used as the only voltage stability indicator in the network information system.

## 6.3 Measurement Interface Validation

While the NIS abilities mentioned in the previous section sounds promising, it is important to validate their correctness and investigate their actual usefulness. The assumptions when deriving the equations, that form the basis of the various parameter calculations and visualizations, might not be suitable for the current power system set-up, or the derived equations may not yield the information intended for the network information system. The MI validation was mainly performed through simulation study, or by using simulation data as input, but some comparisons with the measurement panels in the laboratory were also conducted.

### 6.3.1 Voltage and Current Phasor Measurements

During increasing load power demand, the increasing current magnitude, and angle, changes are evident. The voltage drop across the system impedance is increasing correspondingly, and the real and imaginary part of the voltage drop, are respectively parallel and orthogonal to the current phasor. The phasor diagram performed just as well when simulation results were used as input, as when actual PMU measurements were utilized.

The trend curves illustrating the phasor magnitudes, and angles, proved very informative when studying a time period of laboratory measurements, in retrospect. During varying system impedance, the load voltage was influenced considerably. The switching action is actually inducing an open circuit in the line equivalent, between the two switch states, which effectively results in a load voltage of zero magnitude and arbitrary angle. This behaviour is displayed in Figure 5.35 and 5.36. The confidence in the measurements', and visualized trend curves', validities, has not been diminished by this incident.

When the measurement interface values were compared to the laboratory panels, both the current and voltages were fairly similar. However, the load voltage panel clearly showed different magnitudes for the different line voltages, with the measured phase coincidentally having the largest magnitude. This indicates that

the power system set-up was not perfectly symmetrical. The maximum parameter deviations were 3.84 V, 1.3 V and 0.54 A for the generator line-voltage, load line-voltage and current respectively. The values obtained from the laboratory panels are exposed to human error during gauge readout, which implies that the comparability between the panels and the MI is limited, but it does indicate correct calculations.

### **6.3.2 Frequency Measurements**

During the laboratory experiments, the frequency of the system decreased with increasing load power demand. Its trend curve was very similar to that of the load voltage magnitude, and its minimum value of 45 Hz was reached when the load power demand was at its maximum. It appears to perform as expected, but its significance would be higher in a larger power system, during real-time operation, for example to discover impending area separation. When the frequency measured by the PMU was compared to the value displayed at the generator display, the maximum deviation was 0.23 Hz. Decimals of both digital values displayed, varied during steady state, and a synchronized readout was difficult to perform.

### **6.3.3 Impedance Calculations**

With the simulated phasors as input to the measurement interface, the calculated impedances were almost equal to the impedances calculated directly. The impedance parameters with highest maximum deviation was resistance and reactance of the load impedance, which deviated with  $0.503\ \mu\Omega$  and  $0.498\ \mu\Omega$  respectively. These differences presumably originate from the numerical precision, either from calculations performed in PowerFactory, extraction of numbers from PowerFactory, calculations performed in LabView, extraction of numbers from LabView, or the difference calculations performed in Matlab. In any case, these differences are so small, that from a grid operator perspective, they would be insignificant.

Another interesting observation was that the system impedance changed, when the load impedance decreased, during the laboratory experiment. This was not observed when simulation data was used as input to the MI. The resistance has only a minor dependency of temperature, but the estimated change was quite small as well. The reactance changed by nearly  $2\ \Omega$  from the highest initial value to the lowest value, during the maximum applied load. Some of this might be explained by the frequency dependency of the reactor inductances, but when the calculations considered this aspect as well, the result showed that it did not account for the entire deviation. This might be due to inaccurate frequency measurements, or some unknown phenomena taking effect in the laboratory.

### 6.3.4 Power Calculations

When the simulated voltages and currents from the simulation model was used as input, the active and reactive power calculated in the MI showed a smooth trend curve, comparative to the one provided by PowerFactory. The highest maximum deviation in power calculations, occurred for produced active power by the generator, and deviated with  $0.990\ \mu\text{W}$ . The parameter with the second highest maximum deviation was reactive power produced, at  $0.570\ \mu\text{VAr}$ . This deviation is so small, and as described for the impedance deviations above, it can be neglected for all grid operator purposes.

When the generated active and reactive power, calculated by the MI, was compared to the value displayed at the laboratory panel, it was found to deviate with a value of  $0.3\ \text{kVA}$  for each. Although most of this might be due to uncertainties in readouts from gauges, some of the deviation may also be due to only measuring a single phase at each measurement point, in a three-phase system, and extrapolate the calculated single-phase power. This is a likely source, since the power system was shown not to be perfectly symmetrical.

The form of the estimated voltage-power characteristic in the MI, is fairly accurate, but its maximum active power supplied to the load, is estimated to be larger than the power the system was actually achieving according to the simulation model. Some of the differences stem from varying system impedance estimations from the laboratory experiments, especially when compared to the initial configurations with minimum load power.

Because only the variable load was adjusted during the test, and the variable capacitor remaining constant, the load power factor changed significantly during the increasing load power experiment. With the resistor and capacitor connected in parallel, the load power factor during maximum load power state was difficult to obtain. Additionally, such information about the power system is not expected, and in an actual power grid during normal operation conditions, it can be assumed that the load power factor would not change that substantially, as a result of increased load power.

A second estimation formula was utilized during initial tests to yield a better voltage-power characteristic estimate, and it estimated the actual load voltage-power relationship with lower deviation for high load power demands than the current estimation formula. However, because of the load power factor included in the formula, the estimate deviated considerably when the distance to the maximum load power changed. The second formula would probably have performed better in an actual power grid, but it was useless as a voltage stability indicator in this laboratory set-up, because of considerably changing load power factor.

### 6.3.5 Voltage Stability Indicators

The formula for estimating the minimum short-circuit capacity in the  $VSI_{SCC}$  index, is based on various assumptions regarding the load, at the maximum loadability point, including a constant load power factor as previously mentioned. As this is not the case, in the power system set-up utilized in this thesis, this index performed poorly when based on the phasors acquired from both simulation results, and from laboratory measurements. This is especially apparent during the validation of the MI, since the voltage-power characteristic clearly indicates that the system reaches its loadability limit, while the  $VSI_{SCC}$  never increases beyond 0.7.

At the loadability limit, it should have been closer to one, as the actual short-circuit capacity should have been almost equal to the minimum capacity. However, its maximum value was reached when the system was at the maximum loadability point, which indicates that the assumptions made regarding the maximum loadability, when calculating minimum short-circuit capacity, only results in a wrong magnitude. The indicator may be better suited for a more realistic power system, where the lines are virtually inductive, and the load power factor almost constant, during different load power demands.

The ISI indicator had a simple implementation, and performed well when applied to the simulated phasors. When the load power demand started to increase, the ISI increased in a proportional manner as well. It intersected the stability limit, with the value of one, simultaneously with the power system state reaching its loadability limit, according to the voltage-power relationship. Its simple and direct basis, limits the number of faults occurring, as a result of assumptions, which gives it a large applicability.



## Conclusion

In a wide area monitoring system (WAMS), the main objective is to improve the situational awareness of the grid operator. In order to achieve this, WAMS is based on dynamic real-time measurements performed by PMUs, rather than the stationary information provided by today's SCADA systems. With the high accuracy and sample rate inherent in the PMU itself, and in its connections, it is expected to play a major role in the future smart grids.

Pattern detection of voltage, frequency and power measurements have been emphasized as important study areas, that can aid the grid operators in their decision making process. Automated alarm systems based on these patterns, with the objective of increasing system protection and reliability, can be developed to increase the aid even further. Several voltage stability indicators can be implemented in the network information system (NIS), to improve intuitive readability, in addition to the before-mentioned parameters.

In the course of this thesis, a measurement interface (MI) was developed, with the properties and requirements of a NIS in mind. It contains functionality for displaying the phasors measurements in a phasor digram, several other parameters can be illustrated by trend curves, and the estimated voltage-power characteristic is illustrated in its own type of display.

When the MI utilized simulated phasors acquired from the simulation model, which was subjected to an increasing load power demand event, most of the MI components performed adequately. However, the voltage stability indicator  $VSI_{SCC}$  did not behave as intended, and yielded wrong information regarding the distance until the power system reached its loadability limit. The voltage-power characteristic estimation was based on the maximum power transfer limit, instead of the system's loadability limit, and therefore indicated a slightly higher peak in

consumed active power, than the system achieved during the simulation. Both of these should be investigated further before being utilized as part of a NIS.

During the comparisons between the measurement interface and the laboratory panels, some limitations of the MI was discovered. Since the PMU only uses three signals in total to perform measurements at three different locations in the power system simultaneously, only one of three phases at each location is measured. Since the system was proved to not be perfectly symmetrical, this is the most likely source of errors when comparing the MI to the laboratory measurement panels. In an actual power grid, the PMUs should measure all three phases at each node to increase the accuracy of the NIS.

The voltage stability indicator ISI (impedance stability index), sufficiently indicated the distance to the state, where the system was reaching its loadability limit, during simulations, and whether the current state was located on the upper stable part (during normal operating conditions) of the (nose-)curve, or the lower. Since the power system in the laboratory did not reach its loadability limit during the increasing load power demand experiment, the indicator has not been tested sufficiently during real-time operation to assure its behaviour close to the critical limit.

The phasor diagram, developed in this thesis, provides a highly intuitive visualization of the current state of the system, which significantly increases the situational awareness for the grid operator. The phasor diagram may even prove useful for educational purposes, because of its natural ability to visualize the current state of the system. It also behaved correctly when based on both simulated data, and on phasors measured in the laboratory, and have thus been thoroughly validated.

Trend curves visualizing both phasor magnitudes and angles, system frequency, calculated powers, and impedances, will be great assets in every network information system, and provide valuable information to the grid operator. They are important parameters, since pattern recognition of these can predict impending faults, govern the supply-demand scheduling, analyse primary frequency, or validate models.

All of the parameters developed in this thesis, except the voltage stability indicators and the voltage-power characteristic estimation, have been validated for power system operation, during increasing load power demand, or varying system impedance. Even though the ISI was not tested close to its limit during real-time operation, it performed well on the simulated voltage and current phasors, and should be included among the parameters. The developed NIS based on PMU measurements are sufficiently accurate, greatly improves the situational awareness delivered by the SCADA systems today, and provides invaluable information regarding the real-time power system operation for the grid operators.



# Chapter 8

## Suggestions for Further Work

There are several ways to continue the work of this thesis. First, the theoretical basis of the voltage-power characteristic estimation, and the  $VSI_{SCC}$  indicator, should be reviewed, and their governing assumptions be detected. Their validity to the power system set-up in question should be investigated, before being implemented in the measurement interface library.

The power system set-up, utilized in this thesis, was not well adapted to actual power grid conditions. The main issues arise as a consequence of the high resistance setting for the line equivalent, and with the significantly changing load power factor. If further studies are to be done, the line resistance should be set at a lower value, while keeping the reactance high, and the variable capacitor should either be disconnected, or varied correspondingly to the variable resistor, during the increasing load power demand experiments.

Since the loadability limit of the power system set-up in the lab was never reached, a component providing additional reactance to the system should be included. This was mentioned as a possibility during the power system description provided in Section 4.1, but was not implemented in this thesis due to the system apparently reaching the loadability limit. When it was discovered that the generator was likely reaching its power production limit instead, remaining time until deadline was the limiting factor, for not adding the variable reactor to the power system set-up.

Additionally, another possibility for emulating an actual power grid, would be to run the power system set-up with the load bus connected to the main grid. This would result in a more rigid grid, which is both more applicable to real-time conditions, and would keep the system frequency from deviating as much as it did. This could have kept the system operational, until it reached its actual

loadability limit.

It was discovered during the performed measurements, that the power system was not perfectly symmetrical. Only one input module for the PMU was designed for downscaled measurements, and it had just four input signal sockets available (see Section 4.2.1). Two additional modules of the type NI 9239 should be acquired, and all three phases for each measurement location should be included in the measurements. This requires customization of the measurement interface library, in order for it to take the additional measurements into consideration as well. It would provide better parameter calculations for the three-phase power, both generated and consumed, as well as various impedances and stability indicators.

The next logical step would be to only perform measurements at the load bus, and then try to obtain an accurate state estimation of the power system. This is especially useful in large grids, without needing to perform measurements at every point, or when there is deficiencies in knowledge concerning the power system topology. This approach is linked to increased difficulties when obtaining parameters, such as powers, impedances and voltage stability indicators, which in this thesis was greatly based on the available generator voltage phasor.

# Appendices



# Appendix Contents

<b>A Measurement Interface Template</b>	<b>3</b>
<b>B Matlab script for estimating PV-curve</b>	<b>7</b>
<b>C Layout of Renewable Energy Lab</b>	<b>9</b>
<b>D Measurement Interface Library Overview</b>	<b>11</b>
<b>E Measured Line Equivalent Impedance Values</b>	<b>17</b>
<b>F Plots of Deviations</b>	<b>19</b>
<b>G Phasor Diagram States</b>	<b>21</b>
<b>H Measurement Error Sources</b>	<b>25</b>
<b>Appendix References</b>	<b>27</b>

---

# Appendix A

## Measurement Interface Template

The main components of an operational measurement interface based on the PRL functionality are described in Section 2.4.3. Their visual appearance in a block diagram, and a minimum working example, is illustrated in this chapter. The four attached figures are presented in the order of execution, from left to right.

The required steps for performing measurements, are indicated in Figure A.1, A.2 and A.3. Utilization of the developed subVI named *SaveLoadMeasurement-Data* to save the measured data is illustrated in Figure A.4. A separate buffer containing the measurements to be saved, is starting to build up when the button named *Save data?* from the front panel has been activated. The program must end while the button is active in order for the measurements to be saved.

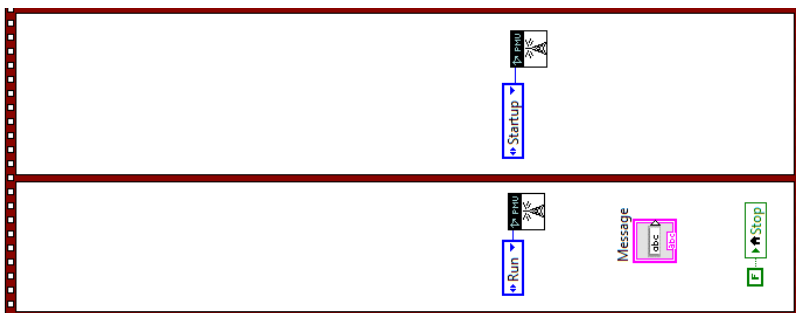


Figure A.1: *The block diagram actions corresponding to step 1 and 2 from the guide provided in Section 2.4.3.*

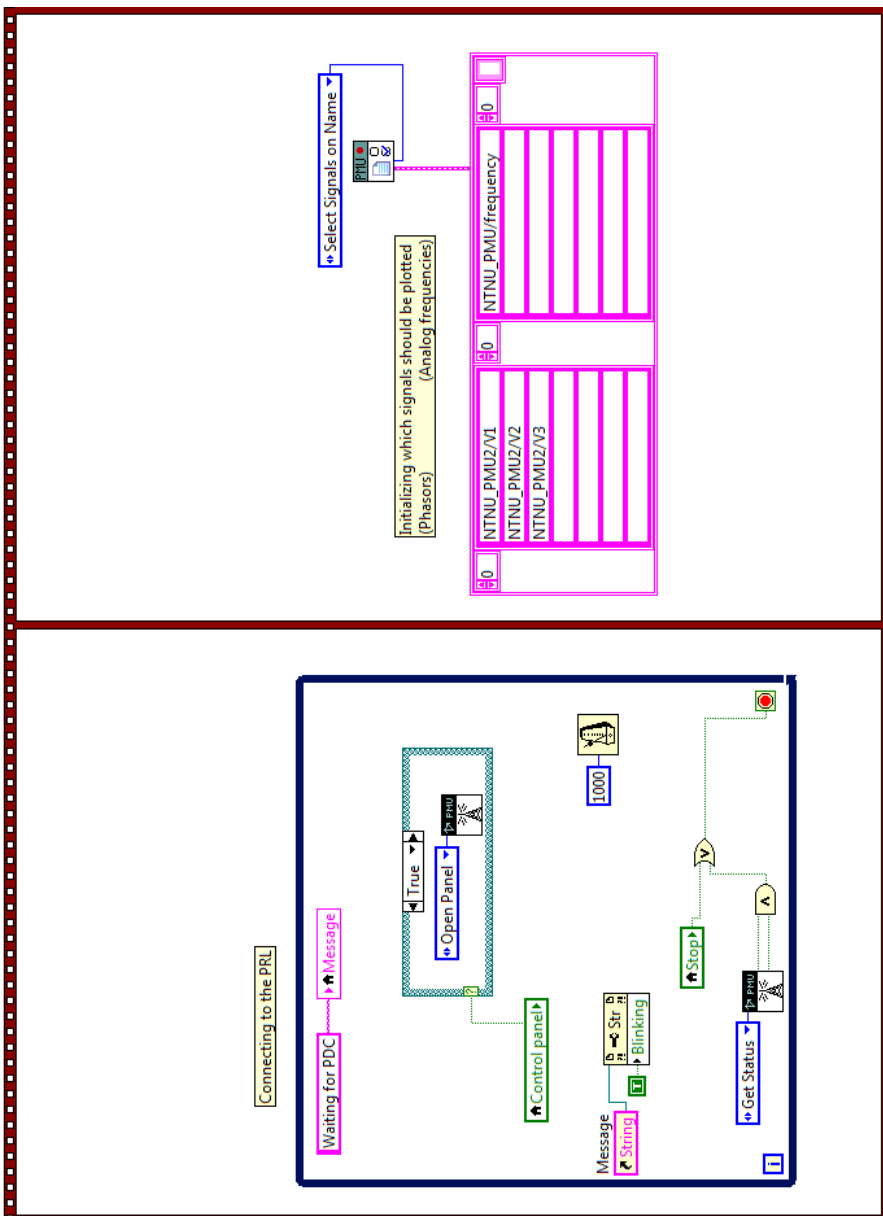


Figure A.2: The block diagram actions corresponding to step 3 and 4 from the guide provided in Section 2.4.3.



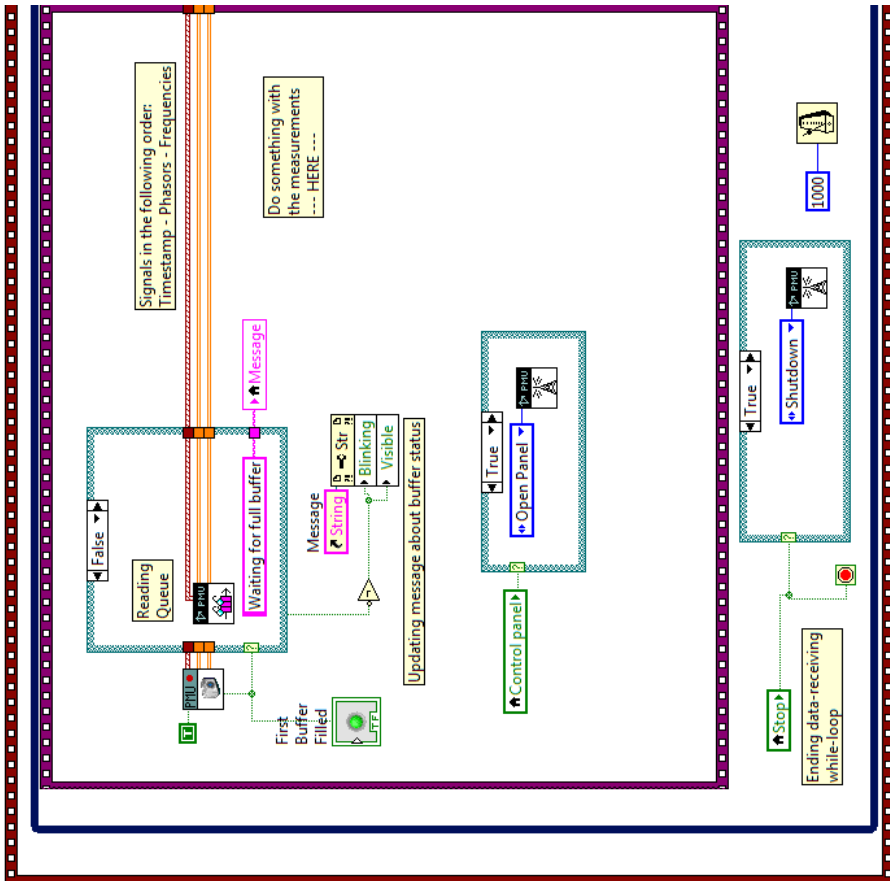


Figure A.3: The block diagram actions corresponding to step 5, 6 and 7 from the guide provided in Section 2.4.3.

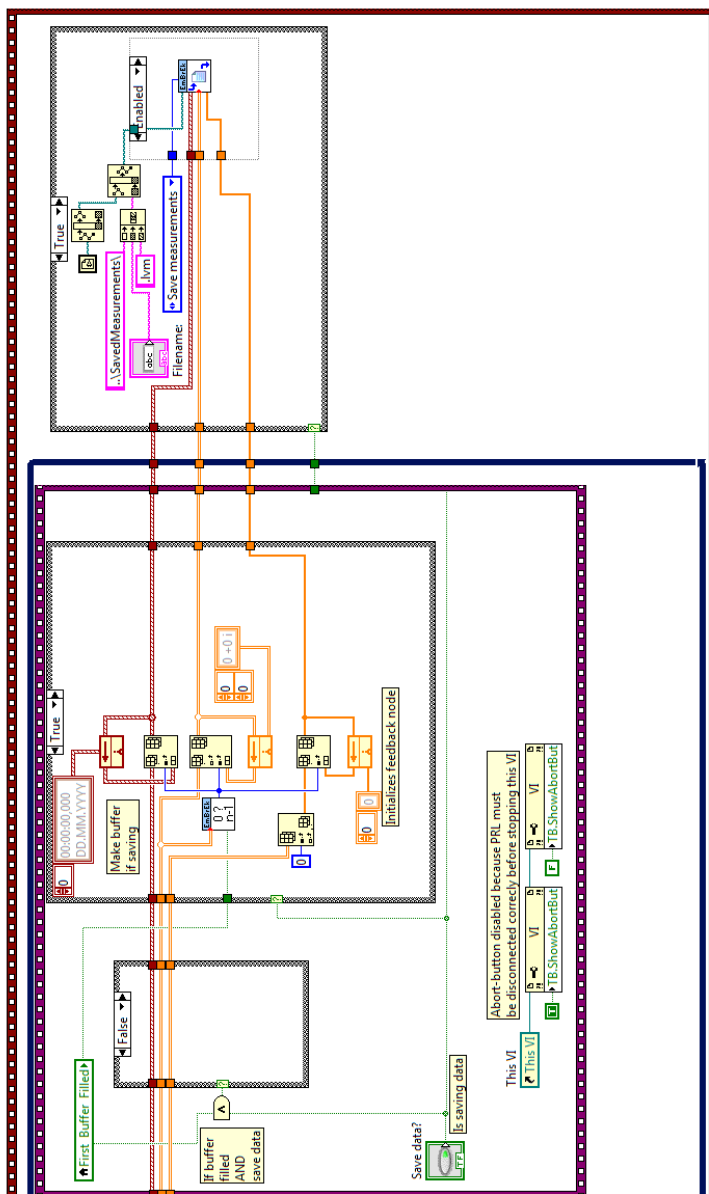


Figure A.4: The block diagram with the subVI *SaveLoadMeasurementData*, presented in Section 4.3.2.1, implemented in order to save the acquired measurements.

# Appendix B

## Matlab script for estimating PV-curve

```
1 %% INITIAL PHASOR VALUES
2 magnitudes = txt2mat('nyMagnitude.txt');
3 angles = txt2mat('nyAngle.txt');
4
5 col = 2;
6 Ugen = magnitudes(1,col) * (cosd(angles(1,col)) + 1i*sind(angles(1,
7   col)));
8 col = col + 1;
9 Uload = magnitudes(1,col) * (cosd(angles(1,col)) + 1i*sind(angles(1,
10  col)));
11 col = col + 1;
12 I = magnitudes(1,col) * (cosd(angles(1,col)) + 1i*sind(angles(1,col)
13  ));
14 col = col + 1;
15 Zsys = (Ugen - Uload)/I;
16 Zload = Uload/I;
17
18 %% PLOTTING OF ACTUAL PV-CURVE
19 input = txt2mat('nyPV.txt');
20 input(:,2) = input(:,2) * 1000 /3; %single-phase in [W]
21 length = size(input);
22 length = length(1);
23
24 %% PROVIDED FORMULA
25 E = abs(Ugen);
26 X = abs(Zsys);
```

```

24 tanphi=0;
25 uProvided = [0:E/1000:E];
26 delta = X.*uProvided.*(sqrt(E^2 + E^2*tanphi^2 - uProvided.^2));
27 pProvided = (-X*uProvided.^2.*tanphi+ delta)/(1+tanphi^2)/X/X;
28
29 %% STORVANN
30 E = abs(Ugen);
31 uStorvann=linspace(0,E,length);
32 p_inner = uStorvann .* sqrt(uStorvann.^2 - abs(Zsys)^2 * (uStorvann
    .^2-E^2));
33 pStorvann = (-uStorvann.^2 + p_inner)/abs(Zsys)^2;
34
35 %% STABILITY BOOK
36 E = abs(Ugen);
37 Vstab = linspace(0,abs(Ugen),length);
38 X = abs(Zsys);
39 phi = angle(Uload) - angle(I);
40 v = Vstab/E;
41 p = -v.^2*sin(phi)*cos(phi) + v*cos(phi).*sqrt(ones(1,length) - v
    .^2*(cos(phi)).^2);
42 Pstab = p .* E^2/X;
43
44 %% BEST ESTIMATE - used in measurement interface
45 uload = linspace(abs(Ugen),0,length); %phase
46 current = (abs(Ugen) - uload) / imag(Zsys);
47 phi = angle(Uload) - angle(I);
48 ploadd = current .* uload * cos(phi); %single-phase
49
50 %% PLOTTING OF ESTIMATED CHARACTERISTICS
51 plot(input(:,2),input(:,1), pProvided,uProvided, pEm,uEm, Pstab,
    Vstab, pBest,uBest, 'Linewidth',2)
52 legend('Actual data', 'Provided formula', 'Storvann', 'Stability book'
    ; 'Best estimate', ...
    'Location', 'SouthEast')
53
54 %axis([0 11000 0 250])
55 ylabel('Load Voltage, U-{'phase'}, [V]')
56 xlabel('Active Load Power CONsumption, S-{'phase'}, [W]')

```

The plot of the power-voltage characteristic estimations is illustrated in Figure 3.12.

# Appendix C

## Layout of Renewable Energy Lab

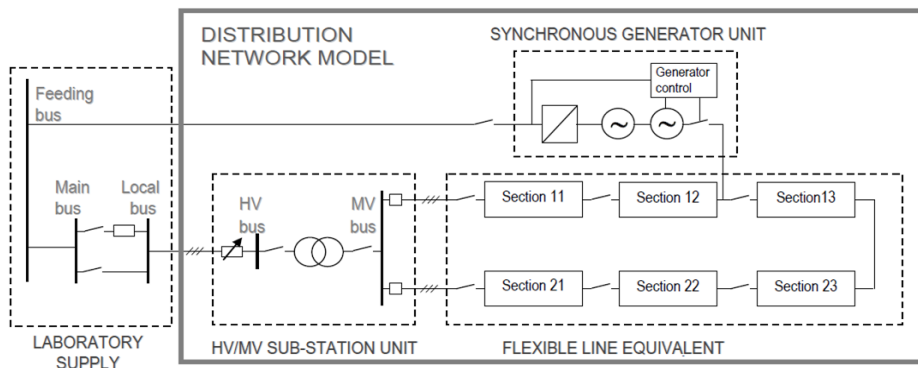
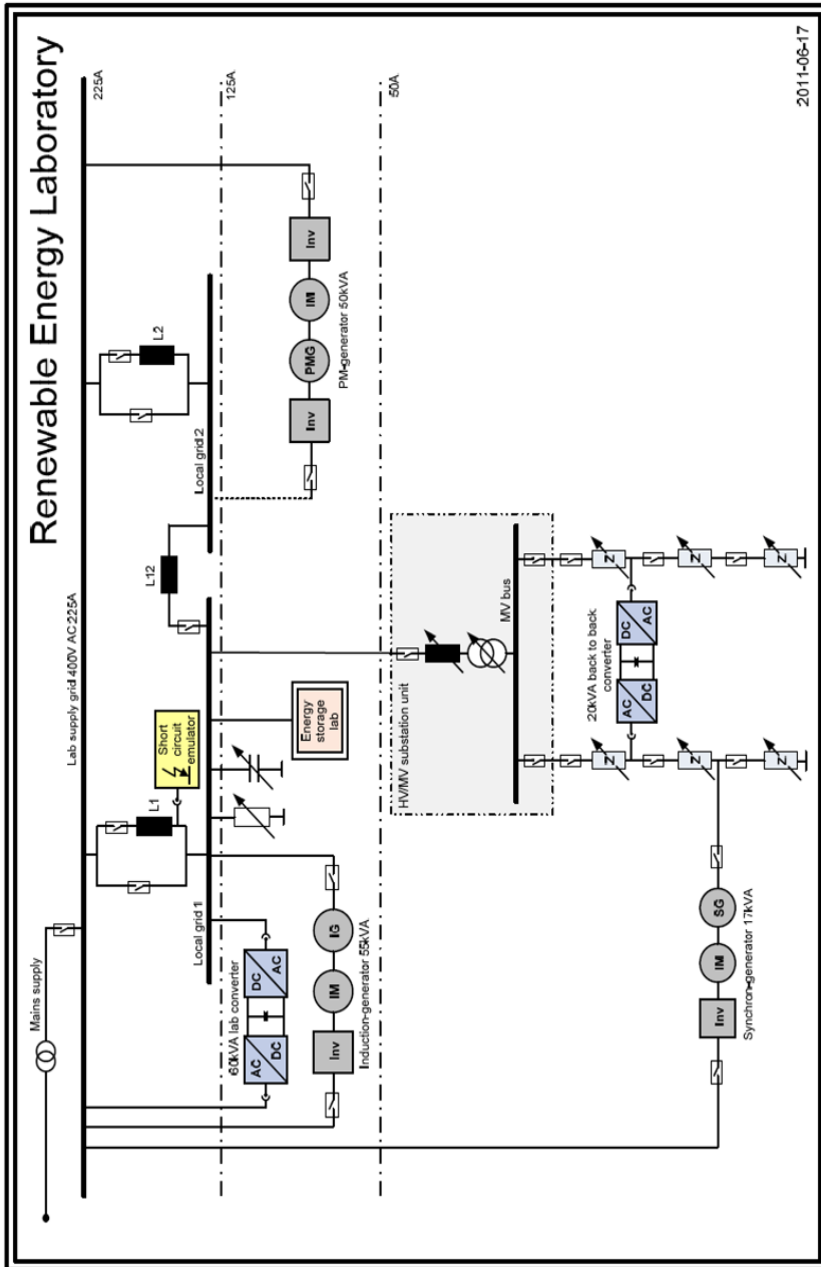


Figure C.1: *Distribution Network Model of the Renewable Energy Laboratory.*

The following diagram shows almost all available components installed in the lab [Pettterteig, 2011, p. 46]. The set-up in this thesis utilized the synchronized generator unit, the line sections with variable impedance between the generator and feeder 2 of the substation unit, the 400V/400V transformer and the variable resistance and reactance connected at the bus named Local grid 1. The local grid 1 bus was disconnected from the Lab supply grid bus during all tests. The important components are extracted from the following figure, and is illustrated with feeder, section numbers and measurement parameters indicated in Figure 4.1.



# Appendix **D**

## Measurement Interface Library Overview

Table D.1: Overview of the different subVIs, listed alphabetically with details about their objectives, inputs and outputs.

Auxiliary	<b>BaseValues</b>	
<i>Objective:</i>	Allows the user to define the pu reference values, which is utilized throughout the other subVIs.	
<i>Input:</i>	None.	
<i>Output:</i>	Reference single-phase power, reference phase-voltage, and reference current.	
Parameter	<b>CalculateImpedanceLoad,</b>	<b>CalculateImpedance-</b>
	<b>System &amp; CalculateImpedanceSystemWfrequency</b>	
<i>Objective:</i>	Calculates the different impedances of the system.	
<i>Input:</i>	PMU measurements either as vector or array(multiple time frames), and a command stating whether the impedance should be outputted as value of vector (multiple time frames).	
<i>Output:</i>	The load impedance, the system impedance, or the system impedance when normalized to 50 Hz, respectively.	

Parameter	<b>CalculatePhasorRepresentations</b>
<i>Objective:</i>	Calculates voltage drops, prepares the phasors for visualization, and (optionally) estimates the emf in the generator.
<i>Input:</i>	PMU measurements, and references to the outputted diagrams for customizing visual appearances, (optional) generator reactance.
<i>Output:</i>	Numerical array, names of the calculated phasors, vector diagram, and a phasor diagram (as XY Graph).

Parameter	<b>CalculatePowerFlow</b>
<i>Objective:</i>	Calculates the generated and consumed active and reactive powers.
<i>Input:</i>	PMU measurements, and choices for outputting the powers as single-phase vs three-phase, and W/kW vs VAr/kVAr.
<i>Output:</i>	Array with the calculated powers, and a string array indicating the units.

Auxiliary	<b>CreatePhasorArrow</b>
<i>Objective:</i>	Adds the arrow head to each phasors visualized in the phasor diagram created in the <i>CalculatePhasorRepresentations</i> subVI.
<i>Input:</i>	Phasor represented as input to the XY Graph, (optional) angle of the arrow head, and (optional) arrow head size constraints.
<i>Output:</i>	Phasor complete with arrow head, represented as input to the XY Graph.

Auxiliary	<b>FindingMostRecentIndex</b>
<i>Objective:</i>	Returning the $n - 1$ index of the measurements to retrieve the most recently measured phasors.
<i>Input:</i>	The PMU measurements.
<i>Output:</i>	The most recent index as numeric value.



Visualization	<b>GraphPlotter</b>
<i>Objective:</i>	Prepares the values for historical visualization.
<i>Input:</i>	Timestamp vector, array of non-complex values, reference to the outputted trend curve, names of the signals contained in the array, and (optional) maximum and minimum values of the Y-axis.
<i>Output:</i>	Trend curve (as a Waveform Chart).
Indicator	<b>Indicator_ISI</b>
<i>Objective:</i>	Calculates the <i>Impedance Stability Index</i> , ISI, for estimation of the voltage stability of the system (loadability limit).
<i>Input:</i>	PMU measurements.
<i>Output:</i>	Array of indicator values with its limit values, and maximum and minimum values of the Y-axis.
Indicator	<b>Indicator_PVcurve</b>
<i>Objective:</i>	Estimates the voltage-power characteristics of the system based on a single state measurement.
<i>Input:</i>	PMU measurement vector (most recently measured state values), a reference to the outputted diagram, and a boolean indicating if the plot should be visualized as pu or phase-voltage versus single-phase power.
<i>Output:</i>	PV-curve (as XY Graph).
Indicator	<b>Indicator_VSI</b>
<i>Objective:</i>	Calculates the <i>Short-Circuit Capacity Index</i> , $VSI_{SCC}$ , for estimation of the voltage stability of the system (loadability limit).
<i>Input:</i>	PMU measurements.
<i>Output:</i>	Array of indicator values with its limit values, and maximum and minimum values of the Y-axis.

Auxiliary	<b>LabMeasurementConverter</b>
<i>Objective:</i>	Converts the measurements with respect to line-voltage versus phase-voltage, transformer phase-shift, and specified converting units.
<i>Input:</i>	PMU measurements, and the converting controls.
<i>Output:</i>	Converted PMU measurements.
Auxiliary	<b>LoadingSetup</b>
<i>Objective:</i>	Simplifies the set-up of the measurement interface that is used for loading off-line measurements or recreating the simulations. The <i>SaveLoadMeasurementData</i> subVI is utilized for loading the saved measurements.
<i>Input:</i>	File name for <i>SavedMeasurements</i> or folder name for <i>SavedSimulations</i> , and a command for choosing loading measurements or loading simulations.
<i>Output:</i>	The complete file path found by the subVI, the phasor angles and magnitudes as dynamic data type, the loaded timestamp values, and the loaded phasor values.
Auxiliary	<b>Normalizer1D &amp; Normalizer2D</b>
<i>Objective:</i>	Converts the phasor measurements to pu magnitude, referring their angles to the load voltage angle, or both.
<i>Input:</i>	PMU measurements, and a command stating which conversion should take place.
<i>Output:</i>	Normalized phasor array.

Auxiliary	<b>ReadLoadedData</b>
<i>Objective:</i>	Simplifies the running loop of the measurement interface that is used for loading off-line measurements or recreating the simulations. It extracts a segment of the entire loaded measurement buffer to be used for each loop.
<i>Input:</i>	Loop index, complete timestamp, measurements and frequency buffers, data segment size, and the number of time frames in the complete buffers.
<i>Output:</i>	Timestamp, measurements and frequency segments, percentage of the complete buffers read, and whether the returned segment is less than the requested data segment size (indicates end of reading).

Auxiliary	<b>SaveLoadMeasurementDataWFrequency</b>
<i>Objective:</i>	Saves the measurements performed by the PMU when performing tests in the lab, and loads the saved data for replaying the original measurement input.
<i>Input:</i>	Filename, Saving/Loading command to switch between the two modes, PMU measurements with their corresponding time stamps when saving, and a boolean indicating whether the frequency should be saved/loaded as well.
<i>Output:</i>	PMU measurements and their corresponding time stamps when loading.



# Appendix **E**

## Measured Line Equivalent Impedance Values

The following page was acquired from [Petterteig, 2011, p. 42], a report where the resistances of the different line equivalent sections, were measured and documented.

### Appendix C3 Breaker status and measured line equivalent resistance values

Switch setting, Equivalent length	L1: 2km	L2: 4 km	L3: 8 km
Inductance, (50 Hz Reactance)	0,6 mH (188 mOhm)	1,24 mH (390 mOhm)	2,48 mH (780 mOhm)

Breaker status and line section resistance for the different equivalent line section.

Equivalent 22 kV line dimension	"Ideal" resistance (wanted value)	Physical resistance - resistor & coil (measured values)	Section 11 & Section 21 (400 A coil)											
			2km				4 km				8 km			
			S3	S4	S5	S6	S3	S4	S5	S6	S3	S4	S5	S6
240 mm <sup>2</sup>	42, 85, 169 mΩ	46, 94, 188 mΩ					0				0	0		0
150 mm <sup>2</sup>	67, 135, 269 mΩ	59, 134, 270 mΩ				0		0			0		0	
120 mm <sup>2</sup>	84, 168, 336 mΩ	84, 171, 326 mΩ	0				0	0		0	0	0	0	0
95 mm <sup>2</sup>	106, 213, 425 mΩ	97, 217 mΩ	0			0			0					
70 mm <sup>2</sup>	143, 286, 572 mΩ	150, 284 mΩ	0	0				0	0	0				
50 mm <sup>2</sup>	200, 400, 799 mΩ	208 mΩ			0									
25 mm <sup>2</sup>	401, 803, 1605 mΩ													

Equivalent 22 kV line dimension	"Ideal" resistance (wanted value)	Physical resistance - resistor & coil (measured values)	Section 12 (200 A coil)											
			2km				4 km				8 km			
			S3	S4	S5	S6	S3	S4	S5	S6	S3	S4	S5	S6
240 mm <sup>2</sup>	42, 85, 169 mΩ	44, 94, 179 mΩ					0				0	0		0
150 mm <sup>2</sup>	67, 135, 269 mΩ	55, 140, 263 mΩ				0		0		0	0		0	0
120 mm <sup>2</sup>	84, 168, 336 mΩ	83 , 170, 315 mΩ	0				0	0		0	0	0	0	0
95 mm <sup>2</sup>	106, 213, 425 mΩ	119, 214, mΩ		0					0	0				
70 mm <sup>2</sup>	143, 286, 572 mΩ	148, 312 mΩ	0	0			0	0	0					
50 mm <sup>2</sup>	200, 400, 799 mΩ	201 mΩ			0									
25 mm <sup>2</sup>	401, 803, 1605 mΩ													

Equivalent 22 kV line dimension	"Ideal" resistance (wanted value)	Physical resistance - resistor & coil (measured values)	Section 22 (200 A coil)											
			2km				4 km				8 km			
			S3	S4	S5	S6	S3	S4	S5	S6	S3	S4	S5	S6
240 mm <sup>2</sup>	42, 85, 169 mΩ	54, 61, 191, mΩ									0			
150 mm <sup>2</sup>	67, 135, 269 mΩ	54, 108, 238 mΩ								0	0			0
120 mm <sup>2</sup>	84, 168, 336 mΩ	101, 181, 353 mΩ				0	0					0		0
95 mm <sup>2</sup>	106, 213, 425 mΩ	101, 228, 424 mΩ				0	0			0			0	
70 mm <sup>2</sup>	143, 286, 572 mΩ	174, 296, 578 mΩ	0					0			0		0	0
50 mm <sup>2</sup>	200, 400, 799 mΩ	221, 414,781 mΩ	0			0			0		0	0	0	0
25 mm <sup>2</sup>	401, 803, 1605 mΩ	407, 771 mΩ			0		0	0	0	0				

Equivalent 22 kV line dimension	"Ideal" resistance (wanted value)	Physical resistance - resistor & coil (measured values)	Section 13 & Section 23 (100 A coil)											
			2km				4 km				8 km			
			S3	S4	S5	S6	S3	S4	S5	S6	S3	S4	S5	S6
240 mm <sup>2</sup>	42, 85, 169 mΩ	30, 94, 186 mΩ					0				0	0		
150 mm <sup>2</sup>	67, 135, 269 mΩ	90, 139,290 mΩ	0					0			0		0	
120 mm <sup>2</sup>	84, 168, 336 mΩ	90, 139, 365 mΩ	0					0			0	0	0	
95 mm <sup>2</sup>	106, 213, 425 mΩ	90, 229, 439 mΩ	0						0					0
70 mm <sup>2</sup>	143, 286, 572 mΩ	135, 287, 590 mΩ		0			0		0		0	0		0
50 mm <sup>2</sup>	200, 400, 799 mΩ	225, 437, 751 mΩ			0					0	0	0	0	0
25 mm <sup>2</sup>	401, 803, 1605 mΩ	434, 748 mΩ				0	0	0	0	0				

# Appendix F

## Plots of Deviations

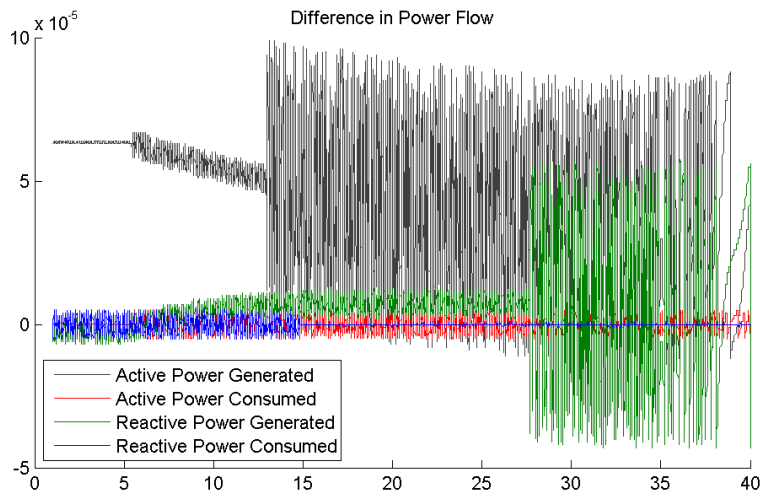


Figure F.1: *Deviations between the powers calculated by the PowerFactory simulation model and the measurement interface when supplied with the same input voltages and current.*

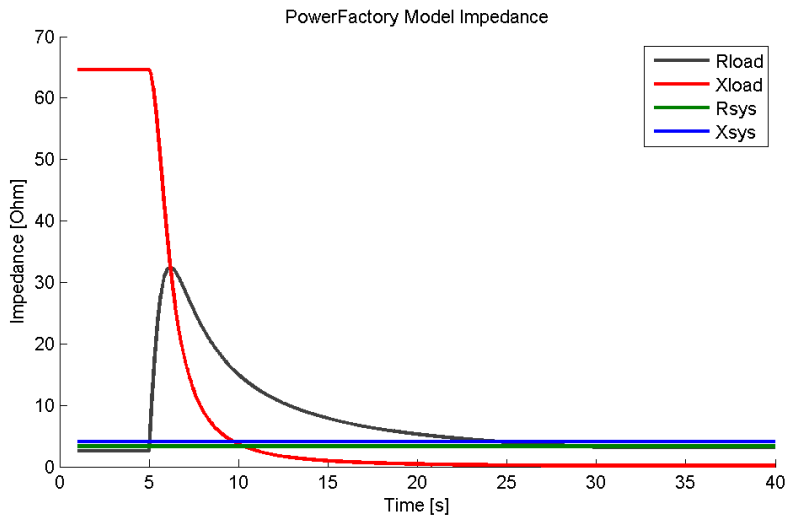


Figure F.2: Impedance calculations performed in Matlab directly based on the simulated voltages and current from the PowerFactory simulation model.

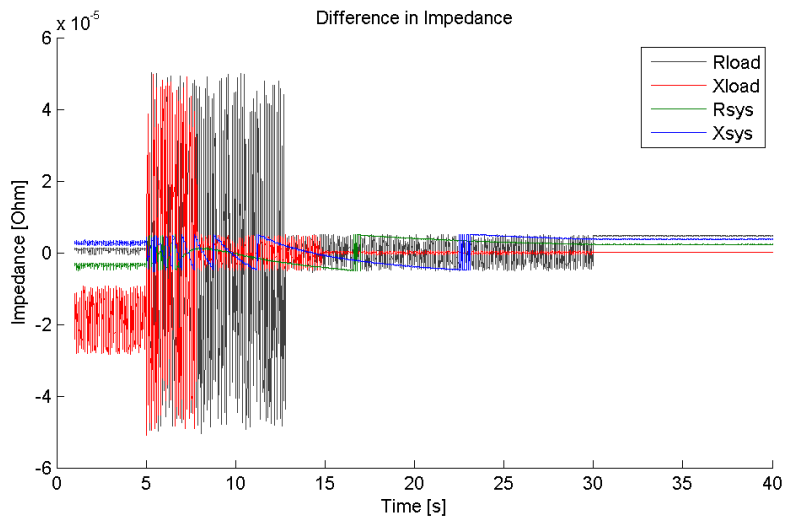


Figure F.3: Deviations between the impedances calculated by the PowerFactory simulation model and the measurement interface when supplied with the same input voltages and current.



# Appendix G

## Phasor Diagram States

Five phasor diagrams illustrating the power system state change during recreation of the scenario *Load: Lab-average* simulated in PowerFactory (Section 5.2.1).

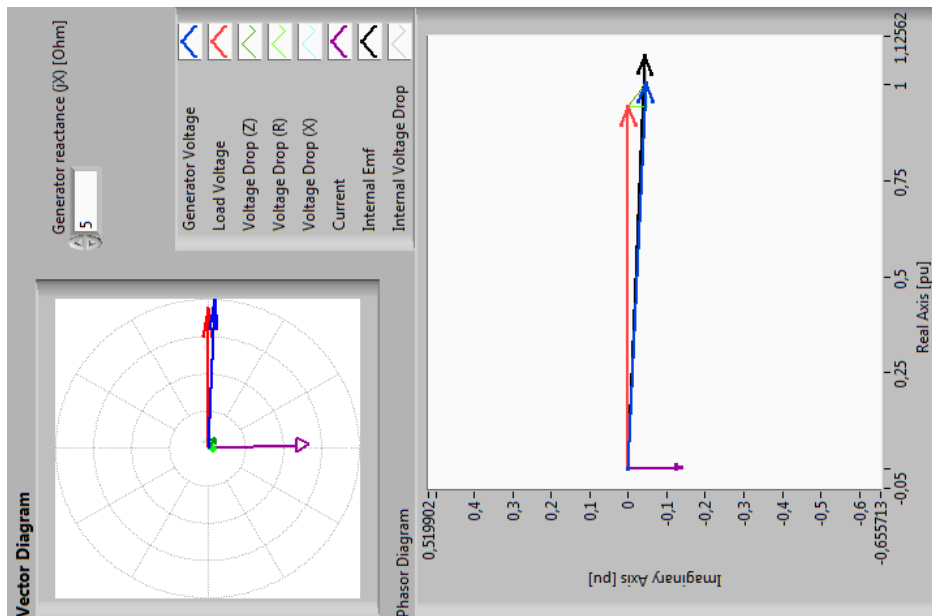


Figure G.1: *First phasor state, equivalent to before simulation scenario Load: Lab-average started.*

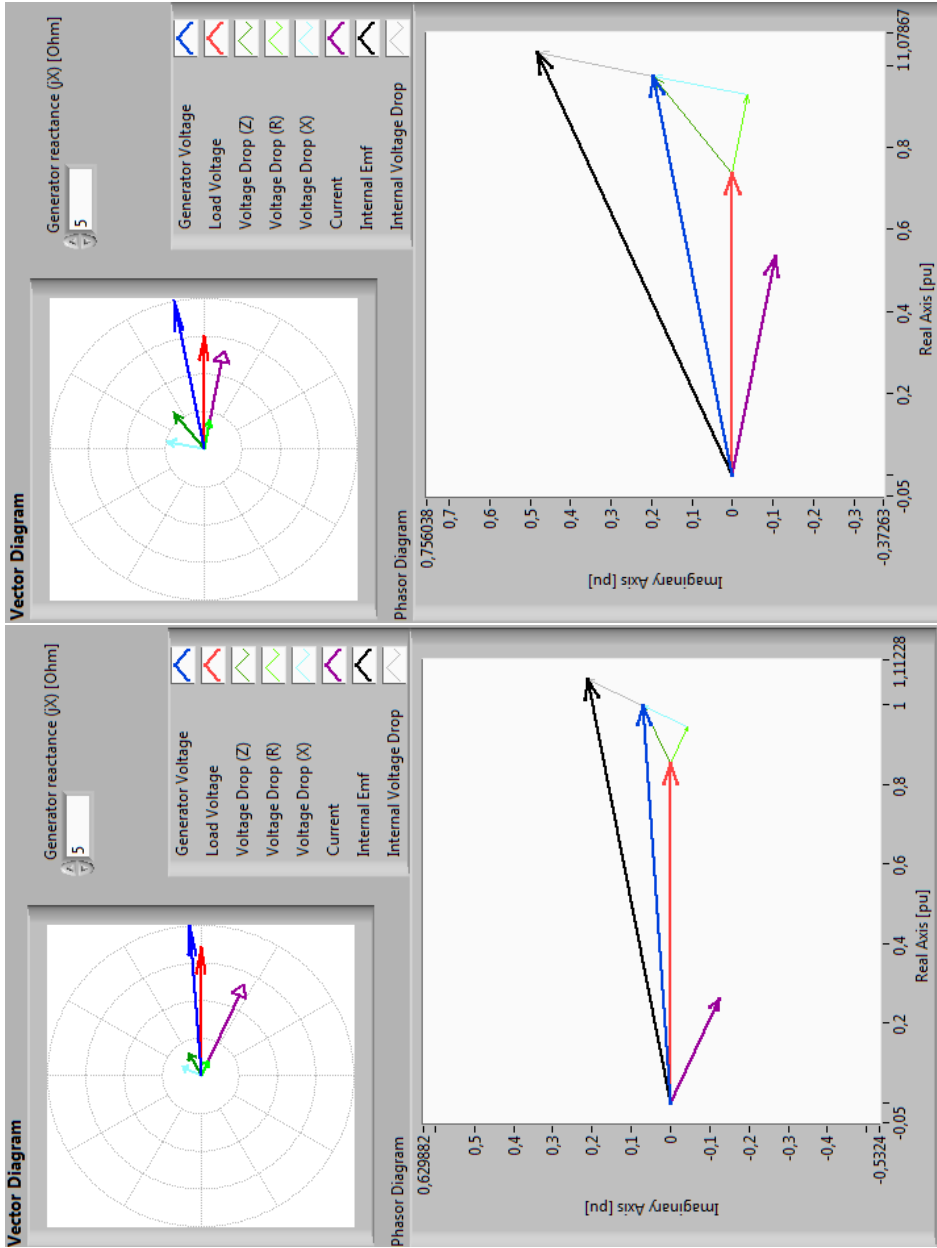


Figure G.2: *Second and third phasor state shown from down/left to top/right, during simulation scenario Load: Lab-average.*

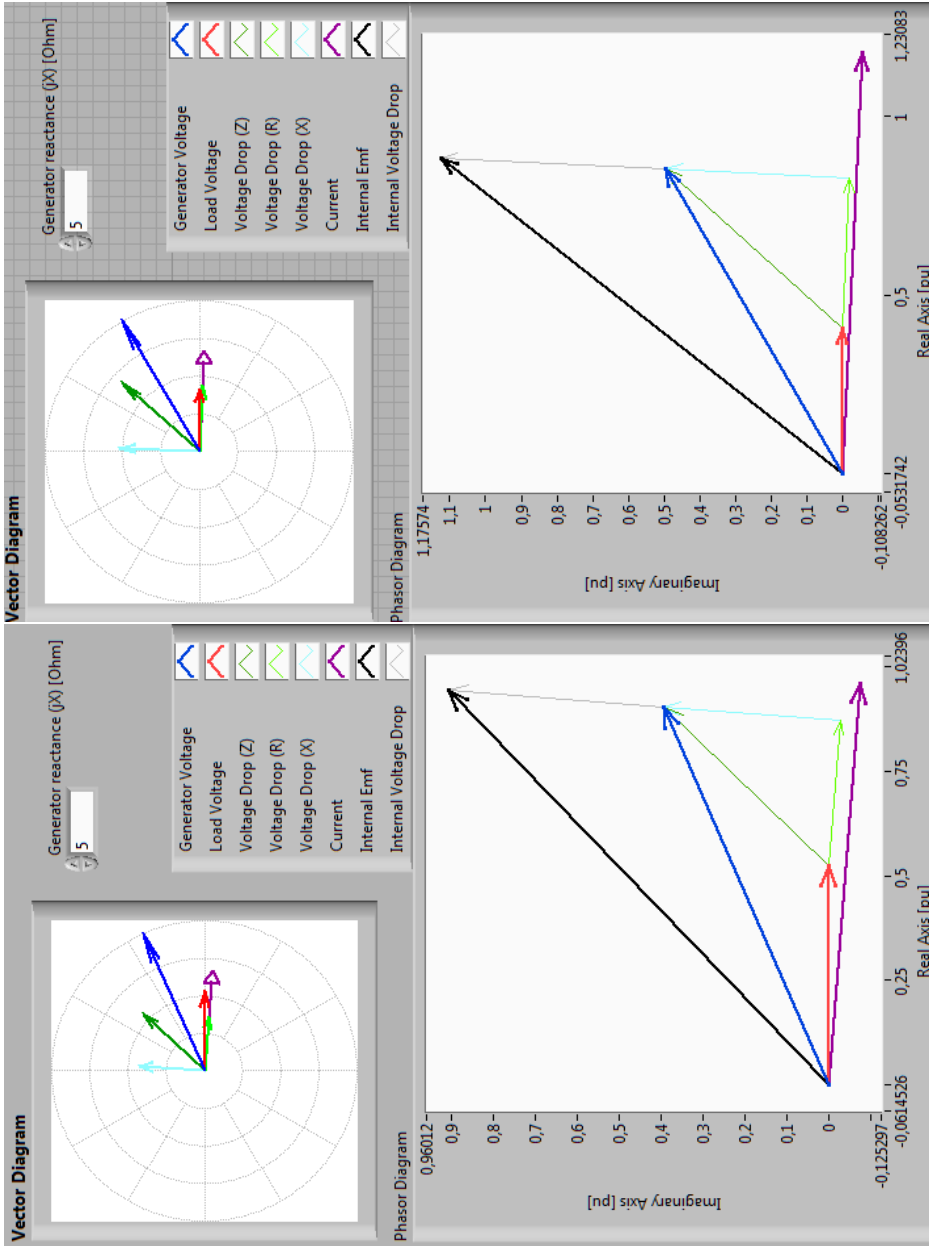


Figure G.3: Fourth and fifth phasor state shown from down/left to top/right, during scenario Load: Lab-average. The fifth indicates the end of the scenario.



# Appendix H

## Measurement Error Sources

Several procedures were performed in order to identify, and preferably eliminate, any possible sources introducing errors in the measurements.

The line-voltage R-S was measured at the Local grid 1 bus with an oscilloscope and the PMU simultaneously. The amplitude was measured with the cursor function of the oscilloscope, which yielded a value of 5.6 V. Divided by the square root of two, this resulted in a rms-value of 3.96 V. The value displayed at the PRL interface was also shown to be 3.96, without some varying trailing decimals. Readouts from oscilloscopes are associated with measurement uncertainties.

The phase was also used in a test where two PMU measurement input sockets were connected to the same phase, in order to discover faults with the different input sockets. The result was identical measurements, and no fault was detected.

To discover whether the phases in each measurement point were perfectly synchronized, the three PMU measurement input sockets were utilized simultaneously. The screen shots of the performed measurements are illustrated in Figure H.1 and H.2 for the generator current and generator voltage respectively, and Table H.1 displays which measurement belongs to which phase.

Table H.1: *PMU input socket measurement's connection with laboratory phases.*

PMU Input socket	$U_{\text{gen}}$	$I_{\text{gen}}$
NTNU.PMU2/V1	R-S	R
NTNU.PMU2/V2	S-T	S
NTNU.PMU2/V3	T-R	T

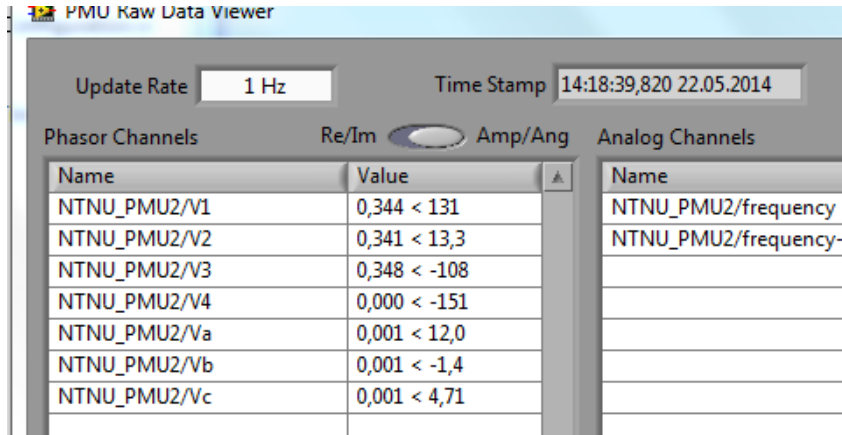


Figure H.1: All current phases measured at the generator by a PMU, where phase  $R$ ,  $S$  and  $T$  are visualized respectively by the PRL interface.

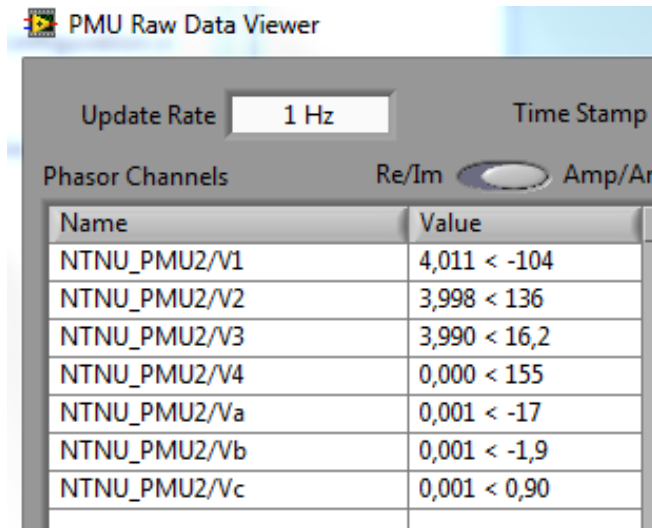


Figure H.2: All line-voltage phases measured at the load by a PMU, which indicates not perfectly symmetrical load line-voltages (according to the PRL interface). The phases  $V1$ ,  $V2$  and  $V3$  corresponds respectively to  $R$ - $S$ ,  $S$ - $T$  and  $T$ - $R$  in the laboratory, and the scaling coefficient is  $10^{-3} \text{ mV/v}$ .

## **Appendix References**

Petterteig, A. (2011). Distribution network laboratory model; consisting of a hv/mv substation model, a synchronous generator dg model and a flexible line equivalent. Technical report, SINTEF Energy Research.